Electrical and Optogenetic Modulation of Cortical Activity to Promote Neuroprotection and Network Reorganization in Non-Human Primates

Jasmine Zhou

A dissertation

submitted in partial fulfillment of the

requirements for the degree of

Doctor of Philosophy

University of Washington

2025

Reading Committee:

Azadeh Yazdan-Shahmorad, Chair

Amy Orsborn

Chet Moritz

Program Authorized to Offer Degree:

Bioengineering

University of Washington

Abstract

Electrical and Optogenetic Modulation of Cortical Activity to Promote Neuroprotection and Network Reorganization in Non-Human Primates

Jasmine Zhou

Chair of the Supervisory Committee:
Azadeh Yazdan-Shahmorad
Department of Bioengineering

Many debilitating neurological conditions arise from abnormal network dynamics and connectivity. Novel neuromodulation techniques, including electrical and optogenetic stimulation, aim to harness the brain's innate plasticity to reorganize neural connections, reduce tissue damage, and improve patient outcomes. To test the feasibility of these emerging neuromodulation approaches while improving their translational potential, my dissertation work applies advanced electrophysiology, histology, and computational tools in the brains of non-human primates (NHPs), evaluating the cortical response to different stimulation paradigms. Chapter 2 addresses the critical need for acute interventions in ischemic stroke, which can prevent irreversible tissue injury and improve functional outcomes. By inducing focal lesions in the sensorimotor cortex of NHPs while recording electrocorticography signals, we evaluated the impact of acute, theta-burst electrical stimulation delivered adjacent to the ischemic infarct. Early stimulation significantly reduced peri-infarct

neuronal depolarization and microglial activation, leading to smaller lesion volumes. This study demonstrated the therapeutic potential of acute electrical stimulation to mitigate excitotoxicity, inflammation, and neural damage following ischemic injury, offering a promising strategy to enhance patient outcomes after stroke. Chapter 3 explores the use of optogenetic tools to modulate cortical network dynamics. By delivering patterned laser illumination to regions expressing an inhibitory opsin, we successfully disrupted functional connectivity in the posterior parietal cortex, reducing gamma-band coherence between targeted locations and the broader network. This selective decoupling highlights the potential of optogenetics to weaken pathological synchrony, complementing prior work using excitatory strategies to enhance connectivity and facilitate recovery. Together, these findings advance the development of targeted neuromodulation therapies aimed at restoring healthy network function in neurological disorders.

Acknowledgement

I would first like to thank my advisor, Dr. Azadah Yazdan-Shahmorad, for her endless support and mentorship. She has been the kindest, most empathetic and inspiring advisor, shaping not only the scientist I am but also the person I aspire to be. She showed me the importance of being my own champion while keeping an open heart to the world. I will always be grateful for her encouragement and for the trust she placed in me to pursue ambitious goals in neuroengineering. I also thank Drs. Chet Moritz and Amy Orsborn for their thoughtful guidance on my dissertation work. Their feedback and insight motivated me to refine my ideas, strengthen my arguments, and grow as an independent researcher. I could not have asked for better committee members to challenge and support me along the way.

I would like to thank my closest collaborator, Dr. Karam Khateeb, who has been a constant source of inspiration since I joined the lab, combining a genuine passion for neuroscience with the ability to ask critical questions. I also want to thank my former colleagues, Drs. Devon Griggs, Julien Bloch, and Tiphaine Belloir, who laid the foundations for our chronic experiments and supported me during the early days of data collection. I thank our undergraduate students, especially Aryaman Gala and Makaha Harmon, for contributing to different stages of my projects and for teaching me to become a better mentor. I'm also thankful to Toni Haun, our lab manager, for her kindness, uplifting conversations, and steady support during difficult times. Finally, to all members of the Yazdan Lab, thank you for creating an environment of trust, collaboration, and friendship. I could not have joined a better community to complete my PhD.

Outside the lab, I am grateful to the wonderful people I met in Seattle who made these six years brighter and more meaningful. Jiahao Wan, Yusi Chen, Zhiyao Li, and Zhiyang Zhang, you have been my family away from home. Thank you for lifting me up during challenges, celebrating milestones big and small, and filling my time here with laughter, comfort, and unforgettable memories. Finally, I want to thank my family, my mother, father, and grandparents, for being the true reason I chose this field and for their unwavering support from afar. You have believed in me unconditionally, even when it meant being separated by distance for years at a time. Every achievement in this dissertation is built upon your sacrifices and encouragement. I am endlessly grateful for your love and strength, and I dedicate this work to you.

Table of Contents

Chapter 1: Introduction

Neurological disorders are the leading cause of disability and the second leading cause of death worldwide, with global prevalence continuing to rise in the past decades (Feigin et al., 2019). According to the Global Burden of Disease Study, neurological conditions affect over one billion people globally, resulting in more than 10 million deaths each year (Vos et al., 2020). At the same time, the burden of long-term disability from conditions such as stroke, epilepsy, Alzheimer's, and Parkinson's disease has also grown substantially, driven by aging populations, improved survival after acute events, and the low likelihood of complete recovery (Feigin et al., 2019; Vos et al., 2020). Addressing this growing challenge will require the development of novel therapeutic strategies that can target underlying circuit dysfunction to improve long-term outcomes across various neurological conditions.

Neuromodulation has recently emerged as a promising technique in the treatment of neurological disorders, offering the opportunity to directly target pathological brain circuits when traditional pharmacological therapies fail (Lewis et al., 2016). Unlike systemic drugs that often lack spatial specificity and are limited by blood-brain barriers, neuromodulation techniques overcome these challenges by delivering targeted stimulation that modifies neural excitability, plasticity, and network dynamics (Dayan et al., 2013; McCormick et al., 2020). Supported by growing evidence from both preclinical and clinical studies, neuromodulation is gaining recognition as an important therapeutic approach to combat brain disorders by reshaping pathological activity patterns (Lewis et al., 2016). Advances in stimulation technologies and modalities, ranging from invasive deep-brain stimulation (DBS) to noninvasive transcranial magnetic stimulation (TMS), have broadened the spectrum of treatable conditions, encompassing both chronic diseases like Parkinson's and treatment-resistant depression (Lozano et al., 2019; Perera et al., 2016), as well as neurological damage such as ischemic stroke and traumatic brain injury (Bao et al., 2020; Hummel & Cohen, 2006; Villamar et al., 2012). As these techniques continue to be refined, neuromodulation offers significant promise for improving recovery and outcomes in patients with neurological conditions that were once considered intractable.

While neuromodulation therapies are most often associated with chronic conditions, their potential application in acute settings warrant further investigation. This gap is highlighted by ischemic stroke, a leading cause of death and disability worldwide (Tsao et al., 2022). Current

acute stroke treatments, such as thrombolysis and thrombectomy, are constrained by narrow time windows and strict eligibility criteria (Brott & Bogousslavsky, 2000; Prabhakaran et al., 2015). As a result, there is an urgent need for additional interventions that can protect vulnerable neural tissue during the acute phase, when injury progression remains early and potentially reversible (Ginsberg, 2008; Powers, 2020). One promising strategy is to design brain stimulation protocols that suppress cortical excitability and interrupt secondary injury mechanisms such as glutamate-mediated excitotoxicity, spreading depolarizations, and inflammatory cascades (Belov Kirdajova et al., 2020; Chamorro et al., 2016). However, implementing neuromodulation acutely poses both scientific and practical challenges. The potential benefits of early stimulation must be carefully balanced against the risks of disrupting fragile and evolving pathophysiology immediately after stroke (Dohmen et al., 2008). In addition, logistical barriers such as limited access to equipment and neurophysiological monitoring (Brasil et al., 2024) may further complicate the use of acute brain stimulation in emergency clinical settings. Given these hurdles, only a limited number of neurostimulation approaches have been tested in acute stroke patients. For example, vagus nerve stimulation (VNS), a technique traditionally used to treat epilepsy and depression, has been shown to be safe and technically feasible when administered within 6 hours after stroke onset (Arsava et al., 2022). While the efficacy of acute VNS in improving functional recovery remains to be established, these preliminary results suggest that early stimulation could be developed into a viable neuroprotective strategy. Collectively, these findings support continued investigation of brain stimulation paradigms for acute neurological injuries, coupled with physiological studies to clarify the neural and cellular mechanisms underlying their therapeutic effects.

Beyond the acute phase, neuromodulation has been well-established for promoting long-term plasticity and functional recovery (Boonzaier et al., 2018; Hummel & Cohen, 2006; Solomons & Shanmugasundaram, 2019). Numerous studies have utilized electrical, magnetic, optogenetic, or sensory stimulation to enhance either synaptic strength between monosynaptic neurons (Bi & Poo, 1998; Caporale & Dan, 2008; Feldman, 2012) or functional connectivity across large-scale cortical networks (Ruggiero et al., 2021; Yazdan-Shahmorad, Silversmith, et al., 2018). For example, repetitive TMS has been shown to improve motor function in stroke survivors by facilitating reorganization of perilesional networks (Hsu et al., 2012). Similarly, paired and activity-dependent stimulation paradigms have been used to strengthen correlated neuronal activity and behaviorally relevant neural pathways in primates (Lucas & Fetz, 2013; Nishimura et al., 2013). In sum, these excitatory approaches primarily aim to increase connectivity, promote coordinated

activity across networks, and drive functional recovery through Hebbian plasticity mechanisms (Kempter et al., 1999). However, not all brain disorders benefit from increased functional connectivity. In conditions such as epilepsy and traumatic brain injury, abnormally high synchrony or hyperconnectivity can disrupt network function and exacerbate symptoms (Englot et al., 2016; Hillary & Grafman, 2017). In these contexts, the goal of neuromodulation therapy shifts from enhancing correlated activity to inducing targeted suppression and neural decoupling. Experimental studies using sensory deprivation or chemogenetic silencing have demonstrated the feasibility of weakening synaptic and functional connections (Allen et al., 2003; Peeters et al., 2020), though it remains unclear whether such decoupling can be achieved consistently across targeted cortical areas. If successful, the capacity to both strengthen and weaken connectivity would establish neuromodulation as a versatile, bidirectional approach for restoring healthy network dynamics and addressing diverse forms of circuit dysfunction across neurological conditions.

A major challenge in the development of neuromodulation therapies lies in translating findings from preclinical animal studies into clinical applications. Much of the work on cortical stimulation for neuroprotection and network reorganization has been conducted in rodent stroke models, which despite their utility, differ substantially from the human brain in terms of scale, cortical architecture, and vascular physiology. These key differences likely contribute to the difficulty of reproducing positive preclinical outcomes in human clinical trials (Cheng et al., 2004; Levy et al., 2016a; Nouri & Cramer, 2011). To bridge this gap, it's crucial to evaluate stimulation paradigms in systems that more closely resemble human neuroanatomy and physiology. Non-human primates (NHPs) represent a highly relevant model in this regard, given their larger brain volume, complex cortical organization, and human-like functional connectivity patterns (Hutchison et al., 2013). For these reasons, my dissertation uses the NHP model to investigate stimulation-induced neuroprotection (Chapter 2) and neuroplasticity (Chapter 3), thereby enhancing the translational relevance of the proposed interventions.

Chapter 2 of this dissertation addresses the gap in acute stroke interventions by investigating strategies to mitigate irreversible tissue injury and improve outcomes. Specifically, we combined electrophysiological and histological approaches to assess the effects of acute electrical stimulation on injury progression and cortical physiology in NHPs. By inducing sensorimotor lesions and monitoring electrocorticographic signals over time, we evaluated the impact of theta-

burst stimulation delivered adjacent to the ischemic infarct. Our results showed that early stimulation significantly reduced peri-infarct neuronal activation, which was accompanied by lower microglial activation and smaller lesion volumes. Together, these findings demonstrate the therapeutic potential of acute electrical stimulation to reduce excitotoxicity, inflammation, and neural damage following ischemic injury, offering a promising strategy to improve patient outcomes after stroke.

Chapter 3 of this dissertation investigates the potential of optogenetic tools to modulate neural dynamics and plasticity in NHPs. Using single-site optogenetic inhibition, we found that repeated modulation reduced gamma band coherence, which serves as a proxy for functional connectivity, between the illuminated site and other recording channels. This continuous reduction indicates effective decoupling of the targeted brain region, demonstrating that optogenetic interventions can selectively weaken neural synchrony within the cortical network. These results complement prior studies using excitatory stimulation to enhance functional connectivity (Yazdan-Shahmorad, Silversmith, et al., 2018). Together, our work establishes a foundation for employing optogenetics to reorganize network structures and highlights its versatility as a tool for both suppressing and strengthening targeted neural circuits.

Finally, Chapter 4 of this dissertation outlines several key considerations for designing effective neuromodulation strategies tailored to specific conditions, including stimulation effects, timing, modality, and translational feasibility. It also highlights future research directions such as monitoring subacute physiological responses, linking neural changes to behavior, developing closed-loop systems, and refining stimulation parameters to improve the spatial precision of network modulation. Together, these efforts will advance the development of next-generation neuromodulation therapies that are adaptive, targeted, and clinically impactful.

Chapter 2: Early Intervention with Electrical Stimulation Reduces Neural Damage After Stroke in Non-Human Primates

Jasmine Zhou[1,2], Karam Khateeb[1,2], and Azadeh Yazdan-Shahmorad[1,2,3]

[1]Department of Bioengineering, University of Washington, Seattle, WA
[2]Washington National Primate Research Center, Seattle, WA
[3]Department of Electrical and Computer Engineering, University of Washington, Seattle, WA

*This work is adapted from our published manuscript: Zhou, J., Khateeb, K. & Yazdan-Shahmorad, A. Early intervention with electrical stimulation reduces neural damage after stroke in non-human primates. *Nat Commun* **16**, 6701 (2025). https://doi.org/10.1038/s41467-025-61948-y

Abstract

For patients with ischemic strokes, acute intervention offers the most critical therapeutic opportunity as it can reduce irreversible tissue injury and improve functional outcomes. However, currently available treatments within the acute window are highly limited and have strict patient selection criteria. Although emerging neuromodulation techniques have been proposed as a treatment for stroke patients suffering chronic disabilities, acute stimulation is rarely studied due to the risk of causing adverse effects related to ischemia-induced electrical instability. Here, we demonstrate that acute cortical electrical stimulation, when administered one hour post-stroke, can provide neuroprotective effects in non-human primate brains. Utilizing state-of-the-art electrophysiology and histology tools, we observed that applying continuous theta burst electrical stimulation directly adjacent to the ischemic lesion significantly reduced peri-infarct neural activity, as evidenced by lower electrocorticography signal power and c-Fos expression. The reduced depolarization is also accompanied by a decrease in neuroinflammation and infarct volume in the sensorimotor cortex. These findings suggest that acute electrical stimulation can be used safely and effectively as an early intervention to enhance the clinical outcomes in ischemic stroke patients.

Introduction

Ischemic stroke is a major type of brain injury that results in high mortality and serious long-term disability for adults, especially in the aging population. Globally, over 7.6 million people suffer from ischemic stroke each year, causing significant health and economic burdens worldwide (Feigin et al., 2021; Tsao et al., 2022). An ischemic stroke happens when blood flow within the brain is interrupted, leading to a lack of oxygen supply, energy depletion, and subsequent neuronal death. Acute intervention within hours after stroke onset offers the most critical therapeutic opportunity to mitigate irreversible tissue injury, thus improving neurological and functional outcomes for stroke patients (Prabhakaran et al., 2015). However, currently available treatments within the acute window are highly limited, and approved interventions such as the administration of tissue plasminogen activator (t-PA) and catheter-based thrombectomy often have strict patient selection criteria (Brott & Bogousslavsky, 2000; Prabhakaran et al., 2015). During the past few decades, there has been a large amount of experimental research and clinical trials on neuroprotective drug therapies targeting acute ischemic stroke, with the aim to interrupt the ischemic cascade and thereby reduce neuronal death (Chamorro et al., 2016; Cheng et al., 2004; Danton & Dietrich, 2004). However, most of the drugs failed to show consistent clinical efficacy when moving from animals to humans (Cook & Tymianski, 2011; Ginsberg, 2008; Shi et al., 2018). Therefore, there is a pressing need to expand the therapeutic options for acute ischemic stroke and improve the translation from bench to bedside to help millions of stroke patients retain the maximum quality of life.

In recent years, novel neuromodulation paradigms such as electrical brain stimulation have been proposed as a promising treatment for ischemic stroke. Most of these stimulation paradigms target the subacute or chronic phase of stroke to promote neural plasticity and functional recovery, rather than reducing permanent ischemic damage (Adkins-Muir & Jones, 2003; Kleim et al., 2003; Khanna et al., 2021; Boonzaier et al., 2018; Popović et al., 2009; Bao et al., 2020). As a result, it might take months of treatment in conjunction with rehabilitative training for only a subset of patients to see positive results from these interventions (Coscia et al., 2019; Levy et al., 2016b; Stinear et al., 2020). Meanwhile, comparing to the chronic implementation of electrical stimulation for stroke, the acute application of such strategy is still relatively rare, especially in larger animal models and humans due to the risk of causing adverse effects and greater tissue damage related to ischemia-induced electrical instability and spreading depolarizations (SDs). It has been widely

reported that perilesional tissues are particularly susceptible to SDs, marked by intense neuronal depolarization waves that can lead to increased metabolic stress, neuronal swelling, and lesion progression (Dohmen et al., 2008; Dreier, 2011; von Bornstädt et al., 2015; Woitzik et al., 2013). However, despite the concern about SDs, a few studies have successfully demonstrated the use of sensory or direct brain stimulation to exert neuroprotection and reduce tissue damage for rodents with acute stroke (Lay et al., 2010; Notturno et al., 2014; Peruzzotti-Jametti et al., 2013; L.-C. Wang et al., 2021; Buetefisch et al., 2023). Similar to neuroprotective drugs, these acute stimulation strategies aim to reduce the irreversible damage caused by the ischemic cascade within hours after stroke onset or after reperfusion by reducing inflammation, oxidative stress, excitotoxicity, and apoptosis, thus preserving the perilesional tissues surrounding the ischemic core (Baba et al., 2009; Bahr Hosseini et al., 2019). While these results from rodent studies are promising, the scale and anatomical differences between rodent and human brains pose significant challenges to the feasibility of clinical translation (Tajiri et al., 2013). Therefore, we need a more comprehensive understanding of how electrical brain stimulation drives changes in the physiology of neuronal networks at scales comparable to that of the human brain before these strategies can be successfully translated from bench to bedside for acute stroke patients.

As a result, two major gaps in knowledge need to be addressed as we seek to implement brain stimulation paradigms for acute ischemic stroke: 1) The protective effect of electrical stimulation needs to be evaluated across large cortical areas in a more clinically relevant animal model. 2) We need to have a better understanding of the mechanisms underlying stimulation-induced changes, from both electrophysiological and cellular perspectives. In this study, we used a novel set of approaches capable of addressing these two gaps to investigate stimulation-induced neuroprotection. We combined a lesion-based toolbox (Khateeb et al., 2022; Stanis et al., 2023), state-of-the-art neurophysiology techniques, and a range of histology markers to study the neuroprotective effects of cortical electrical stimulation following acute ischemic stroke in non-human primates (NHPs). We compared multiple aspects of physiological responses to stimulation from large areas (~3 cm^2) of the macaque sensorimotor cortex for up to 4 hours after stroke onset to interrogate the mechanisms underlying any observed neuroprotection. The unprecedented insights gained from these experiments will inform the development of next-generation brain stimulation paradigms that can be used as an alternative treatment in the acute window after stroke to minimize neuronal damage, reduce severe disabilities, and improve functional outcomes for stroke patients.

Results

In this study, we induced controlled cortical ischemic lesions in the primate sensorimotor cortex using the photothrombotic technique (Khateeb et al., 2022; Labat-gest & Tomasi, 2013; Stanis et al., 2023), which generated focal infarcts by photo-activation of a light-sensitive dye (Rose Bengal) that interrupts local blood flow. The infarct size and location are controlled by setting a constant illumination intensity and aperture size through an opaque light mask placed above the cortical surface (**Fig. 1a,b**). In control monkeys D and E, we collected electrocorticography (ECoG) data through our customized multi-modal interface (**Fig. 1b**), which includes baseline before lesioning, during lesion induction, and up to 3 hours post lesioning to monitor network dynamics around the injury site. In stimulated monkeys F and G, we recorded 1 hour after lesioning and then applied electrical stimulation at approximately 8 mm medial to the lesion center on the ipsilesional hemisphere (**Fig. 1b,c**: blue arrow). The stimulation trains employed a theta burst paradigm with five 1kHz pulses within each burst (Zhou et al., 2022). Each stimulation block lasted 10 minutes, with 2-minute recordings of spontaneous activity in between the blocks to track changes in neurophysiology as stimulation continued (**Fig. 1d**).

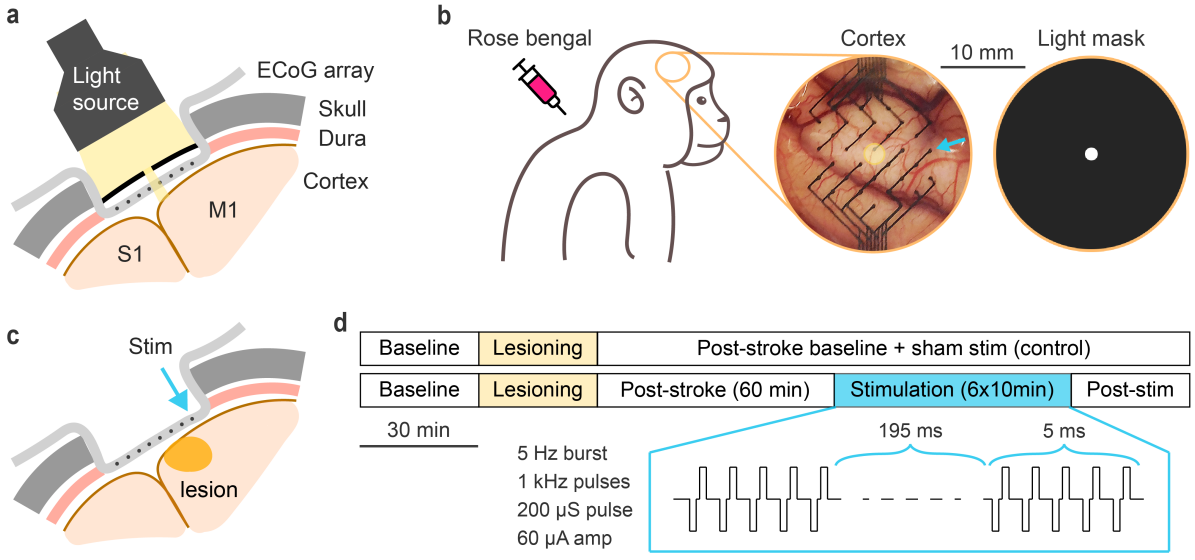

Fig. 1 | Schematics of experimental procedures. a, Illustration of the method and setup to induce photothrombotic lesion in the NHP cortex. **b,** Cortical view of the multi-model artificial dura used to record ECoG. Yellow circle indicates the area illuminated with light source to induce stroke. Blue arrow points to the stimulation electrode. **c,** Illustration of the location of induced lesion and electrical stimulation. **d,** Experimental timeline for the control (monkey D, E) and stimulated groups (monkey F, G). Scale bar indicates 30-min block length.

Reduction in ischemic lesion volume with acute cortical stimulation

To investigate the neuroprotective effects of electrical stimulation following acute ischemic stroke, we first quantified the extent of ischemic injury within the sensorimotor cortex through histological analysis. Specifically, we performed Nissl staining on mounted coronal sections of the brain to evaluate the amount of cell death and estimate lesion volumes in both control (monkey D, E) and stimulated animals (monkey F, G). The loss of Nissl substance at the infarct core led to distinct pale areas and well-defined boundaries on the stained sections (**Fig. 2a**). Using these identified boundaries, we applied edge detection and linear interpolation between sections to reconstruct the brain with the ischemic lesion in 3D space (**Fig. 2b**), including distinct anatomical features of the sensorimotor cortex such as the central sulcus. This reconstruction was used to estimate the lesion volumes in each animal **(Fig. 2c**). We found that in control monkeys D and E which did not receive post-stroke stimulation, the estimated lesion volumes were 35.3 and 28.4 mm^3 respectively, while in stimulated monkeys F and G, the lesion volumes were 20.3 and 15.9 mm^3 respectively. Notably, the ischemic lesions in the stimulated animals were consistently smaller than those in the controls, both in depth and medial-lateral width (**Fig. 2c, d**). As the stimulation pulses were delivered medially from the infarct core on the medial-lateral axis (**Fig. 2b**: blue arrow), these results suggest acute electrical stimulation may have reduced the infarct size by protecting the brain from ischemic injury progression hours after stroke onset.

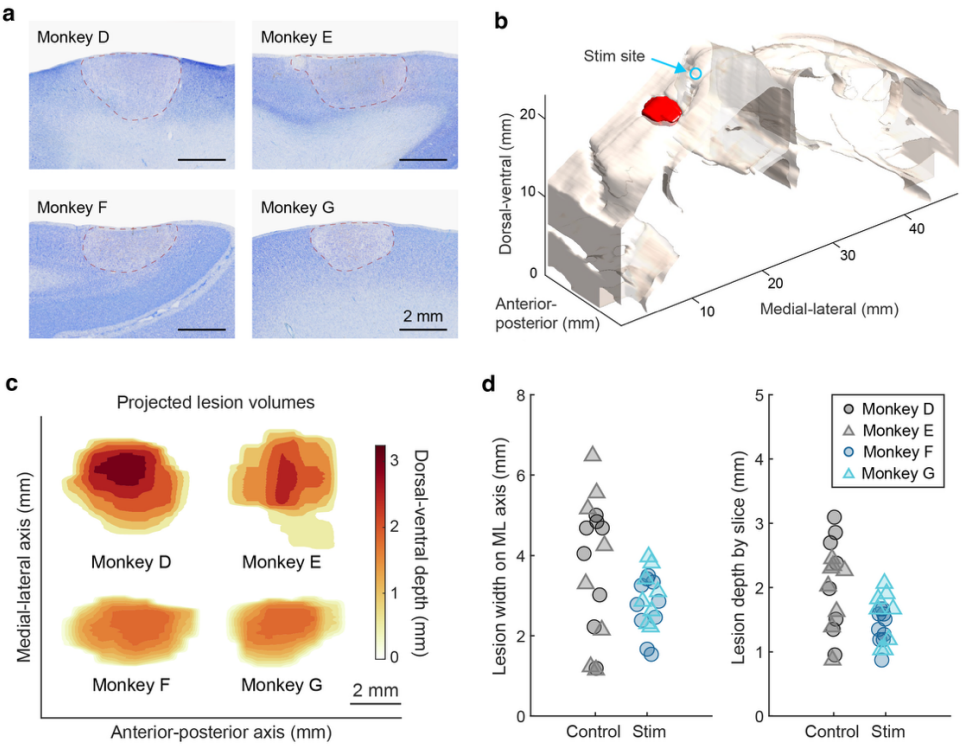

Fig. 2 | Histology analysis of ischemic damage and lesion size. **a,** Nissl-stained coronal slices from each animal, with lesion boundaries marked by dashed lines. Medial and lateral regions outside of the boundaries are considered perilesional (proximal to lesion) for all subsequent analysis. **b,** 3D reconstruction of the cortex and lesion (red) for monkey F. Blue arrow points to the location of stimulation electrode. **c,** Estimated lesion volume comparison projected along the dorsal-ventral axis, onto the anterior-posterior and medial-lateral (ML) axes. Color scale represents lesion depth from the cortical surface. Scale bar indicates 2 mm length on the x and y axes. **d,** Slice by slice comparison of lesion widths and depths for the control (monkeys D and E) and stimulated group (monkeys F and G).

Decrease of post-stroke neural activity by acute electrical stimulation

To further understand the physiological mechanisms underlying the reduced infarct volume as a result of acute electrical stimulation, we incorporated the histological results with the analysis of electrophysiology recordings by identifying the electrodes that overlapped with the reconstructed lesion. We registered the ECoG electrodes found to be within the anatomically defined lesion by overlaying the surgical image and the reconstructed cortex based on the location of and distance between sulci (**Fig. 3a**). After classifying the ipsilesional electrodes in each animal as either lesion or non-lesion, we computed the gamma band (30-59 Hz) signal power at each electrode, since gamma rhythms in the brain have been found to be correlated with neural activity levels and firing rate (Buzsáki & Wang, 2012; Yazdan-Shahmorad et al., 2013). By visualizing the gamma power changes on heatmaps (**Fig. 3b**), we found that in both control and stimulated monkeys, the lesion electrodes showed decreased gamma power as early as 10 minutes after ischemic lesioning, which persisted throughout the 3-hour recordings. This observation confirmed the location of ischemic injury and neuronal death caused by photothrombosis. In addition, we observed a gradual but large-scale downregulation of gamma power across the entire ipsilesional sensorimotor region in response to post-stroke stimulation for monkeys F and G in the stimulation group (**Fig. 3b,** bottom). This was distinctly different from the ECoG activity in control monkeys, as gamma power at some of the non-lesion electrodes was elevated above the baseline at around 90 minutes post lesioning (**Fig. 3b**, top), suggesting hyperactivation of perilesional areas due to focal ischemia. Similar trends can also be seen from the bar plots for each of the control and stimulated monkeys. Here, gamma power at non-lesion electrodes increased from 50 minutes to 90 minutes post-stroke in monkeys D and E (**Fig. 3c**). Meanwhile, for both stimulated monkeys, the perilesional gamma power at 70 to 110 minutes post stroke was significantly lower than their respective pre-stroke baseline (**Fig. 3c**, one-way ANOVA and Bonferroni corrections for multiple comparisons). Together, these results showed that gamma power was mildly suppressed across

the injured sensorimotor cortex as a result of continuous electrical stimulation, suggesting that stimulation delivered from 60 minutes after stroke may prevent excessive neuronal activation and energy depletion caused by the ischemic cascade, thus slowing the lesion progression and reducing neuronal death.

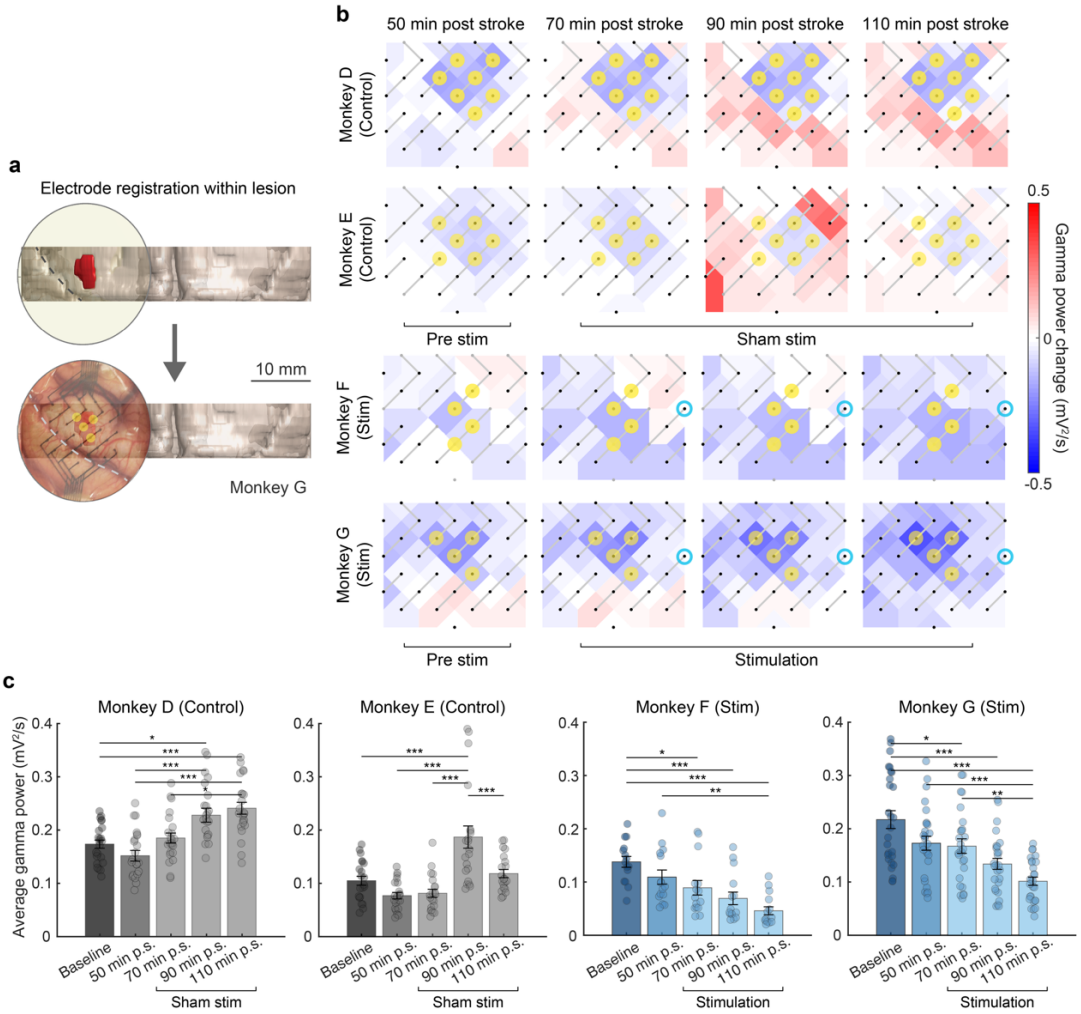

Fig. 3 | Electrophysiological analysis of the ipsilesional cortex after stroke and electrical stimulation. a, Electrode registration within histologically defined lesion using 3D reconstruction and surgery photos of monkey G. Yellow circles indicate lesion electrodes. **b,** Heatmaps of the changes in gamma ECoG power for two control (monkeys D, E) and two stimulated animals (monkeys F, G). Yellow circles indicate lesion electrodes. Blue circles indicate stimulation electrode. **c,** Summary and statistics for gamma ECoG power for non-lesion electrodes in each animal at different time points post stroke (p.s.). Gamma power increased significantly from baseline during sham stimulation periods in both control monkeys, but decreased continuously in both stimulated monkeys. (One-way ANOVA and Bonferroni corrections for multiple comparisons. ***P<0.001, **P<0.01, *P<0.05). Error bars represent mean ±standard error (SE).

Decrease of post-ischemia c-Fos activity due to acute stimulation

To investigate the downregulation of neural activity and its potential neuroprotective effects, we went back to histological tools and performed immunohistochemistry staining of c-Fos, a common cellular marker of neuronal activity. c-Fos is a protein derived from the immediate early gene *c-fos,* which gets transiently expressed in neurons quickly following depolarization in the cerebral cortex, and can be detected reliably using immunohistochemistry up to many hours after intense neuronal activation in primates (Barros et al., 2015; Herrera & Robertson, 1996). Meanwhile, it was also widely reported that c-Fos expression can be temporarily elevated following focal ischemic stroke as part of the injury response (Butler & Pennypacker, 2004; Uemura et al., 1991). Therefore, we applied antibodies against c-Fos protein on the ipsilesional cortex of control (monkey C, D) and stimulated animals (monkey F, G). Monkey E was excluded from all immunostaining procedures and subsequent analyses due to consistently poor immunoreactivity across the sensorimotor cortex, regardless of the antibody tested. These sections were also co-stained with antibodies against the neuronal nuclear marker NeuN to establish precise lesion boundaries and identify neurons for the subsequent analysis. For each animal, we stained 4 coronal sections proximal to the lesion and another 4 sections at areas distal to the lesion to compare perilesional c-Fos to that of a remote region on the same hemisphere. For each proximal section, two images were taken at the medial and lateral sides of the ischemic core (**Fig. 4a**, pink squares). And for each distal section, two images were taken at similar cortical depth (**Fig. 4a**, blue squares). We saw that in control monkeys, there were high levels of c-Fos expression immediately adjacent to the lesion boundary (**Fig. 4b,** top left). By contrast, we saw few neurons expressing c-Fos in stimulated monkeys proximal to the lesion (**Fig. 4b,** bottom left). Both control and stimulated monkeys had low levels of baseline c-Fos expression at distal regions (**Fig. 4b,** right). After calculating the percentage of NeuN-positive cells co-expressing c-Fos, we observed that control monkeys C and D showed significantly higher c-Fos expression in proximal regions compared to distal regions. However, this elevated c-Fos expression was not observed in the stimulated monkeys F and G (**Fig. 4c**, two-sample unpaired t-test). When combining results across animals, we found that the stimulated group exhibited significantly fewer c-Fos-positive neurons at the lesion boundary compared to the control group (**Fig. 4d**). These results suggest that electrical stimulation applied acutely after stroke reduced the intensity of neuronal depolarization and potentially prevented further cell death caused by overactivation of cortical neurons and excitotoxicity surrounding the ischemic core.

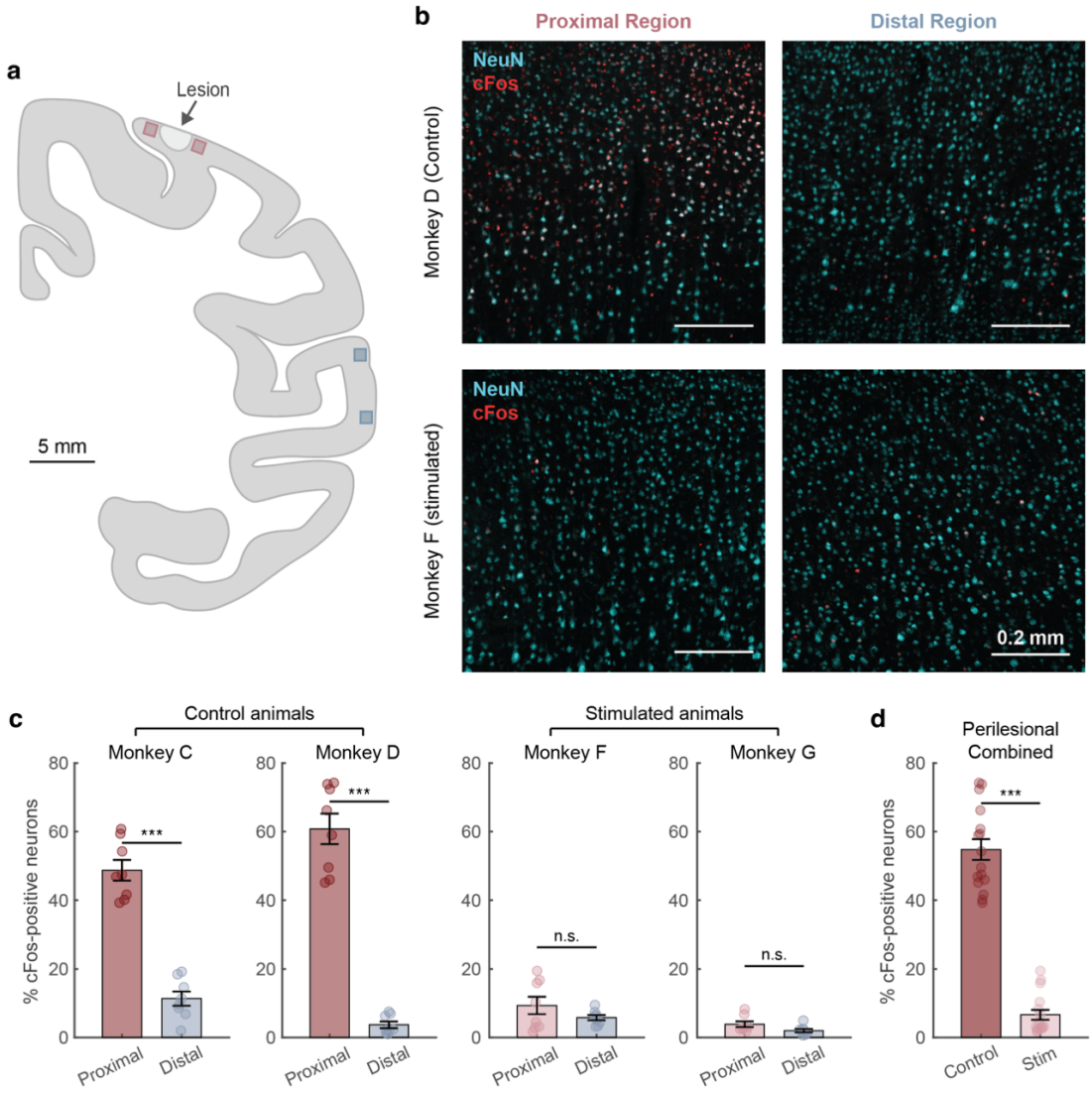

Fig. 4 | Immunohistochemistry analysis of c-Fos to quantify neuronal activation. a, Schematics of a coronal section illustrating confocal imaging locations at the proximal region in pink and distal region in blue. **b,** Representative images of c-Fos (red) and NeuN (cyan) co-staining from monkeys D and F at the proximal and distal regions respectively. **c,** Within-subject comparison of the percentage of neurons co-expressing c-Fos at the proximal versus distal regions. **d**, Between-subject comparison of c-Fos expression in neurons proximal to the lesion, for the control (monkeys C, D) and stimulation group (monkeys F, G). Significance was determined with a two-sample unpaired t-test (***P<0.001). Error bars represent mean ±SE.

Alleviating neuroinflammatory response through acute stimulation

To understand the role of electrical stimulation in reducing excitotoxicity and neuronal death caused by acute ischemic lesion, we evaluated the neuroinflammatory response surrounding the ischemic core by quantifying microglia activation and accumulation in the peri-infarct region.

Glial cells including microglia are known to play a significant role in the ischemic cascade and glutamate excitotoxicity (Belov Kirdajova et al., 2020). Therefore, we applied immunostaining against ionized calcium-binding adapter molecule 1 (Iba1), a widely used intracellular microglial marker (Jurga et al., 2020), on ipsilesional sections of the sensorimotor cortex. Again, these sections were co-stained for NeuN to define the lesion boundaries and select regions of interest (ROIs) for all subsequent image analysis. For monkeys C, D, F, and G respectively, we stained four coronal sections per animal with two proximal and another two distal to the lesion. For the proximal regions, we took four ROIs per section at the medial and lateral sides of the ischemic core (**Fig. 5a**). For the distal regions, we randomly sampled four ROIs per section at similar cortical depths. We observed stronger expression of Iba1 and greater number of Iba1-positive cells in proximal ROIs of the control animals (**Fig. 5b**). Notably, we saw a greater percentage of perilesional microglia with activated morphology in the controls, as characterized by larger cell body area and reduced ramification (**Fig. 5b**: white arrows). After comparing the binarized ROIs from the proximal versus distal regions in each animal, we found significantly greater levels of microglia activation at the lesion boundary only in control animals, reflected by greater percentage coverage of Iba1 staining (**Fig. 5c**: two-sample unpaired t-test, $P<0.001$). When combining results across animals, we found that the stimulated group had a significantly lower level of microglia activation compared to the control group at proximal regions (**Fig. 5d**). Through cell segmentation, we also found that microglia density was higher at proximal regions only in control monkeys (**Fig. 5e**), and the combined proximal microglia density was higher for the control group than for the stimulation group (**Fig. 5f**).

Combining these observations with the smaller lesion volumes, reduced c-Fos expression, and downregulated neural activity in animals receiving stimulation, our findings indicate that post-stroke electrical stimulation can alleviate the inflammatory response and excessive neuronal depolarization in the perilesional cortex, thus exerting neuroprotection by potentially reducing ischemia-induced excitotoxicity. Given this protective effect, cortical electrical stimulation warrants further investigation as a promising therapeutic intervention in the acute phase post-stroke to minimize the irreversible neuronal damage caused by the ischemic cascade.

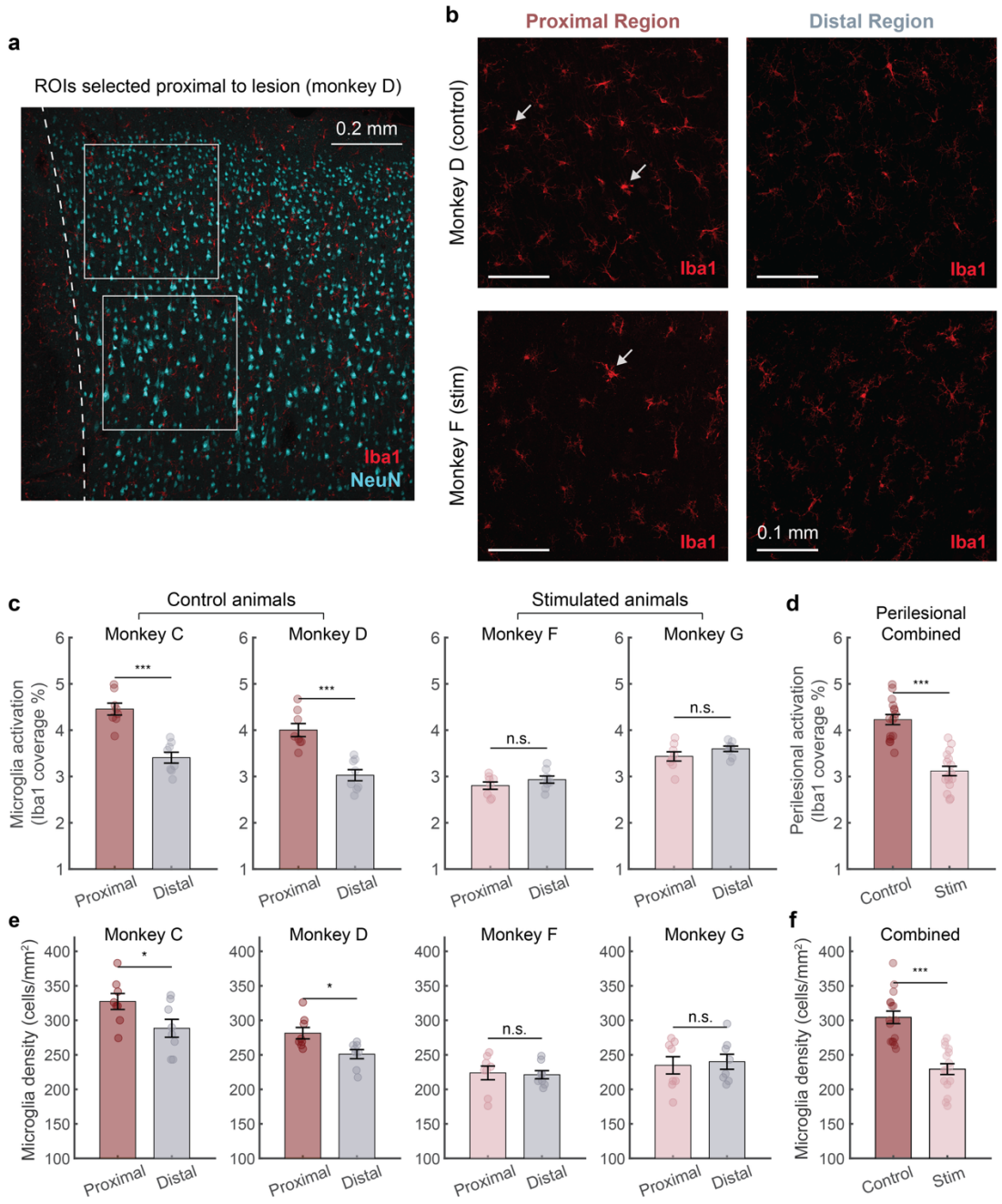

Fig. 5 | Immunohistochemistry analysis of Iba1 to quantify microglial response. a, Confocal image of a perilesional coronal section from monkey D stained for Iba1 (red) and NeuN (green). Dashed line represents the lesion boundary. White squares represent two sample ROIs used for subsequent analysis. **b,** Sample ROIs showing Iba1 immunoreactivity from one control and one stimulated monkey at the proximal and distal regions with respect to the lesion. White arrows point to examples of morphologically activated microglia. **c,** Within-subject analysis of microglia activation as measured by the percentage coverage of Iba1-positive pixels, at proximal versus distal regions for each animal. **d,** Between-subject comparison of perilesional microglia activation for the control (monkeys C and D) and stimulation group (monkeys F and G). Significance was determined with a two-sample unpaired

t-test (***P<0.001). Error bars denote mean ±SE. **e,** Within-subject analysis of microglia density as measured by the number of Iba1-positive cells per unit area, at proximal versus distal regions. **f,** Between-subject comparison of perilesional microglia density for the control (monkeys C and D) and stimulation (monkeys F and G) groups. Significance was determined with a two-sample unpaired t-test (*P<0.05, ***P<0.001). Error bars denote mean ±SE.

Discussion

In this study, we demonstrated potential neuroprotective effects of stimulation acutely following ischemic stroke by integrating advanced electrophysiology and histology techniques with an NHP stroke model. Our results suggest that early electrical stimulation decreases the extent of neuronal cell death by reducing peri-infarct depolarization and inflammation in the sensorimotor cortex of NHPs. These findings highlight the promise of electrical stimulation as a therapeutic strategy to protect the brain and minimize tissue damage during the acute window. Such an approach could play a pivotal role in addressing the global burden of stroke, given that infarct size significantly impacts not only patient mortality but also the functional outcomes of stroke rehabilitation strategies (Chen et al., 2000).

We utilized the photothrombotic method to produce focal ischemic lesions in NHPs. In comparison to other interventions for generating infarcts (J. Fan et al., 2017), our method is less surgically challenging and allows for more robust control of the location and size of infarcts across animals by implementing the same aperture, intensity, and duration of light illumination as demonstrated in our previous work (Khateeb et al., 2022). This technique enabled us to generate controlled focal lesions in the sensorimotor cortex of NHPs while simultaneously collecting ECoG recordings from the affected brain regions to monitor changes in neural activity, making it a valuable and reproducible model for studying acute stroke pathophysiology and evaluating neuroprotective interventions in a large-brain system. Importantly, cortical infarcts are commonly observed in several clinical subtypes of ischemic stroke, including cardioembolic events and large-artery atherosclerosis involving distal vessels, both of which are frequently associated with significant neurological deficits such as aphasia (Adams et al., 1993). Multiple studies report that 30 to 50% of stroke patients experience cortical damage, and that approximately 15% of the overall stroke population present with cortical-only lesions (Corbetta et al., 2015; Kang et al., 2003; Wessels et al., 2006), highlighting the cortex as a critical therapeutic target for acute intervention. Moreover, even in strokes that primarily affect deeper brain regions such as the white

matter, cortical function can still be impacted due to axonal injury (Hinman et al., 2013), network disconnection (Thiebaut de Schotten et al., 2014), secondary neuronal degeneration and apoptosis (Duering et al., 2012). Electrophysiology studies in humans have also shown that both cortical and subcortical stroke can lead to hyperexcitability of the ipsilesional cortex during the acute window (Harquel et al., 2024; Huynh et al., 2016), which may contribute to spreading depolarization, injury progression, or even seizure activity (Fabricius et al., 2008). Therefore, by suppressing cortical overactivation early during acute ischemia, our stimulation paradigm offers a targeted strategy to limit neural damage across a broad range of clinical stroke subtypes. Beyond stroke, this novel intervention also holds promise for other neurological conditions characterized by cortical hyperexcitability and continuous depolarization, including traumatic brain injury (Tehse & Taghibiglou, 2019), underscoring the broader therapeutic relevance and translational potential of our findings.

Mechanisms of stimulation-induced neuroprotection

An hour following stroke induction, we applied repeated electrical stimulation directly adjacent to the lesion on the ipsilesional cortex. The stimulation train contains 5 Hz bursts of biphasic pulses, similar to the theta burst stimulation (TBS) pattern of transcranial magnetic stimulation (TMS) protocols that are widely adopted in the clinic (Chung et al., 2016). However, one major difference is that our stimulation paradigm used five pulses at 1 kHz in contrast to the three 50-100 Hz pulses per burst used in traditional TBS protocol. Stimulation via high frequency pulses at greater than around 200 Hz has been shown to have an inhibitory effect on neuronal firing rates (Beurrier et al., 2001; Yazdan-Shahmorad, Kipke, et al., 2011). While there are many possible mechanisms of action underlying this inhibitory effect, it is likely that these high frequency pulses contribute to recurrent hyperpolarization (Garcia et al., 2005), or generate a transient reduction of excitatory currents in the stimulated neurons, thereby decreasing the excitability and firing rates of postsynaptic cells (Beurrier et al., 2001). Given that our ECoG recordings showed decreasing gamma power during and after stimulation, and that gamma activity in ECoG has been shown to correlate with neuronal firing (Yazdan-Shahmorad et al., 2013), it is likely that applying theta bursts of electrical stimulation on the cortex suppressed peri-infarct neural activity and network excitability through similar mechanisms. It is important to note that high-frequency band power reflects synchronized firing of neuronal populations and has been associated with both synaptic activity (Viswanathan & Freeman, 2007) and action potential generation (Ray et al., 2008). Therefore, the observed reduction in gamma power likely reflects a global suppression of neuronal

output, encompassing both somatic and axonal effects. Moreover, postsynaptic excitability has been shown to play a major role in excitotoxic cell damage after ischemia (Y. Fan et al., 2008; F. Wang et al., 2022), which may explain the protective effect of our inhibitory stimulation paradigm.

Importantly, the observed decrease in c-Fos immunoreactivity in stimulated monkeys suggests that the downregulation of ECoG activity is not a manifestation of the harmful cortical spreading depression, given that an increase in c-Fos expression has been shown to correlate with sustained depolarizations and the subsequent spreading depression in the presence of focal ischemia (Hermann et al., 2001). Furthermore, both *c-fos* mRNA and c-Fos protein expression have been reported as reliable markers for glutamate toxicity, correlating with excitotoxic cell death in cultured neurons (Fernandez et al., 2005; Rogers et al., 2004). These works and the lack of c-Fos positive neurons we found in stimulated animals support our hypothesis that electrical stimulation reduces peri-infarct excitotoxicity, likely through the suppression of neuronal hyperexcitability. Combined with the reduction in lesion size and the electrophysiology results discussed above, our findings provide evidence that electrical stimulation applied one hour after stroke onset produced an inhibitory and neuroprotective effect, without exacerbating tissue damage attributed to spreading depolarization as previously described for early sensory stimulation (von Bornstädt et al., 2015), making this stimulation protocol a safe and promising treatment option for acute ischemic stroke.

To better understand the cellular response to electrical stimulation, we analyzed Iba1 immunoreactivity to assess microglia-mediated neuroinflammation in the perilesional tissues. Since the microglial response during acute stroke involves both cell migration to the infarct and morphological activation through cell body enlargement and process thickening (Yenari et al., 2010), we used two common measures to quantify inflammation: percent area of Iba1 immunoreactivity and Iba1-positive cell density, accounting for both microglia accumulation and activation within a given region (Fox et al., 2020). Based on these measures, the lack of significant microglial response near the lesion boundary in stimulated monkeys suggest that electrical stimulation was able to mitigate neuroinflammation for tissues undergoing the acute ischemic cascade. Given the important role of activated microglia in detecting and propagating the ischemia-induced excitotoxicity (Belov Kirdajova et al., 2020; Yenari et al., 2010), the decreased microglial activation in stimulated tissues may suggest an attenuation of excitotoxic injury as a result of our acute intervention. Nevertheless, additional experiments are essential to further

investigate the interplay between microglial response and other components of the ischemic cascade, such as glutamate signaling and oxidative stress following ischemia and stimulation, to establish the precise mechanisms through which acute stimulation induces neuroprotection.

Together, the reduced c-Fos activity and microglial response near the lesion boundary in stimulated monkeys suggest that electrical stimulation was able to mitigate both cortical depolarization and neuroinflammation for tissues undergoing the acute ischemic cascade, leading to reduced neural damage. These findings are consistent with prior studies in rodents, where cortical stimulation via bipolar electrodes (Baba et al., 2009; L.-C. Wang et al., 2021) and cathodal transcranial direct current stimulation (C-tDCS) (Notturno et al., 2014; Peruzzotti-Jametti et al., 2013) were shown to decrease tissue damage by inhibiting peri-infarct excitability, neuroinflammation, and apoptosis during acute stroke. Furthermore, Our findings also align with the hypothesized neuroprotective mechanisms of many pharmacological agents designed for acute ischemic stroke, which aim at attenuating excitotoxicity due to energy depletion by inhibiting neuronal excitability (Chamorro et al., 2016; Cheng et al., 2004; A. R. Green et al., 2000; F. Wang et al., 2022). Compared to pharmacological treatments, electrical stimulation may offer distinct advantages, particularly for patients who experience severe side effects or allergic reactions to these medications. Future studies could extend the post-stimulation monitoring to determine the optimal dose and duration for stimulation while minimizing potential side effects.

Comparison with alternative brain stimulation techniques towards clinical translation

To understand the spatial distribution of our stimulation effects and compare it with other widely adopted neuromodulation techniques, we simulated the electric field in the underlying cortical tissues. The simulation results suggest that the small electrode size (0.25 mm diameter) and current amplitude (60 μA) in our protocol generated a highly localized electric field (**Fig. 6**), starting at approximately 50 mV/mm directly beneath the electrode and decreasing rapidly to 1 mV/mm near the lesion boundary (~3 mm^2 cortical area stimulated at above ~10mV/mm). Although this field strength and spatial distribution are substantially smaller than those typically used in TMS therapies at motor threshold (~30 cm^2 cortical area stimulated at ~60 to 100 mV/mm) (Numssen et al., 2024; Thielscher & Kammer, 2004), our perilesional stimulation is specifically designed to modulate cortical excitability without inducing widespread neuronal depolarization. Additionally, the observed cellular response also extended beyond the immediate stimulation site, affecting regions as far as the lateral side of the ischemic lesion, as suggested by the changes in ECoG

activity and c-Fos expression. This broader physiological effect is likely attributed to the dense cortical connections that facilitate large-scale excitability changes. This explanation is supported by the extensive studies on intracortical microstimulation (ICMS), where electrodes delivering the stimulation current have a much smaller surface area (Deliano et al., 2009; Kim et al., 2015; Logothetis et al., 2010). For instance, stimulating the thalamic region in NHPs with a microelectrode at similar current amplitudes has been shown to suppress neural activity in its visual cortex projection, likely through synaptic inhibition mechanisms (Logothetis et al., 2010). These studies suggest that even highly localized current source can produce widespread neural effects, supporting the large-scale inhibitory modulation observed with our ECoG stimulation paradigm. Future studies should investigate whether this neuroprotective effect arises specifically from localized stimulation or can also be achieved using more global neuromodulation techniques, thereby facilitating the clinical translation of our findings.

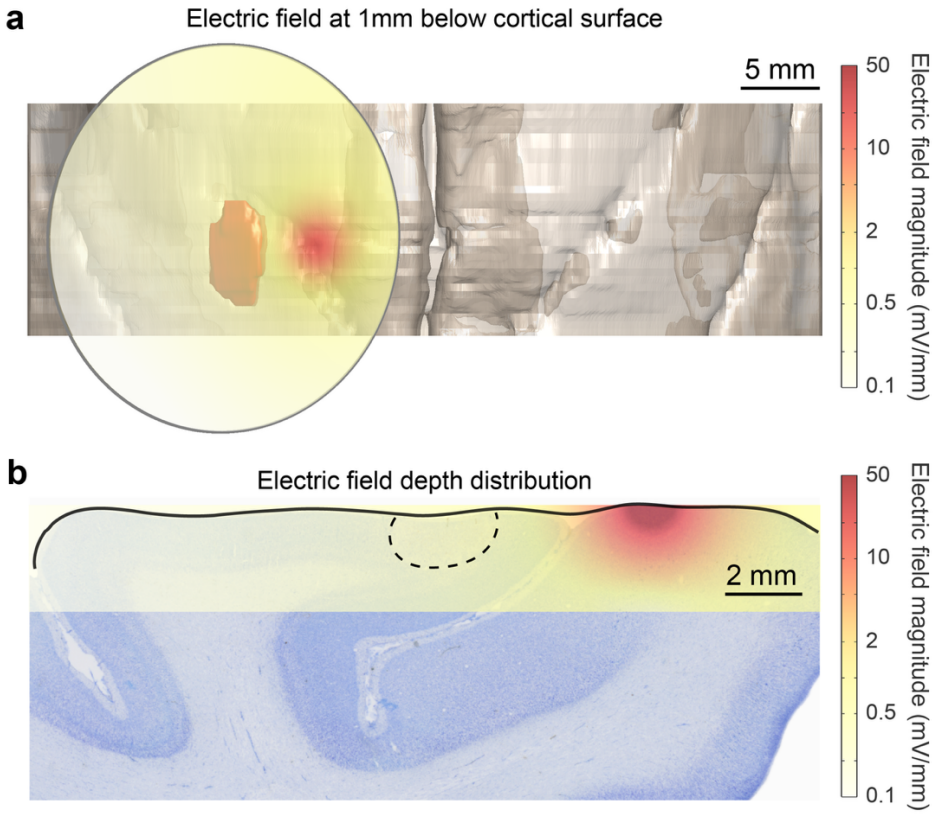

Fig 6. Electric field simulation on the ipsilesional cranial window. **a,** Top view of the 3D cortical reconstruction overlayed with a horizontal slice of the simulated electric field strength, at 1 mm below the cortical surface. **b,** Nissl stained ipsilesional section of monkey F, overlayed with a vertical slice of the simulated electric field (going through the center of stimulation electrode). Dashed line indicates lesion boundary. Black curve represents cortical surface. Color scale is the electric norm in logarithmic scale.

While our electrical stimulation approach requires access to the cortical surface, similar neuromodulatory effects could potentially be achieved noninvasively using existing technologies. For example, a range of TMS paradigms, including the intermittent theta-burst stimulation (iTBS) protocol recently approved by the FDA (Cole et al., 2022), have demonstrated clinical efficacy in treating neurological disorders affecting various brain regions. These findings highlight the potential to develop new TMS paradigms that replicate the electric field distribution and stimulation-induced effects in our current study, paving the way for next-generation therapies targeting acute stroke. On the other hand, existing TMS protocols with reported inhibitory effects can be reevaluated in acute stroke settings to test whether the neuroprotective outcomes are reproduced. For instance, continuous TBS (cTBS) has been shown to reduce cortical excitability in humans by inducing synaptic depression (Huang et al., 2005, 2011; Stagg et al., 2009). Recent clinical trials also showed that suppressing the contralesional neural activity with cTBS improved motor recovery in chronic stroke patients (Vink et al., 2023), highlighting its safety and relevance as a therapeutic option for acute stroke. In addition to various TMS paradigms, tDCS also represents a promising noninvasive alternative, which generates sub-threshold cortical electric field (~ 1 mV/mm) while retaining the ability to modulate neuronal spiking over large cortical areas (Vöröslakos et al., 2018). Various tDCS protocols have already been tested in rodents for acute neuroprotection (Notturno et al., 2014) and in humans for stroke rehabilitation (Solomons & Shanmugasundaram, 2019), demonstrating their strong translational potential for use in acute settings to mitigate inflammation and protect the brain following ischemia.

Limitations

For lesion volume estimation and electrophysiology analysis, we compared results from control monkeys D and E to stimulated monkeys F and G, all of which were lesioned using identical illumination parameters known to produce predictable infarct sizes (Khateeb et al., 2022). However, for immunohistochemistry (IHC) analysis of biomarkers such as NeuN, control monkey E exhibited poor immunofluorescence signals over the sensorimotor cortex. Despite this, Nissl staining revealed consistent cell density and a clear lesion boundary, suggesting that the lack of immunoreactivity was likely due to perfusion fixation issues or subsequent tissue handling steps prior to immunostaining. For example, it has been shown that perfusing the injured brain with fixatives could lead to incomplete and asymmetrical fixation, thus decreasing the immunoreactivity in affected tissues (McFadden et al., 2019). Unlike NeuN staining, Nissl staining

is less susceptible to such perfusion issues, as the dye binds directly to nucleic acids within cells, making it more robust across different fixation and processing conditions (Gittins & Harrison, 2004; Lindroos & Leinonen, 1983). To address this staining challenge, we added monkey C as an additional control and excluded monkey E from all IHC analysis.

It should also be noted that photothrombotic infarcts do not capture all aspects of acute stroke in humans. For example, this technique generates narrow penumbras and is largely constrained to the cortical layers, thereby excluding stroke subtypes that primarily involve subcortical or white matter lesions (Sommer, 2017). Nevertheless, for stroke patients with infarcts that extend into the white matter, suppressing cortical depolarization with our stimulation paradigm could still mitigate the ischemia-induced ionic imbalance and high extracellular glutamate, potentially preventing them from propagating into the affected white matter and thus reducing the excitotoxic damage of oligodendrocytes and myelin (Matute et al., 2013). Meanwhile, in cases involving deep white matter stroke, noninvasive methods like TMS may be preferable due to their ability to generate electric fields that reach greater depths and volumes (Laakso et al., 2018), potentially preventing oligodendrocyte excitotoxicity and subsequent cell death that are central to ischemic white matter injury (Matute et al., 2007). Future research should explore how stimulation-induced effects vary with infarct size and location, focusing on optimizing parameters such as stimulation strength and duration to improve outcomes for larger and deeper infarcts. Such efforts will validate the generalizability of our findings and tailor interventions to patients with varying injury severities.

While our study was limited by a small number of monkeys in both the control and stimulation groups, it is important to recognize the inherent challenges associated with conducting stroke research involving NHPs, particularly those suitable for combined electrophysiology and histology analysis. These NHPs are highly valuable but scarce resources due to ethical and logistical considerations, thus constraining our sample size. Despite this limitation, the unique technology and promising results from this study not only provide valuable insights into the effects of acute stimulation on ischemic damage, but also open many exciting opportunities for future investigation regarding acute stroke intervention in large-brain models. In particular, applying the lesioning toolbox and electrical stimulation to monkeys chronically implanted with our multi-modal interface (D. J. Griggs et al., 2021a) can allow us to study the impact of stimulation well beyond the acute window. Combined with the sensorimotor behavioral capabilities of NHPs, these experiments will deepen our understanding of the mechanisms underlying stimulation-

induced neuroprotection and its effect on functional recovery from days to months after stroke onset. More importantly, investigating the chronic effect of localized electrical stimulation using a reproducible lesioning toolbox in NHPs, which closely resemble human brain anatomy and immune response, can help bridge the gaps between rodent and human studies that have hindered the success of past clinical trials on neuroprotective therapy (Cook & Tymianski, 2011; Shi et al., 2018; Tajiri et al., 2013).

Materials and Methods

Animals subjects and surgical procedures. All animal procedures were approved by the University of Washington Institutional Animal Care and Use Committee and were in accordance with the National Research Council's Guide for the Care and Use of Laboratory Animals. All our animals were housed and maintained at the Washington National Primate Research Center (WaNPRC) accredited by the American Association for Assessment of Laboratory Animal Care (AAALAC). This study used five adult macaques (Control group: monkey C - *Macaca mulatta*, 10.3 kg, 16 years, female; monkey D - *Macaca nemestrina*, 12.8 kg, 14 years, female; monkey E - *Macaca nemestrina*, 13.10 kg, 14 years, female; Stimulation group: monkey F - *Macaca nemestrina*, 13.8 kg, 14 years, female; monkey G - *Macaca nemestrina*, 14.6 kg, 7 years, male) that were part of the Tissue Distribution Program (TDP) at the WaNPRC, which aims to conserve and fully utilize the NHPs no longer needed for other experiments.

Surgical procedures and induction of ischemic lesions. Using standard aseptic technique, the five macaques (monkeys C, D, E, F, G) were anesthetized with isoflurane and placed in a stereotaxic frame. The animals' temperature, oxygen saturation, heart rate, electrocardiographic responses were monitored throughout the procedure. Bilateral craniotomies and durotomies (25 mm diameter) were performed using stereotaxic coordinates that target the sensorimotor cortices (Paxinos et al., 2009). To protect the exposed brain, a transparent silicone artificial dura (monkey C) or a semi-transparent multi-modal artificial dura (monkey D to G) fabricated using previously described methods (D. J. Griggs et al., 2019, 2021b) was implanted bilaterally on top of the sensorimotor cortex, offering optical and electrical access during subsequent procedures. For animals in both the control (monkeys C, D, E) and stimulation groups (monkeys F, G), we induced ischemic lesions using the photothrombotic technique (Khateeb et al., 2022), which

produces focal infarcts by photo-activation of a light-sensitive dye (Rose Bengal). Upon illumination, the intravenously administered dye produced singlet oxygen that damaged endothelial cell membranes, causing platelet aggregation and interrupting local blood flow. To control the infarct size and location, we placed an opaque silicone mask on top of the artificial dura. In monkey C, the mask contains circular apertures of different diameters (0.5, 1.0, and 2.0 mm) to induce control lesions in various sizes. In monkey D to G, the mask has a single aperture located in the center (diameter 1.5 mm) and was placed on one hemisphere (monkeys D, F, and G: left hemisphere; monkey E: right hemisphere). After the mask was in place, each animal was injected with Rose Bengal (20mg/kg) for 5 minutes as we started illuminating the ipsilesional cranial window for 30 minutes through the aperture using an uncollimated white light source.

Histology, lesion reconstruction and size estimation. At around 4 hours after the stroke was induced, animals were deeply sedated and transcardially perfused with phosphate buffered saline (PBS) followed by 4% paraformaldehyde (PFA). The brains were harvested and post-fixed by immersion in 4% PFA for 24 to 48 hours. A coronal block containing the lesioned region was dissected using a custom matrix and then stored at 4 °C in 30% sucrose in PBS. To prepare for staining, the block was frozen and sectioned into 50 µm thick coronal sections using a sliding microtome (Leica). Sliced sections were stored at 4 °C in PBS with 0.02% sodium azide. To evaluate the extent of ischemic damage and neuronal death, we mounted a rostrocaudal series of coronal sections with approximately 0.45 mm separation and then performed Nissl staining on the mounted sections using Thionin acetate. Nissl-stained sections were scanned and registered using a custom software in MATLAB (2019b, MathWorks) for alignment and three-dimensional reconstruction. The registered images were smoothed and binarized so that lesion boundaries on each slice can be identified and visualized within the reconstructed cortex. A more detailed description of the lesion edge detection and reconstruction method can be found in our previous publication (Khateeb et al., 2022). The widths and depths of each lesion within the representative coronal sections were also calculated based on the detected boundary and image resolution. Linear interpolation was used between sections to estimate the lesion volume in each animal. To combine histological information on the ischemic injury with electrophysiology recordings, we overlayed the surgical image taken for each animal on top of its reconstructed cortex based on the location of sulci and other distinct anatomical features. The overlayed images allowed us to register the ECoG electrodes that fell within the estimated lesion area, and classify them into lesion and non-lesion groups for the subsequent electrophysiology analysis.

Electrophysiology recording and electrical stimulation. All electrophysiology recordings and electrical stimulation were performed with Grapevine Nomad processors, four Nano front ends (Ripple Neuro, Salt Lake City, UT), and our customized large-scale multi-modal interface. The design and characterization of this interface with 32 embedded ECoG electrodes can be found in our previous work(D. J. Griggs et al., 2019, 2021b). A skull screw close to the midline and anterior to the ipsilesional cranial window was used as an electrical ground for subsequent recordings. All animals were transitioned from isoflurane to urethane anesthesia prior to ECoG recordings and stayed on urethane until the end of the experiment to allow reliable monitoring of neural activity. In control monkeys D and E, we collected ECoG data bilaterally at 30 kHz sampling frequency, including 30 minutes of baseline before photothrombotic lesioning, 30 minutes during illumination, and up to 3 hours post lesioning to monitor the extent of neuronal damage and network dynamics around the injury site. In stimulated monkeys F and G, we followed the same recording timeline for baseline and illumination periods, and recorded spontaneous neural activity for 1 hour after lesioning. We then applied electrical stimulation through a single ECoG electrode (0.25 mm diameter) approximately 8 mm medial to the lesion center on the ipsilesional (left) hemisphere. We delivered the stimulation trains in 6 blocks lasting 10 minutes each, with 2-minute recordings of spontaneous activity in between the blocks to track changes in neurophysiology as stimulation continued. The stimulation trains had a 5 Hz burst frequency and 5 biphasic charge-balanced pulses at 1 kHz within each burst. The stimulation amplitude was 60 μA and pulse width was 200 μs per phase with 50 μs inter-phase interval.

Electrophysiology data analysis. ECoG signal power calculation was conducted in MATLAB (R2022b, MathWorks). After down-sampling the signal from 30 kHz to 1 kHz, the signals were notch filtered at 60, 120, and 180 Hz. Channels with a power spectral density that did not exhibit the expected curve were excluded from further analysis (1 channel was excluded for monkeys D and G, 2 channels for monkey E, and 14 channels for monkey F). We then filtered the down-sampled signals into the gamma frequency band (30-59 Hz), and split them into two-minute blocks separated by ten minutes across the pre-stroke baseline, post-stroke, and post-stimulation recording periods. We calculated the average signal power of each channel for each two-minute window by squaring the filtered signal and dividing by the elapsed time. To compare power across each two-minute time window, we conducted paired two-sided t-tests with Bonferroni corrections for multiple comparisons (family-wise error rate of 0.05). Pairwise

comparisons of power distributions were only made between baseline and each subsequent two-minute window and between 50 min post-stroke and each subsequent two-minute window following stimulation.

Immunohistochemistry. To evaluate the neuronal activation and neuroinflammatory response near the ischemic lesion, we performed immunostaining with antibodies against c-Fos protein and the microglia/macrophage-specific calcium-binding protein Iba1 respectively. Coronal sections around the lesion in monkeys C, D, F, and G were co-stained with either neuronal nuclear protein NeuN and c-Fos or NeuN and Iba1. Monkey E was excluded for all immunohistochemistry analysis due to lack of immunoreactivity at the cranial window. To replace monkey E, we used tissues from monkey C as an additional control. For this animal, we specifically selected coronal sections containing a single lesion comparable in size to those observed in monkeys D to G. To prepare tissues for staining, coronal sections were first rinsed in 1x PBS and incubated in 1% $NaBH_4$ solution for 1 hour to reduce background autofluorescence, after which they were washed with PBS and incubated in normal donkey serum (NDS) blocking solution (10% NDS and 0.1% triton-X100 in PBS) overnight at 4°C. Sections were then incubated in primary antibodies including either rabbit anti-c-Fos (Abcam ab190289, 1:500 dilution) or goat anti-Iba1 (Abcam ab5076, 1:1000 dilution) plus mouse anti-NeuN (Millipore Sigma MAB377, 1:500 dilution) in NDS blocking solution at 4°C for ~72 hours. Sections were then rinsed in PBS and incubated in secondary antibody mixtures containing either donkey anti-rabbit antibody (Invitrogen #A10042, 1:500 dilution) or donkey anti-goat antibody (Invitrogen #A-11057, 1:500 dilution) conjugated with Alexa Fluor 568, plus donkey anti-mouse antibody conjugated with Alexa Fluor 488 (Invitrogen # A-21202, 1:500 dilution) and DAPI at 4°C overnight. This was followed by rinsing sections in PBS for 5 times and incubating in 1:1 Glycerol-PBS solution for 10 minutes. Sections were mounted onto slides using DABCO mounting media and later imaged using a Nikon A1R HD25 laser scanning confocal microscope.

c-Fos and microglia activation analysis. To estimate the level of c-Fos expression within neurons, we performed NeuN and c-Fos co-staining on four proximal tissue sections per animal, collected from regions adjacent to the lesion. For each of these proximal sections, we acquired two confocal images (Nikon A1R, 20x objective) on either side of the lesion boundary. Additionally, we stained another four sections distal to the lesion (at least 20 mm away) within the same hemisphere, and randomly sampled two regions of interest (ROIs) per section. Custom algorithms

in MATLAB were then used for image analysis, including binarization with adaptive thresholding and image segmentation, applied separately to the NeuN channel (green) and c-Fos channel (red). Neuronal c-Fos expression in each ROI was quantified by calculating the percentage of NeuN-positive cells that co-expressed the c-Fos protein.

To evaluate the level of microglial reactivity, we stained 2 sections per animal proximal to the lesion. For each section, we imaged 4 ROIs within 1mm from the lesion boundary using a 20x objective through the Nikon A1R laser scanning confocal microscope. For each ROI we took z-stack images with 20 μm thickness and created a maximum intensity projection. The projections were converted to 8-bit and inverted so that dark pixels represent Iba1 signals. We then used ImageJ to denoise each ROI by subtracting the background and removing pixel intensity outliers. The ROIs were converted to binary by setting the threshold to one standard deviation below the average pixel intensity and filtering out objects below 150 pixels in size. The percentage area covered by dark pixels, a widely used Iba1 reactivity measure(Fox et al., 2020; T. R. F. Green et al., 2022), was then calculated to estimate the microglia activation level. To quantify microglial density, we used the same binarized images and counted the number of segmented cells in each ROI to estimate the average microglia density at the lesion boundary for each animal. Similar imaging and quantification steps were performed for regions distal to the lesion on the same hemisphere of each animal (4 ROIs per section) to compare microglial density and activation within each of the control and stimulated monkeys.

Electric field stimulation. To estimate the strength of the electric field at the perilesional region, quasi-static simulation was performed using COMSOL Multiphysics in a cylindrical volume that represents the cortical tissue directly below the ipsilesional cranial window. The following parameters and assumptions were used for the simulation, with conductivity values taken from previous literature(Jiang et al., 2020; Wagner et al., 2004). Radius of the cylindrical volume: 12.5 mm; pia conductivity: 0.15 S/m; pia depth: 20 μm; grey matter conductivity: 0.28 S/m; grey matter depth: 3 mm. Surface electrode diameter: 0.25 mm; electrode location: 8 mm medial to the craniotomy center; terminal current from the electrode: 60 μA. In addition, as we performed monopolar stimulation with a distant ground (skull screw located ~20mm anterior of the cranial window close to the midline), the anterior boundary of the top cortical surface was selected as our electric current ground when running the simulation. We modeled the pia mater only on the exposed cortical surface and assumed a homogeneous conductivity for the underlying grey

matter. Pia in the deep sulcus was not segmented due to the variability across animals and its much thinner structure relative to the surrounding grey matter. As the pia has a lower conductivity than grey matter, its omission in the sulcus may overestimate the predicted electric field at the lesion boundary. However, the resulting values are expected to remain within the same magnitude range and thus do not meaningfully alter the interpretation of the simulation results.

Statistics and reproducibility. A total of five monkeys were used in this study, with three animals assigned to the control group (monkeys C, D, E) and two to the stimulation group (monkeys F and G). Given the limited number of animals and the challenge of NHP research, statistical tests were performed within each individual animal. Because of this, the experiments were not randomized, and the investigators were not blinded to group allocation during data collection and analysis. For Nissl-stained tissues, lesion volume estimates were derived from serial coronal slices and their 3D reconstructions. No statistical comparisons were conducted on the Nissl-stained sections or lesion volumes. For immunohistochemistry analysis, proximal and distal regions were compared within each monkey using $n=8$ ROIs per region and two-sided unpaired t-test. Similar results were independently observed across both animals in the control and stimulation groups. The only histological data excluded was the immunohistochemistry sections from monkey E as discussed above. For neurophysiology data, electrodes with abnormal spectral characteristics were excluded from the power analysis. Perilesional ECoG signal power was compared across different time points after stroke using one-way ANOVA with Bonferroni correction for multiple comparisons, with sample size determined by the number of non-lesion electrodes. All electrophysiological and histological findings were independently reproduced in both animals from the control and stimulation groups.

Acknowledgement

We thank Toni Haun, Devon J. Griggs, Christopher English, Britni Curtis, and Sandi Thelen for their help with animal care, experimental preparation, and assistance during surgeries. We also thank Aryaman Gala and Mona Rahimi for their help with histological procedures and preliminary analysis of the Nissl slices. We also thank Drs. Jialing Liu, Chet Moritz, Yukio Nishimura, and Eberhard Fetz for their guidance on the interpretation of our data and their insights on the clinical relevance of our findings.

Funding. J.Z. discloses support for the research described in this study from the National Institute of Neurological Disorders and Stroke of the National Institute of Health [NIH 1R01NS119395] and the Weill Neurohub. K.K. discloses support for the research described in this study from the National Science Foundation Graduate Research Fellowships Program [NSF-GRFP]. A.Y. discloses support for the publication of this study from the National Institute of Neurological Disorders and Stroke of the National Institute of Health [NIH 1R01NS119395], the Washington National Primate Research Center funded by NIH [WaNPRC: NIH P51 OD010425], the American Heart Association, and the Washington Research Foundation.

Data and Code availability. All data supporting the findings of this study are included within the article and the Supplementary Information. All custom MATLAB codes and scripts for electrophysiology signal processing, immunohistochemistry image analysis, and figure generation are available at: https://github.com/jzhou33/stroke_estim.

Chapter 3: Large-Scale Cortical Connectivity Changes Induced by Targeted Optogenetic Modulation in Non-Human Primates

Jasmine Zhou[1,2], Karam Khateeb[1,2], Tiphaine Belloir[2], Azadeh Yazdan-Shahmorad[1,2,3]

[1]Department of Bioengineering, University of Washington, Seattle, WA

[2]Washington National Primate Research Center, Seattle, WA

[3]Department of Electrical & Computer Engineering, University of Washington, Seattle, WA

Abstract

Numerous neurological disorders originate from aberrant neural dynamics and connectivity within the brain. Leveraging the brain's inherent plasticity, targeted neuromodulation techniques can be developed to reorganize specific connections, thus serving as therapies for various brain disorders. Among these techniques, optogenetic tools enable spatiotemporally precise modulation by allowing rapid excitation or inhibition of selected neuronal groups with light. While both single-site and paired optogenetic stimulation can enhance functional connectivity within the brain, it remains unclear whether these tools can also disrupt connections and dissociate specific locations from the broader network. To address this gap, we examined network-level changes following optogenetic inhibition in the posterior parietal cortex (PPC) of two monkeys using a multimodal neural interface. After virally infusing the PPC with a red-shifted inhibitory opsin (Jaws), we delivered 5 blocks of 10-minute, single-site, 5 Hz 638 nm laser illumination at selected locations over the PPC. To monitor the neural dynamics in response to light modulation, we recorded electrocorticography signals before, during, and after each inhibition block. Pairwise coherence between electrodes were computed to estimate the changes in functional connectivity. We found that when targeting locations with strong Jaws expression and significant light-evoked neural response, gamma coherence between the illuminated site and the whole network gradually decreased after each inhibition block. Conversely, no significant changes in gamma coherence were observed during no-stim control sessions or when targeting regions without distinct opsin expression. These findings demonstrate that focal optogenetic inhibition can functionally decouple specific cortical sites, complementing our prior study showing that excitatory optogenetic stimulation selectively enhances sensorimotor connections, thus highlighting the potential of optogenetic intervention to achieve bidirectional modulation of network connectivity.

Introduction

Neurological disorders often arise from a complex interplay of dysfunctional neural circuits and aberrant connections between neuronal populations. Since brain-wide network dynamics and functional connectivity are pivotal in supporting our cognitive and sensorimotor functions, their disruption can lead to a wide variety of pathological conditions that include stroke-related functional impairment (Grefkes & Fink, 2011; Westlake & Nagarajan, 2011) and psychiatric disorders such as schizophrenia (Camchong et al., 2011; Skudlarski et al., 2010; Venkataraman et al., 2012). As a result, the ability to selectively modulate specific neural circuits and connections can provide significant therapeutic benefits in treating these neurological disorders and helping patients regain normal functions (Rowe, 2010).

Recently, novel neuromodulation paradigms have been developed in both preclinical and clinical studies, leveraging the brain's inherent plasticity to modify dysfunctional pathways and restore healthy connectivity patterns (Edwardson et al., 2013; Moorjani et al., 2022; Ruggiero et al., 2021). While many of these techniques rely on electrical stimulation, they often lack the spatial and cell-type specificity needed to precisely target defined neural populations. In contrast, optogenetics has emerged as a powerful tool for manipulating brain activity with spatiotemporal precision and minimal recording artifacts, enabling causal investigations of circuit dynamics (Boyden et al., 2005). This technique, well-established in both rodent and non-human primate (NHP) models (Aravanis et al., 2007; Chuong et al., 2014; El-Shamayleh & Horwitz, 2019; Yazdan-Shahmorad et al., 2016), introduces light-sensitive opsin into targeted neuronal populations, activating or inhibiting them within milliseconds upon light illumination. Despite its advantages, however, the long-term effects of repeated optogenetic modulation on large-scale cortical networks remain poorly understood, particularly in NHPs where circuit organization more closely resembles that of the human brain.

Previous studies have demonstrated that excitatory optogenetic stimulation can enhance neural synchrony (El Hady et al., 2013). Our own work has further shown that both single-site and paired optogenetic stimulation can strengthen functional connectivity between cortical areas (Bloch et al., 2022; Yazdan-Shahmorad, Silversmith, et al., 2018). While a substantial body of research supports the use of excitatory stimulation to promote plasticity and enhance neural connectivity, much less is known about whether inhibitory optogenetic tools can be used to selectively disrupt

specific circuits and mitigate the overactive connections or hyperconnected nodes often seen in pathological brain networks (Whitfield-Gabrieli et al., 2009). Traditional neural inhibition strategies involving pharmacological agents such as GABA agonists often produce widespread neural inhibition, thus lacking the spatial specificity and temporal precision required to study targeted network reorganization (Wiegert et al., 2017). Meanwhile, past studies on sensory deprivation have shown that removing relevant inputs and disrupting correlated activity pathways can lead to use-dependent synaptic depression and connectivity loss (Allen et al., 2003; Bender et al., 2006), although whether this Hebbian-like mechanism can translate to direct cortical interventions remains unexplored. To address this gap, we investigate whether inhibitory optogenetic stimulation can be spatially tailored to suppress neural activity and reduce functional connectivity at targeted cortical sites. If effective, this approach could provide a new strategy for decoupling pathological regions from the broader network, paving the way for personalized neuromodulation strategies to restore healthy network dynamics in the brain.

To address this question, we utilized our lab's large-scale optogenetic interface in combination with a multi-modal artificial dura (MMAD), which was previously implanted in two adult rhesus monkeys (D. J. Griggs et al., 2021a, 2024). This unique interface provides us with stable optical and electrophysiological access to the posterior-parietal cortex (PPC), a region implicated in a variety of high-level cognitive and sensorimotor functions (Cavada & Goldman-Rakic, 1989; Freedman & Ibos, 2018). We also infused the cortical regions covered by the optical window with a red-shifted inhibitory opsin, Jaws, to allow red-light mediated inhibition of targeted locations (Chuong et al., 2014; D. J. Griggs et al., 2024). Electrocorticography (ECoG) signals recorded via the MMAD were continuously monitored, allowing us to estimate the dynamic changes in functional connectivity by measuring pairwise coherence between regions, which represents the level of correlated neural activity (Bowyer, 2016). By employing these state-of-the-art tools, we aim to test the efficacy of optogenetic inhibition in altering large-scale network connectivity in a brain anatomically similar to that of humans. In addition, we compare these inhibitory effects to excitatory stimulation performed in separate sessions over the sensorimotor cortex, allowing us to assess the bidirectional capacity of optogenetic modulation. Together, the results of this study lay the groundwork for future investigations into how targeted inhibitory neuromodulation can be used to modify aberrant neural circuit dynamics and ultimately inform therapeutic interventions for restoring balanced connectivity in neurological and psychiatric disorders.

Materials and Methods

Animals and implantation surgeries

Two adult, male, rhesus macaques (Monkey H: 10 y, 13.5 kg; Monkey L: 10 y, 14.0 kg) with chronically implanted cortical recording chambers were used in this study. All animal care and experiments were approved by the University of Washington's Office of Animal Welfare, the Institutional Animal Care and Use Committee (IACUC), and the Washington National Primate Research Center.

The initial chamber implantation surgery was conducted at 22 months prior to the experiments for monkey H and at 17 months prior to the experiments for monkey L as part of our previous work on developing a large-scale, chronically-stable optogenetic interface in NHPs (D. J. Griggs et al., 2024). Details on the design, implantation, and validation of our multimodal interface can be found in these previous papers (D. J. Griggs et al., 2021a; D. J. Griggs, Bloch, et al., 2022; D. J. Griggs et al., 2024; Iritani et al., 2024). To briefly describe its design, our chamber is made of a titanium cylinder with 23-mm internal diameter (Hybex Innovations, Canada), printed with a custom skirt that fits each animal's skull curvature. During implantation, animals were put under isoflurane anesthesia while their respiration, heart rate, and body temperature were continuously monitored throughout the procedure. Using standard aseptic techniques, we performed unilateral craniotomy and durotomy over the posterior parietal cortex (PPC) on the left hemisphere of each animal, before securing the chamber skirt onto the skull directly above the cranial window with titanium bone screws. A threaded, stainless steel cap (Hybex Innovations) is used to close off the cylinder at the end of surgery, sealing the recording chamber between experimental sessions.

Optogenetic interface

Viral vector delivery. During the same surgical sessions as described above, we performed viral vector infusion in the PPC using convection enhanced delivery (CED), before placing our semi-transparent multimodal artificial dura (D. J. Griggs et al., 2021a) on the cortical surface for subsequent electrophysiology experiments. Detailed descriptions of the CED method can be found in our previous publications (D. Griggs et al., 2023; Khateeb et al., 2019; Yazdan-Shahmorad et al., 2016). For the works presented in this chapter, we infused up to 50 µl of virus

containing the Jaws opsin (rAAV8-hSyn-Jaws-KGC-GFP-ER2, 5.4×10^{12} virus molecules/ml, University of North Carolina Vector Core) at each of the 4-6 locations in each monkey without live MRI monitoring. With this chronic optogenetic interface, we had stable electrophysiology and optical access to the PPC over multiple months for both animals, until another dura resection is performed to remove tissue growth and restore the optical window (D. J. Griggs et al., 2024). In monkey L, we also performed viral vector reinjections following dura resection, at around two years after the initial implantation and infusion surgery to restore the Jaws expression before adding additional experimental sessions (D. J. Griggs et al., 2024).

Electrophysiology system. To perform chronic subdural recordings, we resected the newly grown tissue and implanted a new multimodal artificial dura (MMAD) inside the chamber of each animal, before the start of their respective experimental sessions. As described in our previous work (D. J. Griggs et al., 2021a), we designed the MMAD in collaboration with Ripple Neuro (Salt Lake City, TU, USA), which contains 32 μECoG electrodes and flexible conductive layers printed into transparent layers of medical grade copolymer. This ECoG array was then molded into an artificial dura using similar techniques as described before (Ruiz et al., 2013; Yazdan-Shahmorad et al., 2016), which helps secure the array between native dura and the brain, thus protecting the exposed cortex and reducing tissue growth over time (Figure 6A). As part of the MMAD, the flexible cables of the ECoG array were also stored within the chronic chambers between experimental days. All electrophysiology recordings sessions in this study were performed in awake animals sitting in a primate chair. At the start of each experimental sessions, we connected MMAD cables to the PCB clamp connectors, which were then connected to the Grapevine Nomad processors via Nano front ends for subsequent recordings (Ripple Neuro, Salt Lake City, UT). A customized connector tray was attached to the titanium chamber to secure the PCB clamp connectors, and serve as an attachment for the optical stimulation hardware. A more complete description of the interface design and electrophysiology hardware can be found in our separate manuscript undergoing revision (D. J. Griggs et al., 2024).

Validation of opsin expression. During the chambers implantation surgeries, we virally infused the red-light-activated, inhibitory opsin Jaws into the PPC of each monkey using the CED technique (D. J. Griggs, Garcia, et al., 2022; Yazdan-Shahmorad, Tian, et al., 2018) to produce larger and more uniform pan-neuronal expression of Jaws. The validation of opsin expression after initial injections in Monkey H and L was described in our group's previous work (D. J. Griggs, Bloch, et

al., 2022; D. J. Griggs et al., 2024). The optogenetic experiments demonstrated in this current study were performed at 22 and 17 months after the initial injection for monkeys H and L respectively, and additional sessions were added at 2 months after the reinjection for Monkey L. To test the level of expression at different locations over the optical window, we performed epifluorescence imaging of the GFP fluorescence tag. During epifluorescence imaging, we used a blue light source (NIGHTSEA, SFA-RB Royal Blue, 440-460 nm excitation, Electron Microscopy Sciences) and a green light filter (500-560 nm bandpass) attached to a digital camera with 35mm lens (Nikon D5300, Nikon AF-S DX NIKKOR 35mm). Each quadrant of the optical window was illuminated sequentially during imaging while the camera was kept at a fixed position. The sequential images were then stacked and averaged in Photoshop to improve quality and contrast over the full window. Figure 6B shows the stacked opsin expression map for monkey H (left) and monkey L (right) at around 2.5 months and 4 months after their respective injection surgeries, where high intensity of green fluorescence indicates regions of strong opsin expression at the time of imaging. Locations of positive opsin expression before the start of experiments in each animal were manually identified from these composite images (Figure 6D, light green), including the additional expressing regions following viral reinjections (Figure 6D, light grey).

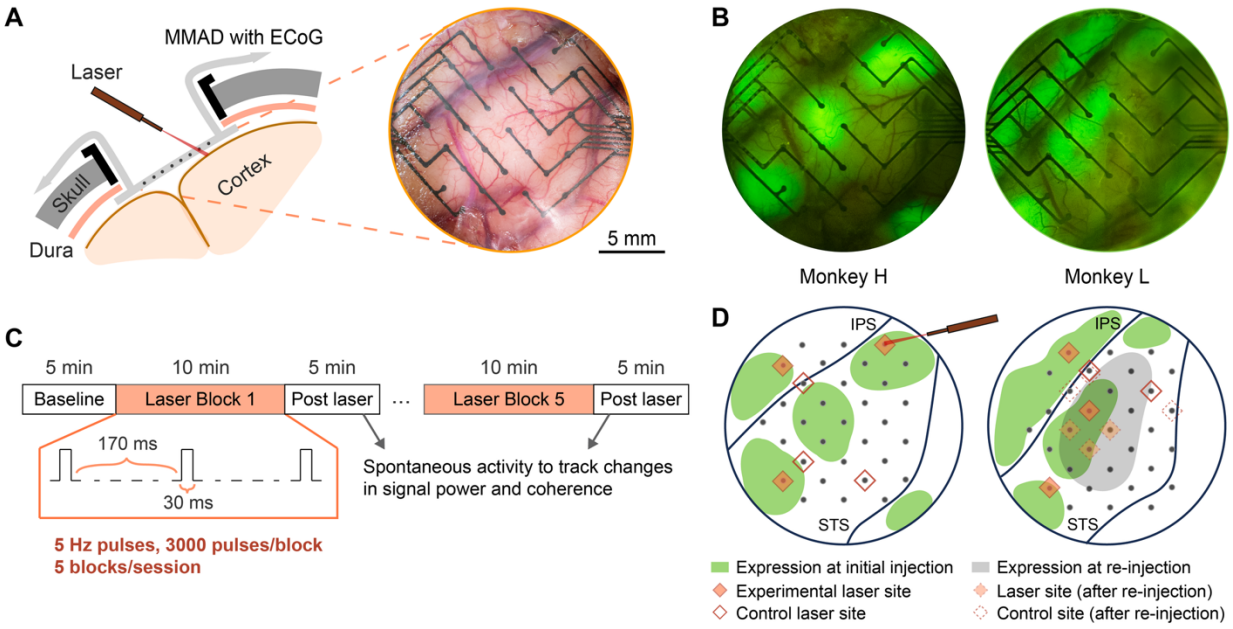

Figure 6. Overview of optogenetic interface and inhibition experiments. **A.** Schematics of the chronically implanted ECoG array and optical window compatible with targeted laser illumination. Zoomed-in area shows a top view of our semi-transparent MMAD placed on top of the PPC of monkey H. **B.** Epifluorescence images of the optical window for monkey H and monkey L, at 2.5 months (H) and 4 months (L) following initial viral infusion. Green indicates areas with high opsin expression (Jaws-GFP). **C.** Schematics of optogenetic inhibition protocols showing the laser illumination parameters and

block designs. **D.** Illustration of opsin expression maps and selected laser locations in monkey H and monkey L (filled diamonds: strong expression; empty diamonds: weak expression; dashed outlines: sessions after re-injection). Light green regions represent initial Jaws expression and light grey indicates expression after reinjection. IPS: intraparietal sulcus; STS: superior temporal sulcus.

Optogenetic inhibition paradigm

For this study, we developed an optogenetic inhibition protocol utilizing a single-site approach with a red fiberoptic laser (core/cladding diameter: 62.5/125 μm, Fiber Systems, USA), building upon the techniques outlined in our earlier work with excitatory optogenetic stimulation (Yazdan-Shahmorad et al., 2016), which allowed us to achieve precise control of the laser position via a customized holder attached to the connector tray. Each experimental session involved selecting a target location on the cortical window covered by electrodes on the MMAD, followed by the application of five 10-minute blocks of 5 Hz pulsed red laser illumination at 638 nm wavelength (Figure 6C). The laser delivered pulses with a duration of 30 ms and current amplitude of 110 mA to generate around 30 mW of light power the fiber tip. We selected 6 target inhibition sites for Monkey H and 12 target sites for Monkey L (including initial and reinjection experiments) across the exposed optical window. To add variability in the light-evoked response, the selected laser locations include both areas of distinctly strong opsin expression (Figure 6D, filled diamonds, 8 sessions) and adjacent regions with weaker expression (Figure 6D, empty diamonds, 8 sessions) as illustrated in the cortical maps. Additionally, we selected one location per animal that displayed no opsin expression and far from any injection site to be our control, based on the epifluorescence images shown in Figure 6B.

Estimation of light evoked neural response

To assess the effect of targeted inhibition on the neural network dynamics, we first characterized the neural response induced by individual laser pulses. The recorded ECoG signals were sampled at 1kHz and filtered into broadband local field potentials (LFPs) for all subsequent processing.

Artifact removal algorithm. The short laser pulses delivered directly above the MMAD electrodes produced a distinct photoelectric artifact that sometimes saturated the recording. To characterize the neural responses, we developed a custom artifact rejection algorithm in MATLAB to remove this low-frequency, high amplitude light-evoked artifact to unmask the neural signals during and immediately after each laser pulse. To do this, we reshaped each 10-min recording block into 3000 trials, where each trial contains 30-ms before laser, 30-ms during laser, and 60-ms after

laser segments (Figure 7A, left). We then averaged the 3000 trials for each of the five blocks to produce five shared artifacts for that experimental session. Next, the first two principal components (PCs) of the shared artifacts were computed to serve as the artifact template in PC space. We then projected each laser trial from the same experimental session onto this PC space, and subtracted the scaled projection of the signal from the original LFP recording in each trial to remove the light artifact while retaining neural signals (Figure 7A, right).

Quantification of evoked response ratio. For each stimulation pulse, we used the welch method to generate power spectral density (PSD) estimates at three time points: 0 to 30 ms before laser start, during laser (30 ms), and 10 to 40 ms post laser (Figure 7A). We then took the ratio of PSDs between during-laser and pre-laser, as well as between post-laser and pre-laser, for each trial at each frequency separately, before averaging across 30-200 Hz and converting to logarithmic scale to compute the evoked response ratios for each during-laser and pre-laser segments. The evoked response was considered significant if the PSD ratios calculated at the laser site was significantly greater than the PSD ratio calculated using randomly shuffled control trials (no laser illumination) undergoing the same artifact rejection procedures (two-sample unpaired t-test).

Estimation of functional connectivity

We estimated the functional connectivity changes between each pair electrodes within the optical window by computing the pairwise coherence between recorded LFPs during spontaneous activity following each laser inhibition block.

Coherence analysis. The magnitude-squared coherence (Cxy) between preprocessed signals at electrodes x and electrode y was computed as a function of the respective power spectral densities of signals x and y (Pxx and Pyy) and their cross-spectral density (Pxy) using 2-sec Hamming windows. We repeated this analysis for every 20 seconds of LFP signals from each 5-minute segments of ECoG recordings (baseline and post-laser blocks in Figure 6C), and calculated the average coherence for theta (4-8 Hz) and gamma (30-59 Hz) frequency bands respectively. The coherence changes for each frequency band were calculated by subtracting the initial baseline coherence from each of the post-laser blocks. At each post-laser time points, we compared the coherence changes between laser site and other channels to the coherence changes between all non-laser channels, using a two-sample unpaired t-test with unequal variances. After performing the same coherence analysis for all experimental and control sessions

and pooling the data from both animals, we grouped the resulting coherence changes based on the session types – laser at strong opsin expression region (with significant evoked response), laser at weak or no expression region (without significant evoked response), and no laser control sessions – to compare the functional connectivity changes across time using one-way ANOVA with post-hoc Bonferroni test for multiple comparisons. Similarly, coherence changes during the extended baseline periods for 8 of the experimental sessions (up to 30 minutes after the last inhibition block) were also computed using the same methods.

Power analysis. To make sure the change in coherence is not a result of fluctuation in frequency-specific signal power, we computed the average band power during each baseline and post-laser periods for theta (4-8 Hz) and gamma (30-59 Hz) frequency ranges, using the Matlab built-in function which integrates the periodogram PSD estimate of the input signal. We then compared any changes in band power at the laser site across time using one-way ANOVA with post-hoc Bonferroni test, where the sample size is the number of sessions in each experimental group.

Excitatory optogenetic stimulation

To test whether the functional connectivity changes between modulation site and the network were specific to our pan-neuronal inhibition paradigm, we compared the effects of inhibitory optogenetic modulation described above to that of excitatory modulation over the sensorimotor cortex. The excitatory dataset was collected from two other rhesus macaques (Monkey G: male, 8 y, 17.5 kg; Monkey J: male, 7 y, 16.5 kg) as part of our previous study demonstrating the feasibility of reshaping cortical connections using optogenetics (Yazdan-Shahmorad, Silversmith, et al., 2018). Full methodological and experimental details can be found in that publication.

Optogenetic interface. The excitatory optogenetic experiments used a similar interface, consisting of a titanium chamber over the sensorimotor cortex and a semi-transparent ECoG array acutely placed over the 25-mm diameter optical window (Yazdan-Shahmorad et al., 2016). This setup provides optical access to the primary somatosensory (S1) and primary motor (M1) cortices where excitatory opsins (C1V1) were selectively expressed in excitatory neurons. During chamber implantation surgeries, viral vectors (AAV5-CamKIIa-C1V1(E122T/E162T)-TS-eYFP-WPRE-hGH) were infused into S1 and M1 cortices on the left hemisphere of each animal. A titanium cylinder was then secured onto the skull, and an artificial dura was inserted to protect the cortical surface. During experimental sessions, the artificial dura was removed and a custom 96-channel μECoG

array (Ledochowitsch et al., 2015) was positioned on the sensorimotor cortex. Optical stimulation of C1V1-expressing neurons was delivered via fiber optic cables (62.5/125 μm, Fiber Systems) connected to a 488 nm laser, with the fiber tip (~20 mW light power) placed directly above the targeted electrode site.

Optogenetic excitation paradigm. Laser stimulation was delivered in five, 10-minute conditioning blocks. Stimulation trains contain 5-ms, 5 Hz laser pulses at either one or two cortical sites in either M1 or S1. When two independent lasers were used, there was a 100-ms delay between pulses at the two laser sites, thus avoiding interference between evoked responses from each light source. In between conditioning blocks for each experimental session, 5 minutes of spontaneous activity was recorded to monitor functional connectivity changes over time.

Neurophysiology and coherence analysis. Neural data was recorded by the μECoG array at a sampling frequency of 24 kHz (Tucker-Davis Technologies system) and down-sampled to 1 kHz. Validation and quantification of the light-evoked neural response was described in the previous publication (Yazdan-Shahmorad, Silversmith, et al., 2018). To analyze the changes in functional connectivity between the modulation site and the network sites, we used the same methods as descripted above, calculating the pairwise coherence between the laser channel and all other M1 and S1 channels for every 20 seconds of broadband LFP signals, using a 2-sec Hamming window. We then computed the average coherence in theta and gamma frequency bands during each of the 5-min spontaneous recordings, and then calculated the changes in coherence from the first baseline period to monitor functional connectivity changes.

Results

Evoked neural response during targeted optogenetic inhibition

In this study, we first confirmed that targeted laser illumination was able to elicit significant neural responses, particularly at sites with strong opsin expression. After implementing the PCA-based light artifact removal (Figure 7A), we used the cleaned, broadband LFP signals to compute the power spectral density (PSD) ratios of before and during laser periods, as well as before and after laser periods, to monitor the transient changes in neural activity. We found that the PSD ratios at the laser site during illumination were not only significantly higher compared to that after

the laser was turned off, but also significantly greater than those at a far channel approximately 6 mm away (Figure 7C, unpaired t-test with Bonferroni correction). These results confirmed a substantial red light evoked neural response that may be counterintuitive, with the estimated neural activity during laser application being markedly higher. Conversely, at locations with minimal opsin expression, the PSD ratios during and after laser application showed no significant differences (Figure 7D), indicating that the laser induced response was spatially specific to the opsin expressing regions, as can be expected from targeted optogenetic modulation.

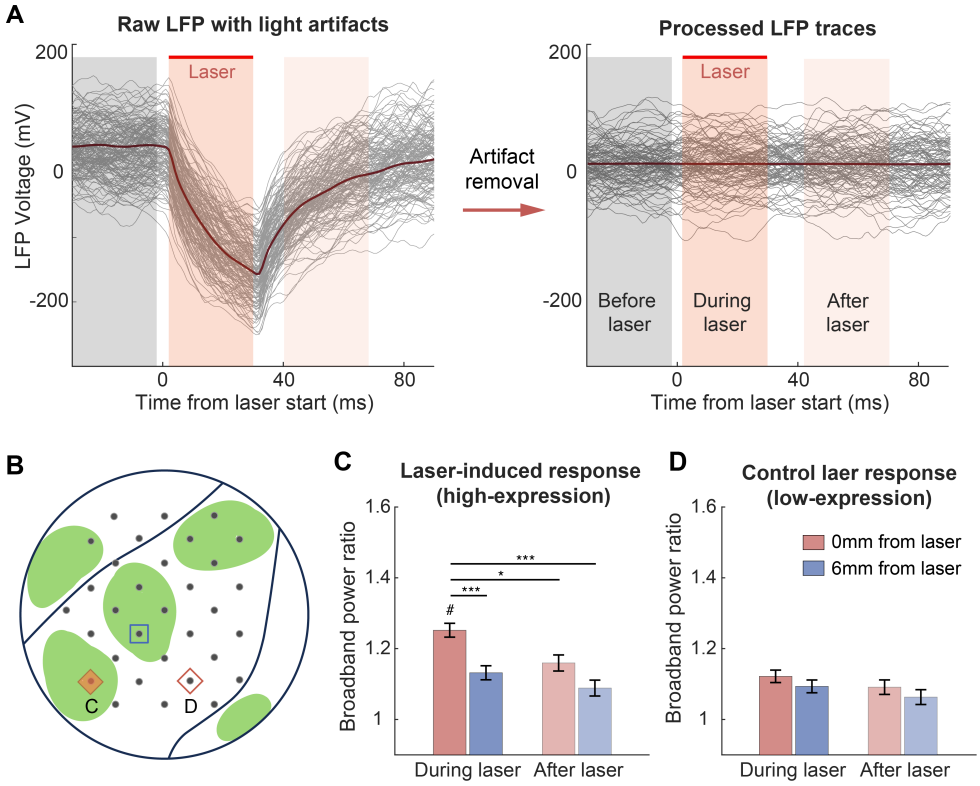

Figure 7. Quantification of laser evoked neural response. **A.** Overview of laser artifact removal pipeline, using dimensionality reduced templates based on trial-averaged traces. **B.** Illustration of sample laser locations in strong (C, solid orange diamond) and weak (D, empty orange diamond) opsin-expressing regions, as well as a far channel at 6 mm away (blue square). **C.** Light evoked neural response when targeting a high-expression region, at the targeted site and a far channel. At the laser site, the PSD ratios during laser was significantly higher than the ratios after laser, or the ratios at far channel, suggesting significant light evoked neural response (paired t-test with Bonferroni correction for multiple comparison, ***: $p < 0.001$, *: $p<0.05$). **D.** PSD ratios quantified at a site with minimal opsin expression, showing no significant differences between during and after laser application, which suggests little or no light-evoked neural response.

Although one might expect the activation of the inhibitory opsin Jaws to reduce LFP signal power, the PSD analysis revealed a local increase in power ratio during laser illumination. Such increase in ECoG activity was also observed when using red LEDs with longer pulse width for global network inhibition (D. J. Griggs et al., 2024). A possible explanation for this observation is that light penetration during optogenetic modulation is most effective in the upper cortical layers, which contain higher percentage of inhibitory GABAergic neurons than deeper tissues such as layers 5 and 6 (Fitzpatrick et al., 1987). As a result, our pan-neuronal inhibition paradigm may have silenced a large population of the inhibitory neurons, leading to higher activity from the excitatory neurons such as layer 5 pyramidal cells. Since the apical dendrites of pyramidal neurons make a substantial contribution to extracellular field recordings (Buzsáki et al., 2012), we observed a net effect of increased LFP power during laser illumination.

Changes in functional connectivity following optogenetic inhibition

After targeted laser was applied at Jaws-expressing regions over the PPC, we found that functional connectivity within the network, as measured by gamma coherence between electrode sites, showed notable reduction following each laser inhibition block. For a session in which the selected laser site exhibits strong Jaws expression and significant light evoked neural response, gamma coherence between the laser-targeted site and the broader network showed greater decrease than the coherence between all non-laser electrodes (Figure 8A, first column, left: unpaired t-test, $p < 0.001$), with the difference becoming more evident at the last post-laser block following 50 minutes of optogenetic inhibition (Figure 8A, first column, right). Meanwhile, this difference was not observed when computing the gamma coherence change between the far channel and the broader network (Figure 8A, first column, blue). To assess the specificity of inhibition induced network response, we evaluated the coherence changes during two types of controls: laser inhibition at no-expression regions (no significant light evoked response) and no-laser sessions with randomly selected sham laser site. We found that for both of these controls, there was no significant difference between the laser site coherence change and the non-laser network coherence change (Figure 8A, lower columns). These results highlight the targeted effects of our optogenetic modulation protocol and its capacity to selectively modulate neural dynamics, disconnecting specific location from the network with spatial precision following continuous application.

Next, we pooled the data from Monkey H (6 sessions) and Monkey L (12 sessions) together into the three groups above (strong expression = 8 sessions, low expression = 8 sessions, no laser control = 5 sessions) and compared functional connectivity changes across time. Significant light-evoked response must be observed during the laser pulses for a session to be classified into the high expression group. We found that gamma coherence changes were largest in sessions targeting regions with strong Jaws expression, where laser site coherence steadily declined across successive post-laser blocks (Figure 8B, top, one-way ANOVA with post-hoc Bonferroni test, n = # electrode pairs x sessions), suggesting a persistent disruption of neural connectivity with longer modulation. In contrast, no significant coherence changes over time were observed during sessions targeting areas with low opsin expression or during no-laser control sessions (Figure 8B, middle and bottom rows). Importantly, gamma-band signal power remained stable across all session types (Figure 8C, one-way ANOVA, n = # sessions), ruling out power fluctuations as a confounding factor in coherence estimates. Together, these findings demonstrate that targeted optogenetic inhibition can selectively and persistently decouple specific cortical sites from large-scale networks, demonstrating its promise as a therapeutic strategy for neurological disorders marked by focal hyperconnectivity.

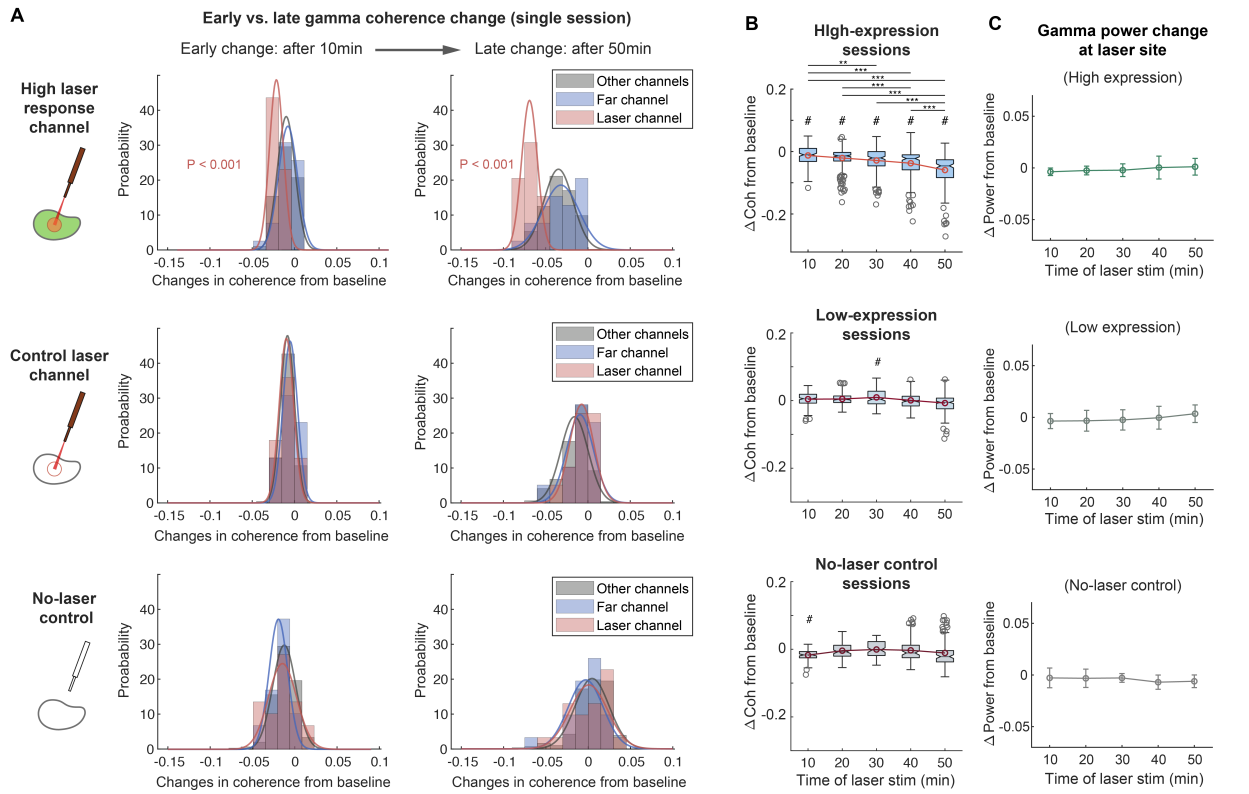

Figure 8. Quantification of functional connectivity as measured by gamma coherence following optogenetic inhibition. **A.** Example histograms of gamma coherence changes after 10 minutes and 50 minutes of laser inhibition for 3 different session types. Red indicates coherence changes between laser site and network. Blue indicates coherence changes from a randomly selected far channel 6 mm from the laser, and grey indicates coherence between rest of the network channels. **B.** Combined gamma coherence changes from laser sites over time for each condition. Blocks with significant changes from the pre-laser baseline are marked by # (paired t-test, $p < 0.001$). n = # electrode pairs across sessions (n = ~240 for high/low expression group; n = ~150 for no-laser control group). Gamma coherence decreased significantly when targeting high-expression regions, but remained relatively stable in low-expression and no-laser control sessions (one-way ANOVA with post-hoc Bonferroni test, ***: $p < 0.001$, **: $p < 0.01$, *: $p < 0.05$). **C.** Changes in gamma band power at the laser site across three session types over time. No significant difference was observed for any of the session type (one-way ANOVA, n = # sessions). Error bars represent mean ± stand error (SE).

Predicting connectivity change using light evoked response

To better understand the relationship between optogenetic inhibition and functional connectivity changes, we examined how gamma coherence between the laser site and the rest of the network was affected by the strength of light-evoked neural responses (Figure 9A). A significant negative correlation was observed between gamma coherence changes and the laser-evoked PSD ratios, at both early (10 minutes) and late (50 minutes) post-laser time points (Figure 9C). Notably, the slope of this relationship became steeper after five laser blocks, indicating that repeated inhibition in regions with strong opsin expression resulted in a more pronounced and sustained disruption of local connectivity. These results highlight the effectiveness of targeted optogenetic inhibition in functionally uncoupling the laser site from its surrounding network, particularly when light illumination induces robust neural responses.

We then extended the analysis to the broader cortical network, assessing coherence changes between all non-laser sites (Figure 9B). Similar to the observations above, we saw that gamma coherence across the network also showed greater reductions in sessions with stronger light-evoked responses at the laser site (Figure 9D, $R^2 = 0.85$), with the relationship being more pronounced after repeated blocks of laser inhibition. However, the slope of these regression lines was notably smaller in magnitude than those observed at the laser site (Figure 9C), indicating that network-wide coherence was less strongly predicted by the neural response during illumination. This suggests that while optogenetic inhibition can propagate its effects across the network, the decoupling is most robust and more directly tied to evoked activity at the site of modulation. These findings indicate that the focal inhibition paradigm used in this study has both local and

global effects on functional connectivity, although with diminishing influence at distant locations. This observation highlights the need for future research on neural inhibition strategies with greater spatial precision to minimize off-target effects.

In addition to gamma-band activity, which closely reflects local neuronal firing, we also examined coherence in slower neural oscillations, particularly the theta rhythm (4-8 Hz) which overlaps with the stimulation frequency used in this study. For each session, we assessed the relationship between light-evoked PSD ratios and theta coherence changes. Unlike the more consistent patterns and stronger correlation observed in the gamma band, theta coherence at the laser site exhibited greater variability across sessions and was less reliably predicted by the strength of the evoked response (Figure 9E), as reflected by lower R-squared values in the regression model. This suggests that, under our optogenetic inhibition paradigm, the modulation of theta coherence may be influenced by additional factors not captured in our current experimental protocol, such as the phase alignment between laser pulses and ongoing theta activity. Therefore, these results underscore the need for future studies to clarify the mechanisms governing theta coherence and its role in shaping network dynamics. Across the broader network, theta coherence changes also showed a shallow but statistically significant negative relationship with the light-evoked PSD ratio after 50 minutes of laser inhibition (Figure 9F, $R^2 = 0.57$). Since this effect was more subtle than in the gamma band, it suggests that theta coherence may reflect broader network states rather than local activity at the stimulation site. Alternatively, theta coherence may be more sensitive to the brain's baseline state or broader cognitive and neuromodulatory context, and therefore less directly tied to the immediate effects of laser-evoked neuronal suppression.

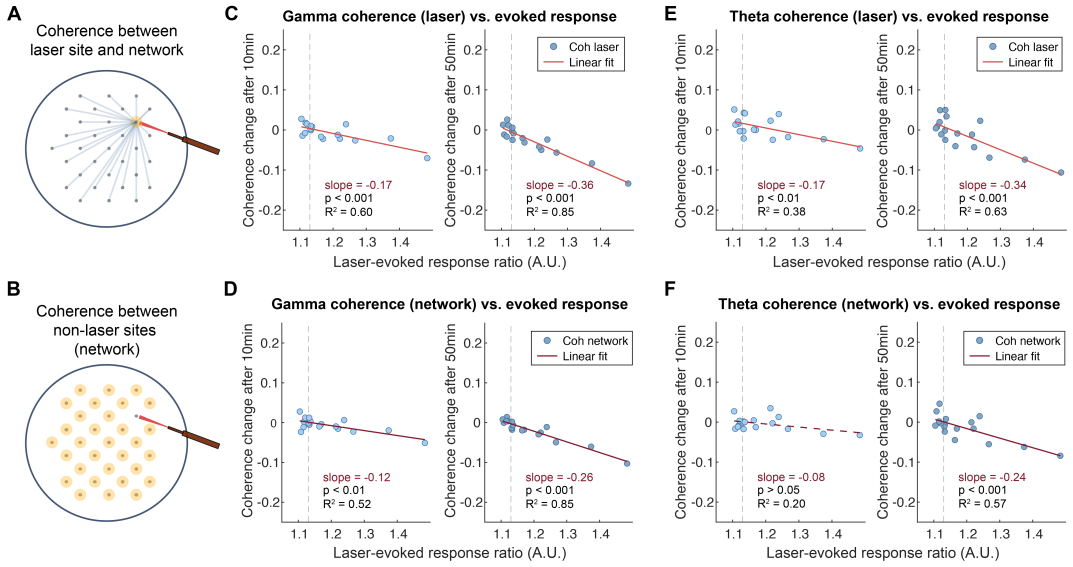

Figure 9. Relationship between laser evoked response and coherence changes for all sessions. **A.** Schematics of coherence quantification between the laser site and other channels in the network, as shown in C and E. **B.** Schematics of network coherence changes (non-laser sites) as shown in D and F. **C.** Gamma coherence changes at the laser site as a function of light-evoked PSD ratios, after fitting a linear regression model, during early (10 min) and late (50 min) modulation periods. Dashed lines indicate average PSD ratio computed using randomly shuffled control trials. **D.** Early and late gamma coherence changes between non-laser sites, analyzed as a function of evoked response ratios using linear regression. **E.** Theta coherence changes at the laser site as a function of evoked PSD ratios. Compared to the gamma band results (C), linear regression showed a weaker relationship between theta coherence change and light-evoked response. **F.** Theta coherence changes between non-laser sites as a function of PSD ratios. The negative relationship is only significant after 50 minutes of repeated laser inhibition.

Variability in theta coherence changes

The relationship between light-evoked neural responses and coherence changes in the previous section highlights the potential of optogenetic interventions to modulate network connectivity. Specifically, gamma coherence exhibited consistent and predictable reductions in response to laser-induced neural suppression at opsin-expressing sites, supporting the use of optogenetics to selectively disrupt functional connections. We next extended our earlier analysis of gamma coherence changes over time (Fig. 8) to the theta band, both within individual sessions and across sessions grouped by experimental condition, to determine whether similar modulation effects were present in lower-frequency neural activity.

In single-session analysis targeting regions with strong expression, we observed a progressive reduction in theta coherence between the laser site and the network from early (after one laser block) to late (after five laser blocks) time points (Figure 10A, top row). At both stages, the laser site showed significantly larger reductions in coherence compared to non-laser channels, suggesting a localized and time-dependent effect of optogenetic inhibition on theta coupling. This local dissociation was not observed in either low-expression or no-laser control sessions (Figure 10A, middle and bottom rows), reinforcing the specificity of the observed modulation.

However, when aggregating theta coherence changes across all sessions for each condition, we found considerable session-to-session variability (Figure 10B). In high-expression sessions, theta coherence showed a broad distribution of changes over the first 30 minutes of modulation, with no consistent trend across sessions (Figure 10B, top row). This variability suggests that theta

coherence may be more sensitive to underlying brain state or trial-level dynamics than gamma coherence. Given that the frequency of our laser (5 Hz) was also in the theta range, the changes in theta coherence might be further dependent on the phases of neural oscillation at which laser pulses were delivered, as described in studies on phase-locked brain stimulation (Widge & Miller, 2019). Nevertheless, after 40–50 minutes of repeated inhibition, we started to see a significant reduction in theta coherence from baseline and early time points (*$p < 0.05$, one-way ANOVA with post-hoc Bonferroni test), pointing toward a delayed, possibly dose-dependent effect. Notably, the distribution of these theta band changes in high-expression sessions remained wider than those observed in the gamma band. Meanwhile, theta band power at the laser channel remained stable across all time points and session types (Figure 10C, n = # sessions, one-way ANOVA), indicating that changes in coherence were not driven by fluctuations in signal power or shifts in oscillatory amplitude, but instead point to altered patterns of network communication.

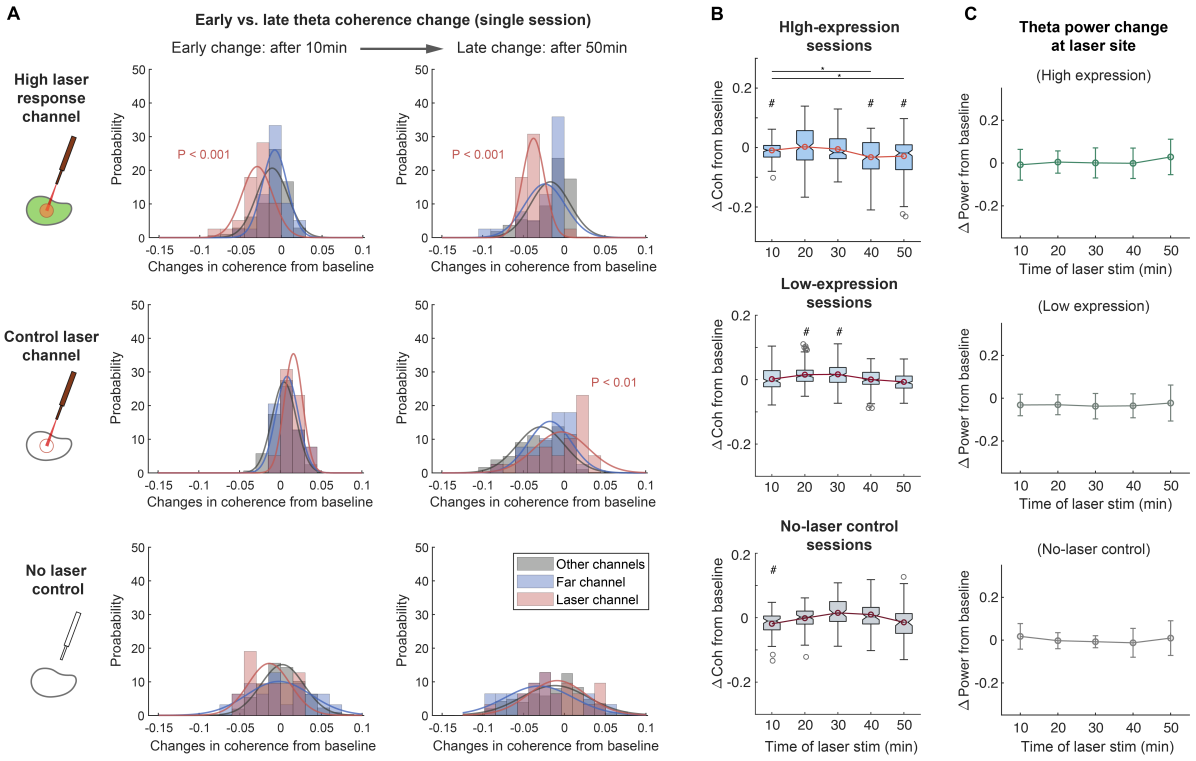

Figure 10. Quantification of theta coherence changes across sessions. **A.** Distribution of theta coherence changes after 10 minutes and 50 minutes of laser inhibition, during one example session for each condition (high-expression, low-expression, no-laser). Red indicates coherence changes between laser site and network. Blue represents a randomly selected far channel (6 mm away), and grey indicates coherence between rest of the network channels. Theta coherence showed greater decrease at the laser site than at other channels for this high-expression session (top row, unpaired t-test). No significant differences were found among the theta coherence changes at the laser site, far

channel, and other non-laser channels for the other two conditions. **B.** Combined theta coherence changes at the laser site across three session types over time. Significant changes in each post-laser block compared to baseline block are marked by # (paired t-test, $p < 0.001$). n = # electrode pairs across sessions (n = ~240 for high/low expression group; n = ~150 for no-laser control group). Although showing high variability, theta coherence decreased significantly from first to last laser block when targeting high-expression regions, but remained relatively stable in the other two conditions (one-way ANOVA with post-hoc Bonferroni test, *: $p < 0.05$). **C.** Changes in theta band power at the laser site over time. No significant difference was observed for any of the session types (one-way ANOVA, n = # sessions). Error bars are mean ±SE.

Connectivity remains suppressed after the end of inhibition

One important question surrounding stimulation-based intervention is the timescale at which the modulation effect lasts after the end of active treatment. Therefore, to assess the persistence of optogenetically induced network changes, we analyzed coherence changes during an extended post-inhibition period, by continuously recording for 30 to 40 minutes after the end of the last laser block. In high-expression sessions, both theta and gamma coherence showed sustained reductions that continued beyond the final inhibition block. As shown by the colormap for one example session in Monkey H, theta coherence between the laser site and the rest of the network progressively declined from early to late time points, and remained suppressed 30 minutes after the laser was turned off (Figure 11A). A similar pattern was observed for gamma coherence, with the decrease in connectivity originating from the laser site and spreading to the network, leading to large-scale and prolonged suppression during extended post-laser periods (Figure 11B).

Furthermore, quantification of all high-expression sessions with extended recordings confirmed these observations. Theta coherence remained significantly lower than baseline immediately after the last laser block and continued to decline modestly over the 30-minute post-inhibition period (Figure 11C; paired t-test, #$p < 0.001$; one-way ANOVA, *$p < 0.05$). Gamma coherence exhibited a comparable pattern, with a robust decrease from baseline that persisted throughout the entire post-laser recording period (Figure 11D; paired t-test, #$p < 0.001$), without signs of recovery. These findings indicate that repeated focal inhibition leads to lasting reductions in both low- and high-frequency functional connectivity, suggesting that the network effects of optogenetic suppression are not transient but can endure well beyond the immediate modulation window.

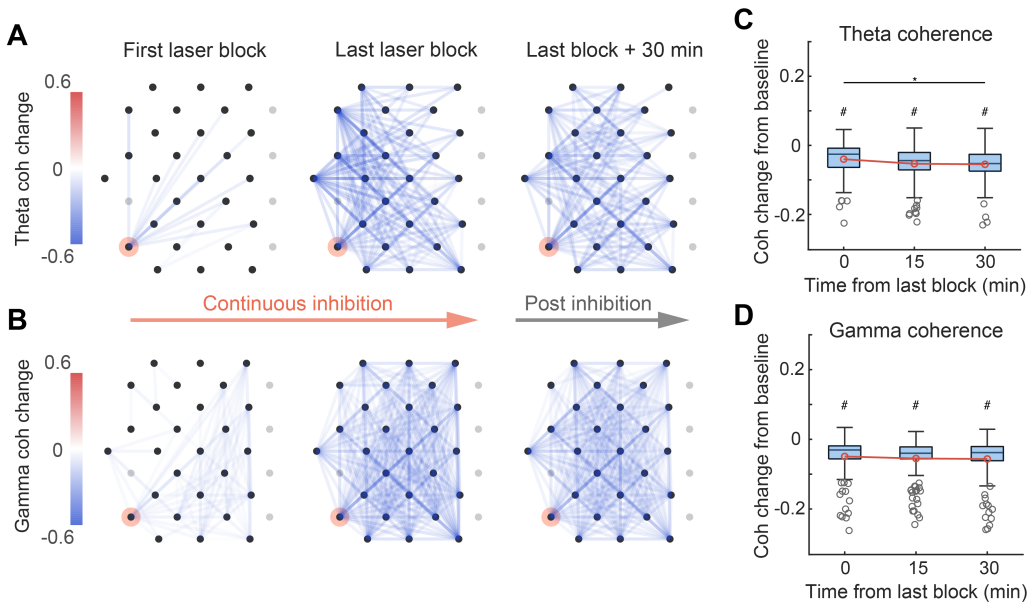

Figure 11. Quantification of coherence changes during extended recordings after optogenetic inhibition ends. **A.** Colormap of theta coherence for an example high-expression session, at early (10 minutes of laser), late (50 minutes of laser), and extended baseline (30 minutes after the last block ends) time points. Pink node represents the laser electrode, and colored edges represent coherence changes from the initial baseline. **B.** Colormap of gamma coherence changes for the session as shown in A, at the same three time points. **C.** Combined theta coherence changes from the laser site for high-expression sessions. Significant changes compared to the initial baseline are marked by # (paired t-test, $p < 0.001$). Theta coherence remained low, with some continuous decrease up to 30 minutes after laser turned off (one-way ANOVA with post-hoc Bonferroni test, *: $p < 0.05$). **D.** Combined gamma coherence changes from the laser site for high-expression sessions, with significant changes marked by # (paired t-test, $p < 0.001$). Gamma coherence remained low (did not return to baseline) up to 30 minutes after laser turned off.

Excitatory optogenetic stimulation enhances functional connectivity

After characterizing the effects of inhibitory optogenetic stimulation on network connectivity, we re-examined whether targeted excitatory stimulation would produce the opposite effect under similar laser parameters and block design, thus strengthening functional connectivity from the stimulated site over time. For this experiment, a 96-channel ECoG array was placed over M1 and S1 cortices, where excitatory opsins (C1V1) were selectively expressed in pyramidal neurons (Figure 12A). For each experimental session, either a single blue laser or two non-interfering lasers with 100-ms delay were used to deliver 5 Hz light pulses during the 10-minute stimulation blocks (Figure 12B). In our previous work, light evoked responses were quantified and showed consistent neural activation over the stimulated cortex after each 5-ms laser pulse (Yazdan-Shahmorad,

Silversmith, et al., 2018). In this study, we assessed the changes in network-wide functional connectivity by measuring coherence between the laser electrode and all other recording channels over the sensorimotor cortex, in both theta and gamma frequency bands following each stimulation block.

Combining the coherence changes across both animals (single-laser: 5 sessions; non-interfering lasers: 7 sessions) revealed a progressive enhancement of laser site coherence after repeated stimulation. In particular, theta coherence between the laser site and the network increased quickly and significantly after each laser block (Figure 12C, n = # electrode pairs across sessions), with changes becoming more pronounced over time (one-way ANOVA with post-hoc Bonferroni test). In contrast, gamma coherence exhibited a more delayed increase after the fourth and fifth stimulation blocks (Figure 12D), suggesting a dose-dependent relationship where sustained excitatory input is required to strengthen higher-frequency connectivity. These differences may reflect distinct roles of theta and gamma bands in mediating global versus local communication. Notably, this pattern contrasts with the effects of inhibitory modulation that led to more rapid and persistent decreases in gamma coherence (Figure 9). Together, these findings demonstrate that cortical connectivity can be selectively modulated in both directions by tailoring the optogenetic paradigm, either strengthened through excitation of pyramidal neurons or weakened through inhibition of all neurons, thus providing a flexible framework for controlled reorganization of large-scale brain networks.

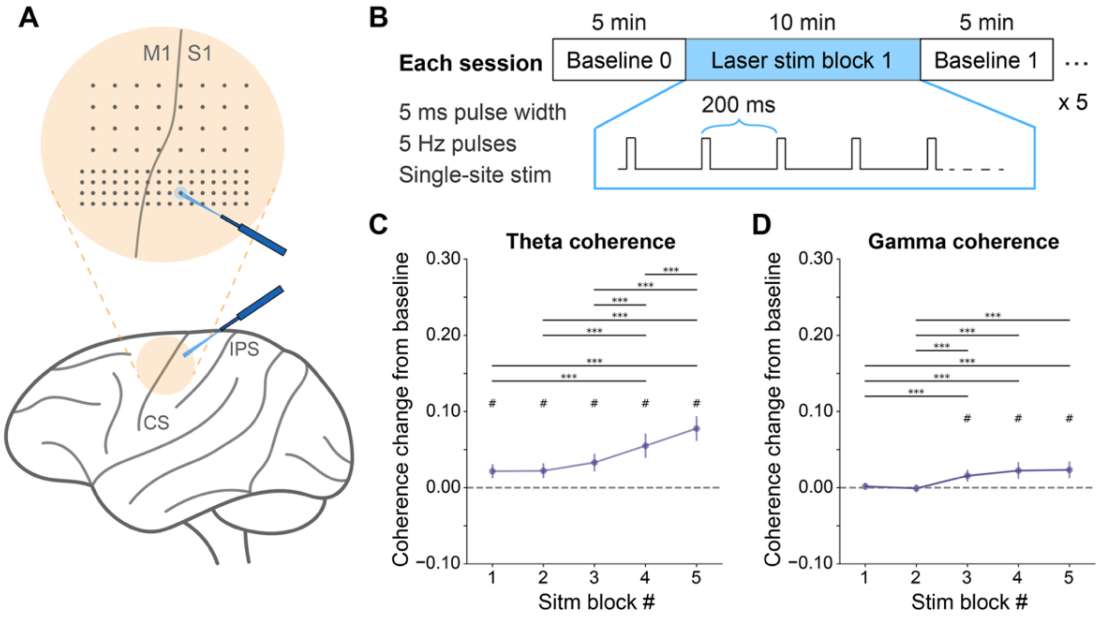

Figure 12. Quantification of coherence changes in response to excitatory optogenetic stimulation. **A.** Schematics of the optogenetic interface and experimental protocol. 96-channel ECoG array covers the M1 and S1 regions with excitatory neurons expressing C1V1 opsin. One or two lasers are placed in varying locations to deliver patterned optical stimulation. **B.** Summary of stimulation parameters and block design. Either one or two non-interfering lasers were used. Each 10-min stimulation is followed by 5-min recording of spontaneous activity. **C.** Theta coherence changes (between laser site and the network) from the initial baseline, for each of the five post-laser blocks, with significant changes marked by # (paired t-test, $p < 0.001$, n = # electrode pairs across sessions). When all experimental sessions are pooled together, theta coherence continuously increased over time, (one-way ANOVA with post-hoc Bonferroni test, ***: $p < 0.001$). **D.** Gamma coherence changes from the initial baseline, which only increased significantly after 30 minutes of laser stimulation. Error bars are mean ±SE.

Discussion

In this study, we demonstrate that targeted optogenetic stimulation can bidirectionally modulate large-scale cortical connectivity in the NHP brain. Using an inhibitory approach, we found that repeated neuronal suppression led to sustained reductions in functional connectivity from the stimulated site, particularly in the gamma band, with effects persisting even after stimulation ended. On the other hand, we found that excitatory stimulation gradually enhanced coherence between laser site and the broader network in a dose-dependent manner, with gamma-band responses emerging only after prolonged stimulation. Together, our findings suggest that cortical networks can be selectively reorganized in either direction through the careful design of neuromodulation paradigms.

The contrasting coherence responses in theta and gamma frequencies highlight the varied effects of optogenetic modulation on different aspects of network dynamics. In the past, we have shown that stimulation of excitatory neurons over the sensorimotor cortex strengthened the functional connectivity between M1 and S1 (Yazdan-Shahmorad, Silversmith, et al., 2018), with significant increases seen specifically in the theta band, which was positively correlated with the amplitude of stimulus-evoked responses. Moreover, since changes in stimulus-evoked coherence were shown to predict shifts in baseline coherence from the stimulation site, this supports a Hebbian-like mechanism underlying the observed connectivity changes. In contrast, our current study demonstrates that pan-neuronal optogenetic inhibition of the PPC leads to a reliable decrease in gamma coherence, while theta coherence exhibited more variable responses across sessions.

This divergence may reflect fundamental differences in how excitatory and inhibitory modulation engage distinct network rhythms. High-frequency ECoG power is often correlated with local firing rates (Dubey & Ray, 2020; Yazdan-Shahmorad et al., 2013), although recent evidence indicates that high-gamma activity may also reflect summed postsynaptic potentials rather than purely local spiking activity (Lei et al., 2025). By contrast, low gamma oscillations (~30 to 60 Hz) are tightly coupled to fast-spiking parvalbumin interneurons, which synchronize excitatory populations and regulate temporal coordination within local circuits (Buzsáki & Wang, 2012; Gouwens et al., 2010; Sohal et al., 2009). Therefore, pan-neuronal optogenetic inhibition via Jaws expression likely disrupts this synchrony and shifts the excitation–inhibition balance, leading to robust suppression of gamma coherence. In contrast, theta rhythms involve broader cortico-cortical interactions and are modulated by diverse interneuron subtypes (Bezaire et al., 2016; Cardin, 2018; Stark et al., 2013), which maintain recurrent connections and contribute to feedback inhibition. As a result, theta coherence may be more susceptible to fluctuations in cognitive or brain states, especially when the inhibition is not cell-type specific, leading to greater variability across sessions compared to gamma coherence. On the other hand, repeated stimulation of pyramidal cells likely amplifies correlated neuronal activity within existing pathways, promoting synaptic strengthening based on the Hebbian learning and spike-timing dependent plasticity (Caporale & Dan, 2008; Kempter et al., 1999), particularly at theta frequency that reflects recurrent excitation and long-range integration (Bezaire et al., 2016). Under these conditions, recruitment of fast-spiking interneurons may occur indirectly, potentially explaining the delayed increase in gamma coherence. These distinctions highlight the need to account for cell-type specificity and circuit-level interactions when designing neuromodulation paradigms aimed at modulating specific network rhythms or communication modes.

Mechanisms of stimulation-induced neuroplasticity

As discussed above, our results showing progressive increases in theta and gamma coherence following repeated excitatory optogenetic stimulation are consistent with Hebbian principles of activity-dependent plasticity, where sequential co-activation of presynaptic and postsynaptic neurons strengthen their connections (Hebb, 2002; Kempter et al., 1999). In larger scale networks, single-site optogenetic excitation likely enhances the excitability and correlated firing of neurons within and across cortical areas, leading to cumulative increases in functional connectivity over time. This Hebbian learning hypothesis is also supported by previous works using activity dependent (Lucas & Fetz, 2013; Nishimura et al., 2013; Song et al., 2013) or paired open-loop

electrical stimulation (Rebesco & Miller, 2011; Seeman et al., 2017) to promote plasticity and increase connections between targeted brain regions.

In contrast, the effects of repeated optogenetic inhibition are less well characterized in the context of long-term neuroplasticity. Our results show that pan-neuronal inhibition using repeated pulse train leads to a sustained reduction in gamma coherence, which may reflect a Hebbian-like mechanism that operates in reverse. Although Hebbian plasticity traditionally describes the strengthening of connections through correlated activity, it also implies that connections which are repeatedly inactive or uncoordinated may weaken over time, a concept sometimes referred to as activity- or experience-dependent depression (Feldman, 2009; Malenka & Bear, 2004). For our experiments, temporally patterned inhibition may disrupt spike timing across cortical sites, reducing the likelihood of synchronized firing needed to reinforce connectivity. Similar forms of activity-dependent synaptic weakening have been observed in sensory cortices during periods of reduced input or sensory deprivation, leading to diminished synaptic strength and long-range decoupling (Allen et al., 2003; Bender et al., 2006). Note that this differs from anti-Hebbian models (Koch et al., 2013) that require precise timing between pre and postsynaptic spikes to induce long-term depression (LTD). Instead, our findings support a more general form of network desynchronization-induced depression, in which lack of correlated activity across the circuit leads to prolonged reductions in functional connectivity. This explanation is also supported by previous neural imaging studies, where chemogenetic silencing of the anterior cingulate area, a highly connected region in the prefrontal cortex, led to reduced neural synchrony and significant decreases in whole-brain functional connectivity (Peeters et al., 2020).

Considerations for neuromodulation therapy

The ability to bidirectionally reorganize functional connectivity through targeted optogenetic stimulation has important implications for developing effective stimulation-based therapies. Many neurological and psychiatric disorders are characterized by abnormal network connections. This can manifest either as excessive connectivity, such as in epilepsy (Englot et al., 2016) and schizophrenia (Camchong et al., 2011; Venkataraman et al., 2012), or as disrupted connectivity, as seen following stroke (Grefkes & Fink, 2011) and in neurodegenerative diseases (Amboni et al., 2015). Our findings suggest that optogenetic inhibition can reduce excessive synchronization and decouple overactive network nodes, offering a potential strategy for suppressing pathological hyperconnectivity. Conversely, repeated excitatory stimulation led to progressive increases in

coherence, particularly in the theta frequency band often associated with long-range integration, indicating a therapeutic potential for strengthening communication between brain regions that have become functionally disconnected due to disease or injury. This dual capability, selectively weakening or strengthening targeted pathways, offers a powerful framework for restoring balanced connectivity in a circuit-specific manner.

Although optogenetic intervention is not yet clinically viable in the cortex due to the need for genetic modification and light delivery hardware implantation, the mechanistic insights gained from these studies provide valuable guidance for advancing other neuromodulation modalities. This includes invasive techniques such as intracortical microstimulation (ICMS) and noninvasive methods such as transcranial magnetic stimulation (TMS). The choice of stimulation modality and parameters should be informed by several factors: the anatomical location of the target area, the desired spatial and temporal resolution, tolerance for off-target effects, and most importantly, the intended direction of connectivity modulation. For instance, when large-scale suppression of network activity is needed, such as reducing pathological connectivity between a deep brain region and its projection areas, a well-established inhibitory TMS protocol termed continuous theta burst stimulation (cTBS) may be applied to transiently reduce neuronal excitability and induce LTD-like effects (Huang et al., 2005, 2011).

Meanwhile, achieving selective excitation of specific neuronal cell type without optogenetics remains challenging, although adjusting the frequency of stimulation may help facilitate the recruitment of particular populations. For example, higher frequency pulses (~100 Hz) tend to preferentially activate fast-spiking interneurons due to their rapid membrane kinetics and firing properties (Eles et al., 2021; Markram et al., 2004). In contrast, pyramidal neurons can be effectively engaged across a broader range of frequencies (10–100 Hz), depending on additional factors such as current amplitude, pulse width, and electrode depth or configuration (Lee et al., 2024; Tehovnik et al., 2006; Yazdan-Shahmorad, Lehmkuhle, et al., 2011). These stimulation parameters, together with electrode placement, determine the activation thresholds of different neuronal populations and thereby determine which cell type will be preferentially recruited during electrical stimulation. Understanding this selective recruitment is also important when designing brain stimulation therapies aimed at altering network synchronization in specific frequency bands, given the differential sensitivity of theta and gamma coherence to excitatory versus inhibitory modulation as demonstrated in our study. Ultimately, translating circuit-level insights from

optogenetic experiments into clinically viable strategies will be crucial for developing precise neuromodulation interventions tailored to specific disorders and patient needs.

Limitations and future directions

Although many neuromodulation studies have used the ratio of evoked responses between stimulated and surrounding sites as a proxy for network connectivity (Seeman et al., 2017; Yazdan-Shahmorad, Silversmith, et al., 2018), this approach was not optimal for our Jaws-mediated optogenetic inhibition experiments. Inhibitory stimulation does not reliably generate a secondary evoked potential, making it difficult to use trial-aligned responses to infer connectivity between sites. Instead, we quantified pairwise coherence between channels during spontaneous activity, which is easier to record and more generalizable across both experimental and clinical settings since it does not require additional stimulation pulses. Moreover, coherence has been shown to correlate well with evoked-response measures of connectivity (Yazdan-Shahmorad, Silversmith, et al., 2018). Nonetheless, coherence can also be influenced by session-specific factors such as baseline fluctuations, arousal level, and global brain state, which should be considered when interpreting its use as a measure of neural connectivity for future experiments involving different subjects or behavioral tasks.

Another important consideration for future work is the long-term stability of opsin expression. In our study, the epifluorescence signal from the initial injections declined over the course of two years, prompting us to perform a reinjection in one animal to enable additional experiments. Although significant light-evoked responses were observed before each experimental session, the duration of functional expression after each injection and the extent to which reinjection restored expression remain to be validated. These findings highlight the need for systematic, longitudinal approaches to track the changes in opsin expression, for example with weekly epifluorescence imaging or other chronic readouts. Developing reliable methods to monitor and sustain stable expression will be essential for chronic experiments and will directly inform the translational feasibility of optogenetic neuromodulation.

Finally, because of the open-loop nature of our optogenetic stimulation protocol and a lack of behavioral correlates during recordings, it remains unclear what specific mechanisms drive the session-to-session variability observed in certain frequency bands. A promising future direction is to incorporate phase-resolved analysis during optogenetic inhibition, as growing evidence from

brain stimulation studies suggests that the timing of stimulation pulse relative to the oscillatory phase can critically influence both the magnitude and direction of induced physiological and neuroplastic changes (Widge, 2024; Widge & Miller, 2019; Zanos et al., 2018). Future work can incorporate real-time phase estimation during inhibition blocks to assess whether coherence changes can be enhanced by aligning light pulses to specific phases of the ongoing rhythm. Additionally, designing closed-loop optogenetic paradigms that deliver lights at behaviorally or physiologically relevant time points may also help mitigate the variability observed across sessions, further informing how temporal alignment shapes targeted neuroplasticity. Such approaches would also improve the translational relevance of optogenetic stimulation, informing next-generation neuromodulation strategies that adapt in real time to ongoing brain dynamics of individual subjects.

Acknowledgement

We thank Toni Haun, Julien Bloch, Devon Griggs, Anne Pierce, Noah Stanis, and Felix Schwock for helping with animal care and chronic chamber maintenance. We thank Kacie Woodward, Christopher English, Britni Curtis, Sandi Thelen, and Amanda Heatherly for their support during surgeries and post-surgery care. Finally, we thank Makaha Harmon and Julien Bloch for their help with developing signal preprocessing pipelines using preliminary data not included in this work.

Chapter 4: Summary and Future Directions

Considerations for tailoring neuromodulation strategy

Designing effective neurostimulation methods to treat neurological conditions requires careful consideration of multiple parameters, including the choice between excitatory versus inhibitory paradigms, the timing and modality of stimulation, and the feasibility of translating these approaches into clinical settings. The previous two chapters of the dissertation highlight how these variables critically shape the outcomes of stimulation-based therapies, and thus should be investigated further to guide the development of targeted, patient-specific interventions.

First, we should consider the desired neuromodulatory direction. Excitatory paradigms, such as those utilizing electrical or optogenetic stimulation to increase excitability and induce neuronal firing, have been widely explored for their ability to strengthen functional connectivity and promote neuroplasticity. However, in pathological conditions characterized by hyperexcitability, such as acute stroke and epilepsy, inhibitory approaches may become more beneficial. In Chapter 2, we show that theta-burst stimulation can protect the ischemic tissues by suppressing post-stroke hyperactivity and reducing perilesional depolarization in the cortex. In Chapter 3, we demonstrate that optogenetic inhibition can effectively decouple targeted cortical regions, reducing gamma-band coherence across the network, contrasting with the effects of excitatory stimulation which enhances connectivity. These findings suggest that neuromodulation strategies must be tailored to the specific pathological context, and that inhibitory paradigms may offer greater therapeutic benefits during neural hyperactivity or excessive synchronization.

The timing of stimulation represents another critical consideration. In Chapter 2, we found that early application of electrical stimulation within hours after stroke onset leads to reduced neural excitability, inflammation, and lesion volume. These results emphasize the importance of intervening during the acute window when neural injury within the penumbra is still reversible. By contrast, stimulation in the subacute or chronic phases would require different parameters or targets to support long-term recovery. For example, to improve motor performance during chronic stroke (weeks to months after onset), excitatory stimulation strategies such as those discussed in Chapter 3 can be beneficial for targeting the ipsilesional cortex to increase excitability, promote neuroplasticity, and restore lost connections (Boonzaier et al., 2018;

Edwardson et al., 2013). This temporal difference indicates that neuromodulation strategies should adapt dynamically to the injury stage and rehabilitation progress, shifting from acute neuroprotection to chronic network reorganization (Figure 13) to maximize functional recovery.

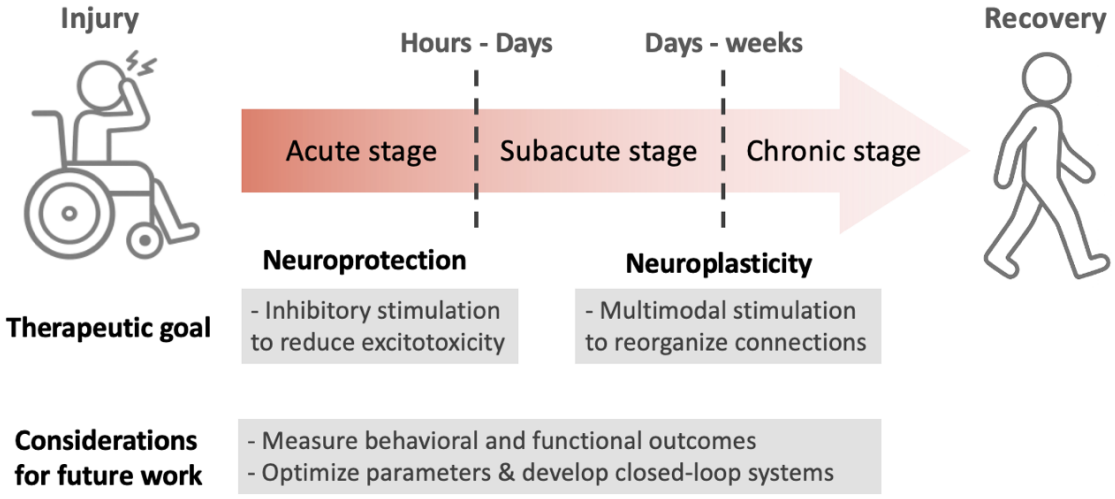

Figure 13. Key considerations for developing tailored neuromodulation therapies. Acute stage interventions should target neuroprotection via inhibitory paradigms that mitigates excitotoxicity, with future work centered on behavioral and functional outcome measures. Interventions in the subacute to chronic stage should promote neuroplasticity and network reorganization, supported by future development of closed-loop systems that adapt to dynamic brain states.

When considering stimulation modality, electrical and optogenetic approaches each offer distinct advantages. Electrical stimulation is clinically established, versatile, and straightforward to apply from the surface of the brain, making it well-suited for acute interventions and broad cortical modulation. On the other hand, optogenetic stimulation provides cell-type-specific and spatially precise control of neural activity, offering a level of selectivity not achievable with electrical methods. Our demonstration of stable opsin expression and consistent light-evoked responses over several months in the primate cortex also supports the feasibility of implementing complex optogenetic tools in large brains similar to those of humans. However, translating these invasive tools into clinical use will require further advancements in gene-delivery systems and optical stimulation hardware to satisfy patient safety and regulatory standards. Nonetheless, insights gained from this dissertation can be validated and extended using clinically approved, non-invasive neuromodulation techniques such as TMS or focused ultrasound stimulation. These approaches could potentially allow us to target broader or deeper brain regions, laying the groundwork for developing next-generation neuromodulation therapies tailored to a variety of neurological conditions.

Future research directions for stimulation-based therapy

Evaluation of stimulation effects in the subacute phase after stroke

Building on the findings of this dissertation, future research should further explore the therapeutic potential of stimulation-based interventions in ischemic stroke and other neural injuries. One key direction involves evaluating post-stroke and post-stimulation physiology at approximately one to two weeks after stroke onset, to capture both the progression of injury and the early stages of recovery. While our results show that early stimulation within hours of injury reduced acute hyperexcitability, it remains unclear whether this intervention could retain neuroprotective benefits and improve neurological outcomes beyond the acute window. Additionally, many cellular markers of glutamate-mediated excitotoxicity and neuroinflammation only become detectable after ~24 hours (Belov Kirdajova et al., 2020; Rawlinson et al., 2020), highlighting the importance of evaluating these delayed injury responses. Together, electrophysiological and histological analyses at these later stages will be essential to determine how cortical excitability, inflammation, and circuit integrity evolve over time, and whether targeted stimulation continues to mitigate secondary damage or supports a more favorable environment for recovery.

Behavioral response to neurophysiological changes

In parallel, chronic behavioral studies are essential to directly evaluate the long-term impact of early stimulation on sensorimotor function (Figure 13). While our acute experiments suggest that stimulation can reduce infarct size and mitigate excitotoxicity, it remains critical to determine whether these neuroprotective effects lead to significant behavioral improvements, an important step in assessing the clinical relevance of our proposed intervention. By training monkeys to perform motor tasks (e.g., center-out reaching) that engage the affected brain regions, and monitoring performance over time in groups receiving early or sham stimulation, we can establish a more causal relationship between acute stimulation and functional outcomes. Additionally, novel behavioral paradigms can also be developed to probe the effects of optogenetic modulation and altered PPC connectivity on sensory, motor, and cognitive functions, particularly in tasks requiring hand-eye coordination and sensorimotor integration (Andersen et al., 1997; Freedman & Ibos, 2018). These future studies will provide crucial insights into how specific stimulation protocols can be implemented to facilitate rehabilitation, offering a framework for developing neuromodulation strategies aligned with patient-specific therapeutic needs.

Optimizing the spatial scale of stimulation effects

Another important future direction of this work involves systematically exploring the parameter space to optimize the spatial resolution and extent of stimulation-induced effects. Both electrical and optogenetic strategies modulate neural activity across different spatial scales, influenced by factors such as electrode size and placement (e.g., surface vs. intracortical) for electrical stimulation, as well as targeted cell types, opsin kinetics, and light delivery methods for optogenetic approaches. In both modalities, parameters such as pulse amplitude, frequency, and duration each plays a critical role in determining the spread and magnitude of neural activation or suppression, thus affecting the induced changes in network excitability and neuroplasticity. A deeper understanding of how these variables interact will be essential for tailoring brain stimulation to specific therapeutic goals while minimizing off-target effects. For instance, focal inhibition may be ideal for treating localized hyperexcitability, whereas stimulation that generates broader electric fields may be more appropriate for deep injuries or for promoting large-scale network reorganization during recovery. Given the huge parameter space, it may not be feasible to systematically test every possible combination experimentally. However, large-scale and high-density neural recordings paired with computational modeling can provide efficient ways to characterize and predict the spatial profiles of different stimulation protocols. In the future, these tools can help identify parameters that balance specificity and efficacy depending on the physiological context, enabling the design of safe neuromodulation strategies tailored to the needs of specific brain disorders.

Development of closed-loop systems

Finally, an important next step toward tailoring neuromodulation therapies is the development of closed-loop stimulation systems that utilize real-time neurophysiological feedback to adjust stimulation timing, location, and parameters. For example, future studies could explore phase-locked or activity-triggered optogenetic protocols that deliver precisely timed pulses aligned with specific oscillatory phases or network states. Similar approaches in clinical brain stimulation techniques, such as DBS and TMS protocols, have been shown to enhance stimulation efficacy and modulate local oscillations (Widge, 2024; Zrenner et al., 2018), leading to more consistent therapeutic outcomes while minimizing off-target effects. In the context of ischemic injury, closed-loop strategies could adapt to the evolving needs of damaged neural tissues, applying inhibitory paradigms to suppress local hyperactivity during acute phases and then transitioning

to excitatory protocols in the subacute stage to promote neuroplasticity and recovery (Figure 13). In such systems, the sensing component would distinguish between states of excessive activity and reduced neural response, dynamically adjusting the stimulation mode to match the brain's condition. When combined with the optimized spatial targeting discussed earlier, this technology could pave the path for precision neuromodulation therapies, where stimulation parameters are continuously adapted not only to the stage of injury but also to millisecond-scale dynamics unique to each patient's network physiology. By aligning novel stimulation paradigms with the brain's continuously changing functional state, these closed-loop approaches have the potential to maximize therapeutic efficacy, minimize unintended effects, and actively guide the brain toward functional recovery. Ultimately, these advances could transform neuromodulation therapy from a static intervention into a dynamic, personalized tool for promoting neural repair and improving rehabilitation outcomes.

References

Adams, H. P., Bendixen, B. H., Kappelle, L. J., Biller, J., Love, B. B., Gordon, D. L., & Marsh, E. E. (1993). Classification of subtype of acute ischemic stroke. Definitions for use in a multicenter clinical trial. TOAST. Trial of Org 10172 in Acute Stroke Treatment. *Stroke*, *24*(1), 35–41. https://doi.org/10.1161/01.STR.24.1.35

Adkins-Muir, D. L., & Jones, T. A. (2003). Cortical electrical stimulation combined with rehabilitative training: Enhanced functional recovery and dendritic plasticity following focal cortical ischemia in rats. *Neurological Research*, *25*(8), 780–788. https://doi.org/10.1179/016164103771953853

Allen, C. B., Celikel, T., & Feldman, D. E. (2003). Long-term depression induced by sensory deprivation during cortical map plasticity in vivo. *Nature Neuroscience*, *6*(3), 291–299. https://doi.org/10.1038/nn1012

Amboni, M., Tessitore, A., Esposito, F., Santangelo, G., Picillo, M., Vitale, C., Giordano, A., Erro, R., de Micco, R., Corbo, D., Tedeschi, G., & Barone, P. (2015). Resting-state functional connectivity associated with mild cognitive impairment in Parkinson's disease. *Journal of Neurology*, *262*(2), 425–434. https://doi.org/10.1007/s00415-014-7591-5

Andersen, R. A., Snyder, L. H., Bradley, D. C., & Xing, J. (1997). Multimodal representation of space in the posterior partietal cortex and its use in planning movements. *Annual Review of Neuroscience*, *20*, 303–330.

Aravanis, A. M., Wang, L.-P., Zhang, F., Meltzer, L. A., Mogri, M. Z., Schneider, M. B., & Deisseroth, K. (2007). An optical neural interface: In vivo control of rodent motor cortex with integrated fiberoptic and optogenetic technology. *Journal of Neural Engineering*, *4*(3), S143. https://doi.org/10.1088/1741-2560/4/3/S02

Arsava, E. M., Topcuoglu, M. A., Ay, I., Ozdemir, A. O., Gungor, I. L., Togay Isikay, C., Nazliel, B., Kozak, H. H., Ozturk, S., Yilmaz, İ. A., Dora, B., Ay, H., Unal, A., Ozel, T., Sorgun, M. H., Bahadır, E. A., Peker, E., Aykac, O., Mehdiyev, Z., … McClure, C. (2022). Assessment of safety and feasibility of non-invasive vagus nerve stimulation for treatment of acute stroke. *Brain Stimulation*, *15*(6), 1467–1474. https://doi.org/10.1016/j.brs.2022.10.012

Baba, T., Kameda, M., Yasuhara, T., Morimoto, T., Kondo, A., Shingo, T., Tajiri, N., Wang, F., Miyoshi, Y., Borlongan, C. V., Matsumae, M., & Date, I. (2009). Electrical Stimulation of the Cerebral Cortex Exerts Antiapoptotic, Angiogenic, and Anti-Inflammatory Effects in Ischemic Stroke Rats Through Phosphoinositide 3-Kinase/Akt Signaling Pathway. *Stroke*, *40*(11), e598–e605. https://doi.org/10.1161/STROKEAHA.109.563627

Bahr Hosseini, M., Hou, J., Bikson, M., Iacoboni, M., Gornbein, J., & Saver, J. L. (2019). Central Nervous System Electrical Stimulation for Neuroprotection in Acute Cerebral Ischemia. *Stroke*, *50*(10), 2892–2901. https://doi.org/10.1161/STROKEAHA.119.025364

Bao, S., Khan, A., Song, R., & Kai-yu Tong, R. (2020). Rewiring the Lesioned Brain: Electrical Stimulation for Post-Stroke Motor Restoration. *Journal of Stroke*, *22*(1), 47–63. https://doi.org/10.5853/jos.2019.03027

Barros, V. N., Mundim, M., Galindo, L. T., Bittencourt, S., Porcionatto, M., & Mello, L. E. (2015). The pattern of c-Fos expression and its refractory period in the brain of rats and monkeys. *Frontiers in Cellular Neuroscience*, *9*. https://www.frontiersin.org/articles/10.3389/fncel.2015.00072

Belov Kirdajova, D., Kriska, J., Tureckova, J., & Anderova, M. (2020). Ischemia-Triggered Glutamate Excitotoxicity From the Perspective of Glial Cells. *Frontiers in Cellular Neuroscience*, *14*. https://www.frontiersin.org/articles/10.3389/fncel.2020.00051

Bender, K. J., Allen, C. B., Bender, V. A., & Feldman, D. E. (2006). Synaptic Basis for Whisker Deprivation-Induced Synaptic Depression in Rat Somatosensory Cortex. *Journal of Neuroscience*, *26*(16), 4155–4165. https://doi.org/10.1523/JNEUROSCI.0175-06.2006

Beurrier, C., Bioulac, B., Audin, J., & Hammond, C. (2001). High-Frequency Stimulation Produces a Transient Blockade of Voltage-Gated Currents in Subthalamic Neurons. *Journal of Neurophysiology*, *85*(4), 1351–1356. https://doi.org/10.1152/jn.2001.85.4.1351

Bezaire, M. J., Raikov, I., Burk, K., Vyas, D., & Soltesz, I. (2016). Interneuronal mechanisms of hippocampal theta oscillations in a full-scale model of the rodent CA1 circuit. *eLife*, *5*, e18566. https://doi.org/10.7554/eLife.18566

Bi, G., & Poo, M. (1998). Synaptic Modifications in Cultured Hippocampal Neurons: Dependence on Spike Timing, Synaptic Strength, and Postsynaptic Cell Type. *Journal of Neuroscience*, *18*(24), 10464–10472.

Bloch, J., Greaves-Tunnell, A., Shea-Brown, E., Harchaoui, Z., Shojaie, A., & Yazdan-Shahmorad, A. (2022). Network structure mediates functional reorganization induced by optogenetic stimulation of non-human primate sensorimotor cortex. *iScience*, *25*(5). https://doi.org/10.1016/j.isci.2022.104285

Boonzaier, J., van Tilborg, G. A. F., Neggers, S. F. W., & Dijkhuizen, R. M. (2018). Noninvasive Brain Stimulation to Enhance Functional Recovery After Stroke: Studies in Animal Models. *Neurorehabilitation and Neural Repair*, *32*(11), 927–940. https://doi.org/10.1177/1545968318804425

Bowyer, S. M. (2016). Coherence a measure of the brain networks: Past and present. *Neuropsychiatric Electrophysiology*, *2*(1), 1. https://doi.org/10.1186/s40810-015-0015-7

Boyden, E. S., Zhang, F., Bamberg, E., Nagel, G., & Deisseroth, K. (2005). Millisecond-timescale, genetically targeted optical control of neural activity. *Nature Neuroscience*, *8*(9), Article 9. https://doi.org/10.1038/nn1525

Brasil, S., Chesnut, R., & Robba, C. (2024). Noninvasive neuromonitoring in acute brain injured patients. *Intensive Care Medicine*, *50*(6), 960–963. https://doi.org/10.1007/s00134-024-07406-7

Brott, T., & Bogousslavsky, J. (2000). Treatment of Acute Ischemic Stroke. *New England Journal of Medicine*, *343*(10), 710–722. https://doi.org/10.1056/NEJM200009073431007

Buetefisch, C. M., Wei, L., Gu, X., Epstein, C. M., & Yu, S. P. (2023). Neuroprotection of Low-Frequency Repetitive Transcranial Magnetic Stimulation after Ischemic Stroke in Rats. *Annals of Neurology*, *93*(2), 336–347. https://doi.org/10.1002/ana.26509

Butler, T. L., & Pennypacker, K. R. (2004). Temporal and regional expression of Fos-related proteins in response to ischemic injury. *Brain Research Bulletin*, *63*(1), 65–73. https://doi.org/10.1016/j.brainresbull.2003.12.005

Buzsáki, G., Anastassiou, C. A., & Koch, C. (2012). The origin of extracellular fields and currents—EEG, ECoG, LFP and spikes. *Nature Reviews Neuroscience*, *13*(6), 407–420. https://doi.org/10.1038/nrn3241

Buzsáki, G., & Wang, X.-J. (2012). Mechanisms of Gamma Oscillations. *Annual Review of Neuroscience*, *35*, 203–225. https://doi.org/10.1146/annurev-neuro-062111-150444

Camchong, J., MacDonald, A. W., III, Bell, C., Mueller, B. A., & Lim, K. O. (2011). Altered Functional and Anatomical Connectivity in Schizophrenia. *Schizophrenia Bulletin*, *37*(3), 640–650. https://doi.org/10.1093/schbul/sbp131

Caporale, N., & Dan, Y. (2008). Spike Timing–Dependent Plasticity: A Hebbian Learning Rule. *Annual Review of Neuroscience*, *31*(1), 25–46. https://doi.org/10.1146/annurev.neuro.31.060407.125639

Cardin, J. A. (2018). Inhibitory Interneurons Regulate Temporal Precision and Correlations in Cortical Circuits. *Trends in Neurosciences*, *41*(10), 689–700. https://doi.org/10.1016/j.tins.2018.07.015

Cavada, C., & Goldman-Rakic, P. S. (1989). Posterior parietal cortex in rhesus monkey: I. Parcellation of areas based on distinctive limbic and sensory corticocortical connections. *Journal of Comparative Neurology*, *287*(4), 393–421. https://doi.org/10.1002/cne.902870402

Chamorro, Á., Dirnagl, U., Urra, X., & Planas, A. M. (2016). Neuroprotection in acute stroke: Targeting excitotoxicity, oxidative and nitrosative stress, and inflammation. *The Lancet Neurology*, *15*(8), 869–881. https://doi.org/10.1016/S1474-4422(16)00114-9

Chen, C.-L., Tang, F.-T., Chen, H.-C., Chung, C.-Y., & Wong, M.-K. (2000). Brain lesion size and location: Effects on motor recovery and functional outcome in stroke patients. *Archives of Physical Medicine and Rehabilitation*, *81*(4), 447–452. https://doi.org/10.1053/mr.2000.3837

Cheng, Y. D., Al-Khoury, L., & Zivin, J. A. (2004). *Neuroprotection for ischemic stroke: Two decades of success and failure*. *1*(1), 10.

Chung, S. W., Hill, A. T., Rogasch, N. C., Hoy, K. E., & Fitzgerald, P. B. (2016). Use of theta-burst stimulation in changing excitability of motor cortex: A systematic review and meta-analysis. *Neuroscience & Biobehavioral Reviews*, *63*, 43–64. https://doi.org/10.1016/j.neubiorev.2016.01.008

Chuong, A. S., Miri, M. L., Busskamp, V., Matthews, G. A. C., Acker, L. C., Sørensen, A. T., Young, A., Klapoetke, N. C., Henninger, M. A., Kodandaramaiah, S. B., Ogawa, M., Ramanlal, S. B., Bandler, R. C., Allen, B. D., Forest, C. R., Chow, B. Y., Han, X., Lin, Y., Tye, K. M., … Boyden, E. S. (2014). Noninvasive optical inhibition with a red-shifted microbial rhodopsin. *Nature Neuroscience*, *17*(8), 1123–1129. https://doi.org/10.1038/nn.3752

Cole, E. J., Phillips, A. L., Bentzley, B. S., Stimpson, K. H., Nejad, R., Barmak, F., Veerapal, C., Khan, N., Cherian, K., Felber, E., Brown, R., Choi, E., King, S., Pankow, H., Bishop, J. H., Azeez, A., Coetzee, J., Rapier, R., Odenwald, N., … Williams, N. R. (2022). Stanford Neuromodulation Therapy (SNT): A Double-Blind Randomized Controlled Trial. *American Journal of Psychiatry*, *179*(2), 132–141. https://doi.org/10.1176/appi.ajp.2021.20101429

Cook, D. J., & Tymianski, M. (2011). Translating promising preclinical neuroprotective therapies to human stroke trials. *Expert Review of Cardiovascular Therapy*, *9*(4), 433–449. https://doi.org/10.1586/erc.11.34

Corbetta, M., Ramsey, L., Callejas, A., Baldassarre, A., Hacker, C. D., Siegel, J. S., Astafiev, S. V., Rengachary, J., Zinn, K., Lang, C. E., Connor, L. T., Fucetola, R., Strube, M., Carter, A. R., & Shulman, G. L. (2015). Common behavioral clusters and subcortical anatomy in stroke. *Neuron*, *85*(5), 927–941. https://doi.org/10.1016/j.neuron.2015.02.027

Coscia, M., Wessel, M. J., Chaudary, U., Millán, J. del R., Micera, S., Guggisberg, A., Vuadens, P., Donoghue, J., Birbaumer, N., & Hummel, F. C. (2019). Neurotechnology-aided interventions for upper limb motor rehabilitation in severe chronic stroke. *Brain*, *142*(8), 2182–2197. https://doi.org/10.1093/brain/awz181

Danton, G. H., & Dietrich, W. D. (2004). The Search for Neuroprotective Strategies in Stroke. *American Journal of Neuroradiology*, *25*(2), 181–194.

Dayan, E., Censor, N., Buch, E. R., Sandrini, M., & Cohen, L. G. (2013). Noninvasive brain stimulation: From physiology to network dynamics and back. *Nature Neuroscience*, *16*(7), 838–844. https://doi.org/10.1038/nn.3422

Deliano, M., Scheich, H., & Ohl, F. W. (2009). Auditory Cortical Activity after Intracortical Microstimulation and Its Role for Sensory Processing and Learning. *Journal of Neuroscience*, *29*(50), 15898–15909. https://doi.org/10.1523/JNEUROSCI.1949-09.2009

Dohmen, C., Sakowitz, O. W., Fabricius, M., Bosche, B., Reithmeier, T., Ernestus, R.-I., Brinker, G., Dreier, J. P., Woitzik, J., Strong, A. J., & Graf, R. (2008). Spreading depolarizations occur in human ischemic stroke with high incidence. *Annals of Neurology*, *63*(6), 720–728. https://doi.org/10.1002/ana.21390

Dreier, J. P. (2011). The role of spreading depression, spreading depolarization and spreading ischemia in neurological disease. *Nature Medicine*, *17*(4), Article 4. https://doi.org/10.1038/nm.2333

Dubey, A., & Ray, S. (2020). Comparison of tuning properties of gamma and high-gamma power in local field potential (LFP) versus electrocorticogram (ECoG) in visual cortex. *Scientific Reports*, *10*(1), Article 1. https://doi.org/10.1038/s41598-020-61961-9

Duering, M., Righart, R., Csanadi, E., Jouvent, E., Hervé, D., Chabriat, H., & Dichgans, M. (2012). Incident subcortical infarcts induce focal thinning in connected cortical regions. *Neurology*, *79*(20), 2025–2028. https://doi.org/10.1212/WNL.0b013e3182749f39

Edwardson, M. A., Lucas, T. H., Carey, J. R., & Fetz, E. E. (2013). New modalities of brain stimulation for stroke rehabilitation. *Experimental Brain Research*, *224*(3), 335–358. https://doi.org/10.1007/s00221-012-3315-1

El Hady, A., Afshar, G., Broeking, K., Schlüter, O., Geisel, T., Stühmer, W., & Wolf, F. (2013). Optogenetic stimulation effectively enhances intrinsically generated network synchrony. *Frontiers in Neural Circuits*, *7*. https://doi.org/10.3389/fncir.2013.00167

Eles, J. R., Stieger, K. C., & Kozai, T. D. Y. (2021). The temporal pattern of intracortical microstimulation pulses elicits distinct temporal and spatial recruitment of cortical neuropil and neurons. *Journal of Neural Engineering*, *18*(1), 015001. https://doi.org/10.1088/1741-2552/abc29c

El-Shamayleh, Y., & Horwitz, G. D. (2019). Primate optogenetics: Progress and prognosis. *Proceedings of the National Academy of Sciences*, *116*(52), 26195–26203. https://doi.org/10.1073/pnas.1902284116

Englot, D. J., Konrad, P. E., & Morgan, V. L. (2016). Regional and global connectivity disturbances in focal epilepsy, related neurocognitive sequelae, and potential mechanistic underpinnings. *Epilepsia*, *57*(10), 1546–1557. https://doi.org/10.1111/epi.13510

Fabricius, M., Fuhr, S., Willumsen, L., Dreier, J. P., Bhatia, R., Boutelle, M. G., Hartings, J. A., Bullock, R., Strong, A. J., & Lauritzen, M. (2008). Association of seizures with cortical spreading depression and peri-infarct depolarisations in the acutely injured human brain. *Clinical Neurophysiology*, *119*(9), 1973–1984. https://doi.org/10.1016/j.clinph.2008.05.025

Fan, J., Li, Y., Fu, X., Li, L., Hao, X., & Li, S. (2017). Nonhuman primate models of focal cerebral ischemia. *Neural Regeneration Research*, *12*(2), 321–328. https://doi.org/10.4103/1673-5374.200815

Fan, Y., Deng, P., Wang, Y.-C., Lu, H.-C., Xu, Z. C., & Schulz, P. E. (2008). Transient cerebral ischemia increases CA1 pyramidal neuron excitability. *Experimental Neurology*, *212*(2), 415–421. https://doi.org/10.1016/j.expneurol.2008.04.032

Feigin, V. L., Nichols, E., Alam, T., Bannick, M. S., Beghi, E., Blake, N., Culpepper, W. J., Dorsey, E. R., Elbaz, A., Ellenbogen, R. G., Fisher, J. L., Fitzmaurice, C., Giussani, G., Glennie, L., James, S. L., Johnson, C. O., Kassebaum, N. J., Logroscino, G., Marin, B., … Vos, T. (2019). Global, regional, and national burden of neurological disorders, 1990–2016: A systematic analysis for the Global

Burden of Disease Study 2016. *The Lancet Neurology*, *18*(5), 459–480. https://doi.org/10.1016/S1474-4422(18)30499-X

Feigin, V. L., Stark, B. A., Johnson, C. O., Roth, G. A., Bisignano, C., Abady, G. G., Abbasifard, M., Abbasi-Kangevari, M., Abd-Allah, F., Abedi, V., Abualhasan, A., Abu-Rmeileh, N. M., Abushouk, A. I., Adebayo, O. M., Agarwal, G., Agasthi, P., Ahinkorah, B. O., Ahmad, S., Ahmadi, S., … Murray, C. J. L. (2021). Global, regional, and national burden of stroke and its risk factors, 1990–2019: A systematic analysis for the Global Burden of Disease Study 2019. *The Lancet Neurology*, *20*(10), 795–820. https://doi.org/10.1016/S1474-4422(21)00252-0

Feldman, D. E. (2009). Synaptic Mechanisms for Plasticity in Neocortex. *Annual Review of Neuroscience*, *32*(Volume 32, 2009), 33–55. https://doi.org/10.1146/annurev.neuro.051508.135516

Feldman, D. E. (2012). The Spike-Timing Dependence of Plasticity. *Neuron*, *75*(4), 556–571. https://doi.org/10.1016/j.neuron.2012.08.001

Fernandez, M., Pirondi, S., Antonelli, T., Ferraro, L., Giardino, L., & Calzà, L. (2005). Role of c-Fos protein on glutamate toxicity in primary neural hippocampal cells. *Journal of Neuroscience Research*, *82*(1), 115–125. https://doi.org/10.1002/jnr.20608

Fitzpatrick, D., Lund, J. S., Schmechel, D. E., & Towles, A. C. (1987). Distribution of GABAergic neurons and axon terminals in the macaque striate cortex. *Journal of Comparative Neurology*, *264*(1), 73–91. https://doi.org/10.1002/cne.902640107

Fox, P., Mithal, D. S., Somogyi, J. R., Vien, A. C., Sanchez, R. M., & Koh, S. (2020). Dexamethasone after early-life seizures attenuates increased susceptibility to seizures, seizure-induced microglia activation and neuronal injury later in life. *Neuroscience Letters*, *728*, 134953. https://doi.org/10.1016/j.neulet.2020.134953

Freedman, D. J., & Ibos, G. (2018). An Integrative Framework for Sensory, Motor, and Cognitive Functions of the Posterior Parietal Cortex. *Neuron*, *97*(6), 1219–1234. https://doi.org/10.1016/j.neuron.2018.01.044

Garcia, L., D'Alessandro, G., Bioulac, B., & Hammond, C. (2005). High-frequency stimulation in Parkinson's disease: More or less? *Trends in Neurosciences*, *28*(4), 209–216. https://doi.org/10.1016/j.tins.2005.02.005

Ginsberg, M. D. (2008). Neuroprotection for ischemic stroke: Past, present and future. *Neuropharmacology*, *55*(3), 363–389. https://doi.org/10.1016/j.neuropharm.2007.12.007

Gittins, R., & Harrison, P. J. (2004). Neuronal density, size and shape in the human anterior cingulate cortex: A comparison of Nissl and NeuN staining. *Brain Research Bulletin*, *63*(2), 155–160. https://doi.org/10.1016/j.brainresbull.2004.02.005

Gouwens, N. W., Zeberg, H., Tsumoto, K., Tateno, T., Aihara, K., & Robinson, H. P. C. (2010). Synchronization of Firing in Cortical Fast-Spiking Interneurons at Gamma Frequencies: A Phase-

Resetting Analysis. *PLOS Computational Biology*, *6*(9), e1000951. https://doi.org/10.1371/journal.pcbi.1000951

Green, A. R., Hainsworth, A. H., & Jackson, D. M. (2000). GABA potentiation: A logical pharmacological approach for the treatment of acute ischaemic stroke. *Neuropharmacology*, *39*(9), 1483–1494. https://doi.org/10.1016/S0028-3908(99)00233-6

Green, T. R. F., Murphy, S. M., & Rowe, R. K. (2022). Comparisons of quantitative approaches for assessing microglial morphology reveal inconsistencies, ecological fallacy, and a need for standardization. *Scientific Reports*, *12*(1), Article 1. https://doi.org/10.1038/s41598-022-23091-2

Grefkes, C., & Fink, G. R. (2011). Reorganization of cerebral networks after stroke: New insights from neuroimaging with connectivity approaches. *Brain*, *134*(5), 1264–1276. https://doi.org/10.1093/brain/awr033

Griggs, D., Belloir, T., Zhou, J., & Yazdan-Shahmorad, A. (2023). Convection Enhanced Delivery of Viral Vectors. In M. A. G. Eldridge & A. Galvan (Eds.), *Vectorology for Optogenetics and Chemogenetics* (pp. 223–244). Springer US. https://doi.org/10.1007/978-1-0716-2918-5_12

Griggs, D. J., Bloch, J., Fisher, S., Ojemann, W. K. S., Coubrough, K. M., Khateeb, K., Chu, M., & Yazdan-Shahmorad, A. (2022). Demonstration of an Optimized Large-scale Optogenetic Cortical Interface for Non-human Primates. *2022 44th Annual International Conference of the IEEE Engineering in Medicine & Biology Society (EMBC)*, 3081–3084. https://doi.org/10.1109/EMBC48229.2022.9871332

Griggs, D. J., Bloch, J., Stanis, N., Zhou, J., Fisher, S., Jahanian, H., & Yazdan-Shahmorad, A. (2024). A large-scale optogenetic neurophysiology platform for improving accessibility in NHP behavioral experiments. *bioRxiv*, 2024.06.25.600719. https://doi.org/10.1101/2024.06.25.600719

Griggs, D. J., Garcia, A. D., Au, W. Y., Ojemann, W. K. S., Johnson, A. G., Ting, J. T., Buffalo, E. A., & Yazdan-Shahmorad, A. (2022). Improving the Efficacy and Accessibility of Intracranial Viral Vector Delivery in Non-Human Primates. *Pharmaceutics*, *14*(7), Article 7. https://doi.org/10.3390/pharmaceutics14071435

Griggs, D. J., Khateeb, K., Philips, S. A., Chan, J. W., Ojemann, W. K. S., & Yazdan-Shahmorad, A. (2019). Optimized large-scale optogenetic interface for non-human primates. *Optogenetics and Optical Manipulation 2019*, *10866*, 7–15. https://doi.org/10.1117/12.2511317

Griggs, D. J., Khateeb, K., Zhou, J., Liu, T., Wang, R., & Yazdan-Shahmorad, A. (2021a). Multi-modal artificial dura for simultaneous large-scale optical access and large-scale electrophysiology in non-human primate cortex. *Journal of Neural Engineering*, *18*(5), 055006. https://doi.org/10.1088/1741-2552/abf28d

Griggs, D. J., Khateeb, K., Zhou, J., Liu, T., Wang, R., & Yazdan-Shahmorad, A. (2021b). Multi-modal artificial dura for simultaneous large-scale optical access and large-scale electrophysiology in

non-human primate cortex. *Journal of Neural Engineering*, *18*(5), 055006. https://doi.org/10.1088/1741-2552/abf28d

Harquel, S., Cadic-Melchior, A., Morishita, T., Fleury, L., Witon, A., Ceroni, M., Brügger, J., Meyer, N. H., Evangelista, G. G., Egger, P., Beanato, E., Menoud, P., Van de Ville, D., Micera, S., Blanke, O., Léger, B., Adolphsen, J., Jagella, C., Constantin, C., … Hummel, F. C. (2024). Stroke Recovery–Related Changes in Cortical Reactivity Based on Modulation of Intracortical Inhibition. *Stroke*, *55*(6), 1629–1640. https://doi.org/10.1161/STROKEAHA.123.045174

Hebb, D. O. (2002). *The Organization of Behavior: A Neuropsychological Theory*. Psychology Press. https://doi.org/10.4324/9781410612403

Hermann, D. M., Kilic, E., Hata, R., Hossmann, K.-A., & Mies, G. (2001). Relationship between metabolic dysfunctions, gene responses and delayed cell death after mild focal cerebral ischemia in mice. *Neuroscience*, *104*(4), 947–955. https://doi.org/10.1016/S0306-4522(01)00125-7

Herrera, D. G., & Robertson, H. A. (1996). Activation of c-fos in the brain. *Progress in Neurobiology*, *50*(2), 83–107. https://doi.org/10.1016/S0301-0082(96)00021-4

Hillary, F. G., & Grafman, J. H. (2017). Injured Brains and Adaptive Networks: The Benefits and Costs of Hyperconnectivity. *Trends in Cognitive Sciences*, *21*(5), 385–401. https://doi.org/10.1016/j.tics.2017.03.003

Hinman, J. D., Rasband, M. N., & Carmichael, S. T. (2013). Remodeling of the Axon Initial Segment After Focal Cortical and White Matter Stroke. *Stroke*, *44*(1), 182–189. https://doi.org/10.1161/STROKEAHA.112.668749

Hsu, W.-Y., Cheng, C.-H., Liao, K.-K., Lee, I.-H., & Lin, Y.-Y. (2012). Effects of Repetitive Transcranial Magnetic Stimulation on Motor Functions in Patients With Stroke. *Stroke*, *43*(7), 1849–1857. https://doi.org/10.1161/STROKEAHA.111.649756

Huang, Y.-Z., Edwards, M. J., Rounis, E., Bhatia, K. P., & Rothwell, J. C. (2005). Theta Burst Stimulation of the Human Motor Cortex. *Neuron*, *45*(2), 201–206. https://doi.org/10.1016/j.neuron.2004.12.033

Huang, Y.-Z., Rothwell, J. C., Chen, R.-S., Lu, C.-S., & Chuang, W.-L. (2011). The theoretical model of theta burst form of repetitive transcranial magnetic stimulation. *Clinical Neurophysiology*, *122*(5), 1011–1018. https://doi.org/10.1016/j.clinph.2010.08.016

Hummel, F. C., & Cohen, L. G. (2006). Non-invasive brain stimulation: A new strategy to improve neurorehabilitation after stroke? *The Lancet Neurology*, *5*(8), 708–712. https://doi.org/10.1016/S1474-4422(06)70525-7

Hutchison, R. M., Womelsdorf, T., Gati, J. S., Everling, S., & Menon, R. S. (2013). Resting-state networks show dynamic functional connectivity in awake humans and anesthetized macaques. *Human Brain Mapping*, *34*(9), 2154–2177. https://doi.org/10.1002/hbm.22058

Huynh, W., Vucic, S., Krishnan, A. V., Lin, C. S.-Y., & Kiernan, M. C. (2016). Exploring the Evolution of Cortical Excitability Following Acute Stroke. *Neurorehabilitation and Neural Repair*, *30*(3), 244–257. https://doi.org/10.1177/1545968315593804

Iritani, R., Belloir, T., Griggs, D. J., Ip, Z., Anderson, Z., & Yazdan-Shahmorad, A. (2024). A Neural Implant Design Toolbox for Nonhuman Primates. *Journal of Visualized Experiments : JoVE*, *204*, 10.3791/66167. https://doi.org/10.3791/66167

Jiang, J., Truong, D. Q., Esmaeilpour, Z., Huang, Y., Badran, B. W., & Bikson, M. (2020). Enhanced tES and tDCS computational models by meninges emulation. *Journal of Neural Engineering*, *17*(1), 016027. https://doi.org/10.1088/1741-2552/ab549d

Jurga, A. M., Paleczna, M., & Kuter, K. Z. (2020). Overview of General and Discriminating Markers of Differential Microglia Phenotypes. *Frontiers in Cellular Neuroscience*, *14*. https://www.frontiersin.org/articles/10.3389/fncel.2020.00198

Kang, D.-W., Chalela, J. A., Ezzeddine, M. A., & Warach, S. (2003). Association of Ischemic Lesion Patterns on Early Diffusion-Weighted Imaging With TOAST Stroke Subtypes. *Archives of Neurology*, *60*(12), 1730–1734. https://doi.org/10.1001/archneur.60.12.1730

Kempter, R., Gerstner, W., & van Hemmen, J. L. (1999). Hebbian learning and spiking neurons. *Physical Review E*, *59*(4), 4498–4514. https://doi.org/10.1103/PhysRevE.59.4498

Khanna, P., Totten, D., Novik, L., Roberts, J., Morecraft, R. J., & Ganguly, K. (2021). Low-frequency stimulation enhances ensemble co-firing and dexterity after stroke. *Cell*, *184*(4), 912-930.e20. https://doi.org/10.1016/j.cell.2021.01.023

Khateeb, K., Bloch, J., Zhou, J., Rahimi, M., Griggs, D. J., Kharazia, V. N., Le, M. N., Wang, R. K., & Yazdan-Shahmorad, A. (2022). A versatile toolbox for studying cortical physiology in primates. *Cell Reports Methods*, *2*(3), 100183. https://doi.org/10.1016/j.crmeth.2022.100183

Khateeb, K., Griggs, D. J., Sabes, P. N., & Yazdan-Shamorad, A. (2019). Convection Enhanced Delivery (CED) of Optogenetic Adeno-associated viral (AVV) vector to the Cortex of Rhesus Macaques under guidance of online MRI images. *Journal of Visualized Experiments : JoVE*, *147*, 10.3791/59232. https://doi.org/10.3791/59232

Kim, S., Callier, T., Tabot, G. A., Gaunt, R. A., Tenore, F. V., & Bensmaia, S. J. (2015). Behavioral assessment of sensitivity to intracortical microstimulation of primate somatosensory cortex. *Proceedings of the National Academy of Sciences*, *112*(49), 15202–15207. https://doi.org/10.1073/pnas.1509265112

Kleim, J. A., Bruneau, R., VandenBerg, P., MacDonald, E., Mulrooney, R., & Pocock, D. (2003). Motor cortex stimulation enhances motor recovery and reduces peri-infarct dysfunction following ischemic insult. *Neurological Research*, *25*(8), 789–793. https://doi.org/10.1179/016164103771953862

Koch, G., Ponzo, V., Lorenzo, F. D., Caltagirone, C., & Veniero, D. (2013). Hebbian and Anti-Hebbian Spike-Timing-Dependent Plasticity of Human Cortico-Cortical Connections. *Journal of Neuroscience*, *33*(23), 9725–9733. https://doi.org/10.1523/JNEUROSCI.4988-12.2013

Laakso, I., Murakami, T., Hirata, A., & Ugawa, Y. (2018). Where and what TMS activates: Experiments and modeling. *Brain Stimulation*, *11*(1), 166–174. https://doi.org/10.1016/j.brs.2017.09.011

Labat-gest, V., & Tomasi, S. (2013). Photothrombotic Ischemia: A Minimally Invasive and Reproducible Photochemical Cortical Lesion Model for Mouse Stroke Studies. *Journal of Visualized Experiments : JoVE*, *76*, 50370. https://doi.org/10.3791/50370

Lay, C. C., Davis, M. F., Chen-Bee, C. H., & Frostig, R. D. (2010). Mild Sensory Stimulation Completely Protects the Adult Rodent Cortex from Ischemic Stroke. *PLOS ONE*, *5*(6), e11270. https://doi.org/10.1371/journal.pone.0011270

Ledochowitsch, P., Yazdan-Shahmorad, A., Bouchard, K. E., Diaz-Botia, C., Hanson, T. L., He, J.-W., Seybold, B. A., Olivero, E., Phillips, E. A. K., Blanche, T. J., Schreiner, C. E., Hasenstaub, A., Chang, E. F., Sabes, P. N., & Maharbiz, M. M. (2015). Strategies for optical control and simultaneous electrical readout of extended cortical circuits. *Journal of Neuroscience Methods*, *256*, 220–231. https://doi.org/10.1016/j.jneumeth.2015.07.028

Lee, S. Y., Kozalakis, K., Baftizadeh, F., Campagnola, L., Jarsky, T., Koch, C., & Anastassiou, C. A. (2024). Cell-class-specific electric field entrainment of neural activity. *Neuron*, *112*(15), 2614-2630.e5. https://doi.org/10.1016/j.neuron.2024.05.009

Lei, T., Scheid, M. R., Glaser, J. I., & Slutzky, M. W. (2025). *Active Dissociation of Intracortical Spiking and High Gamma Activity* (p. 2025.07.10.663559). bioRxiv. https://doi.org/10.1101/2025.07.10.663559

Levy, R. M., Harvey, R. L., Kissela, B. M., Winstein, C. J., Lutsep, H. L., Parrish, T. B., Cramer, S. C., & Venkatesan, L. (2016a). Epidural Electrical Stimulation for Stroke Rehabilitation: Results of the Prospective, Multicenter, Randomized, Single-Blinded Everest Trial. *Neurorehabilitation and Neural Repair*, *30*(2), 107–119. https://doi.org/10.1177/1545968315575613

Levy, R. M., Harvey, R. L., Kissela, B. M., Winstein, C. J., Lutsep, H. L., Parrish, T. B., Cramer, S. C., & Venkatesan, L. (2016b). Epidural Electrical Stimulation for Stroke Rehabilitation: Results of the Prospective, Multicenter, Randomized, Single-Blinded Everest Trial. *Neurorehabilitation and Neural Repair*, *30*(2), 107–119. https://doi.org/10.1177/1545968315575613

Lewis, P. M., Thomson, R. H., Rosenfeld, J. V., & Fitzgerald, P. B. (2016). Brain Neuromodulation Techniques: A Review. *The Neuroscientist*, *22*(4), 406–421. https://doi.org/10.1177/1073858416646707

Lindroos, O. F. C., & Leinonen, L. M. (1983). Rapid Nissl Staining for Frozen Sections of Fresh Brain. *Stain Technology*, *58*(4), 240–242. https://doi.org/10.3109/10520298309066795

Logothetis, N. K., Augath, M., Murayama, Y., Rauch, A., Sultan, F., Goense, J., Oeltermann, A., & Merkle, H. (2010). The effects of electrical microstimulation on cortical signal propagation. *Nature Neuroscience*, *13*(10), 1283–1291. https://doi.org/10.1038/nn.2631

Lozano, A. M., Lipsman, N., Bergman, H., Brown, P., Chabardes, S., Chang, J. W., Matthews, K., McIntyre, C. C., Schlaepfer, T. E., Schulder, M., Temel, Y., Volkmann, J., & Krauss, J. K. (2019). Deep brain stimulation: Current challenges and future directions. *Nature Reviews. Neurology*, *15*(3), 148–160. https://doi.org/10.1038/s41582-018-0128-2

Lucas, T. H., & Fetz, E. E. (2013). Myo-Cortical Crossed Feedback Reorganizes Primate Motor Cortex Output. *Journal of Neuroscience*, *33*(12), 5261–5274. https://doi.org/10.1523/JNEUROSCI.4683-12.2013

Malenka, R. C., & Bear, M. F. (2004). LTP and LTD: An Embarrassment of Riches. *Neuron*, *44*(1), 5–21. https://doi.org/10.1016/j.neuron.2004.09.012

Markram, H., Toledo-Rodriguez, M., Wang, Y., Gupta, A., Silberberg, G., & Wu, C. (2004). Interneurons of the neocortical inhibitory system. *Nature Reviews Neuroscience*, *5*(10), 793–807. https://doi.org/10.1038/nrn1519

Matute, C., Alberdi, E., Domercq, M., Sánchez-Gómez, M.-V., Pérez-Samartín, A., Rodríguez-Antigüedad, A., & Pérez-Cerdá, F. (2007). Excitotoxic damage to white matter. *Journal of Anatomy*, *210*(6), 693–702. https://doi.org/10.1111/j.1469-7580.2007.00733.x

Matute, C., Domercq, M., Pérez-Samartín, A., & Ransom, B. R. (2013). Protecting White Matter From Stroke Injury. *Stroke*, *44*(4), 1204–1211. https://doi.org/10.1161/STROKEAHA.112.658328

McCormick, D. A., Nestvogel, D. B., & He, B. J. (2020). Neuromodulation of Brain State and Behavior. *Annual Review of Neuroscience*, *43*(Volume 43, 2020), 391–415. https://doi.org/10.1146/annurev-neuro-100219-105424

McFadden, W. C., Walsh, H., Richter, F., Soudant, C., Bryce, C. H., Hof, P. R., Fowkes, M., Crary, J. F., & McKenzie, A. T. (2019). Perfusion fixation in brain banking: A systematic review. *Acta Neuropathologica Communications*, *7*(1), 146. https://doi.org/10.1186/s40478-019-0799-y

Moorjani, S., Walvekar, S., Fetz, E. E., & Perlmutter, S. I. (2022). Movement-dependent electrical stimulation for volitional strengthening of cortical connections in behaving monkeys. *Proceedings of the National Academy of Sciences*, *119*(27), e2116321119. https://doi.org/10.1073/pnas.2116321119

Nishimura, Y., Perlmutter, S. I., Eaton, R. W., & Fetz, E. E. (2013). Spike-Timing-Dependent Plasticity in Primate Corticospinal Connections Induced during Free Behavior. *Neuron*, *80*(5), 1301–1309. https://doi.org/10.1016/j.neuron.2013.08.028

Notturno, F., Pace, M., Zappasodi, F., Cam, E., Bassetti, C. L., & Uncini, A. (2014). Neuroprotective effect of cathodal transcranial direct current stimulation in a rat stroke model. *Journal of the Neurological Sciences*, *342*(1), 146–151. https://doi.org/10.1016/j.jns.2014.05.017

Nouri, S., & Cramer, S. C. (2011). Anatomy and physiology predict response to motor cortex stimulation after stroke. *Neurology*, *77*(11), 1076–1083. https://doi.org/10.1212/WNL.0b013e31822e1482

Numssen, O., Kuhnke, P., Weise, K., & Hartwigsen, G. (2024). Electric-field-based dosing for TMS. *Imaging Neuroscience*, *2*, 1–12. https://doi.org/10.1162/imag_a_00106

Paxinos, G., Huang, X.-F., & Toga, A. (2009). *The Rhesus Monkey Brain in Stereotaxic Coordinates*. Academic Press.

Peeters, L. M., Hinz, R., Detrez, J. R., Missault, S., De Vos, W. H., Verhoye, M., Van der Linden, A., & Keliris, G. A. (2020). Chemogenetic silencing of neurons in the mouse anterior cingulate area modulates neuronal activity and functional connectivity. *NeuroImage*, *220*, 117088. https://doi.org/10.1016/j.neuroimage.2020.117088

Perera, T., George, M. S., Grammer, G., Janicak, P. G., Pascual-Leone, A., & Wirecki, T. S. (2016). The Clinical TMS Society Consensus Review and Treatment Recommendations for TMS Therapy for Major Depressive Disorder. *Brain Stimulation*, *9*(3), 336–346. https://doi.org/10.1016/j.brs.2016.03.010

Peruzzotti-Jametti, L., Cambiaghi, M., Bacigaluppi, M., Gallizioli, M., Gaude, E., Mari, S., Sandrone, S., Cursi, M., Teneud, L., Comi, G., Musco, G., Martino, G., & Leocani, L. (2013). Safety and Efficacy of Transcranial Direct Current Stimulation in Acute Experimental Ischemic Stroke. *Stroke*, *44*(11), 3166–3174. https://doi.org/10.1161/STROKEAHA.113.001687

Popović, D., Sinkaer, T., & Popović, M. (2009). Electrical stimulation as a means for achieving recovery of function in stroke patients. *NeuroRehabilitation*, *25*, 45–58. https://doi.org/10.3233/NRE-2009-0498

Powers, W. J. (2020). Acute Ischemic Stroke. *New England Journal of Medicine*, *383*(3), 252–260. https://doi.org/10.1056/NEJMcp1917030

Prabhakaran, S., Ruff, I., & Bernstein, R. A. (2015). Acute Stroke Intervention: A Systematic Review. *JAMA*, *313*(14), 1451–1462. https://doi.org/10.1001/jama.2015.3058

Rawlinson, C., Jenkins, S., Thei, L., Dallas, M. L., & Chen, R. (2020). Post-Ischaemic Immunological Response in the Brain: Targeting Microglia in Ischaemic Stroke Therapy. *Brain Sciences*, *10*(3), Article 3. https://doi.org/10.3390/brainsci10030159

Ray, S., Crone, N. E., Niebur, E., Franaszczuk, P. J., & Hsiao, S. S. (2008). Neural Correlates of High-Gamma Oscillations (60–200 Hz) in Macaque Local Field Potentials and Their Potential Implications in Electrocorticography. *Journal of Neuroscience*, *28*(45), 11526–11536. https://doi.org/10.1523/JNEUROSCI.2848-08.2008

Rebesco, J. M., & Miller, L. E. (2011). Enhanced detection threshold for *in vivo* cortical stimulation produced by Hebbian conditioning. *Journal of Neural Engineering*, *8*(1), 016011. https://doi.org/10.1088/1741-2560/8/1/016011

Rogers, A., Schmuck, G., Scholz, G., & Williams, D. C. (2004). C-fos mRNA Expression in Rat Cortical Neurons During Glutamate-Mediated Excitotoxicity. *Toxicological Sciences*, *82*(2), 562–569. https://doi.org/10.1093/toxsci/kfh279

Rowe, J. (2010). Connectivity Analysis is Essential to Understand Neurological Disorders. *Frontiers in Systems Neuroscience*, *4*. https://doi.org/10.3389/fnsys.2010.00144

Ruggiero, R. N., Rossignoli, M. T., Marques, D. B., de Sousa, B. M., Romcy-Pereira, R. N., Lopes-Aguiar, C., & Leite, J. P. (2021). Neuromodulation of Hippocampal-Prefrontal Cortical Synaptic Plasticity and Functional Connectivity: Implications for Neuropsychiatric Disorders. *Frontiers in Cellular Neuroscience*, *15*. https://doi.org/10.3389/fncel.2021.732360

Ruiz, O., Lustig, B. R., Nassi, J. J., Cetin, A., Reynolds, J. H., Albright, T. D., Callaway, E. M., Stoner, G. R., & Roe, A. W. (2013). Optogenetics through windows on the brain in the nonhuman primate. *Journal of Neurophysiology*, *110*(6), 1455–1467. https://doi.org/10.1152/jn.00153.2013

Seeman, S. C., Mogen, B. J., Fetz, E. E., & Perlmutter, S. I. (2017). Paired Stimulation for Spike-Timing-Dependent Plasticity in Primate Sensorimotor Cortex. *The Journal of Neuroscience*, *37*(7), 1935–1949. https://doi.org/10.1523/JNEUROSCI.2046-16.2017

Shi, L., Rocha, M., Leak, R. K., Zhao, J., Bhatia, T. N., Mu, H., Wei, Z., Yu, F., Weiner, S. L., Ma, F., Jovin, T. G., & Chen, J. (2018). A new era for stroke therapy: Integrating neurovascular protection with optimal reperfusion. *Journal of Cerebral Blood Flow & Metabolism*, *38*(12), 2073–2091. https://doi.org/10.1177/0271678X18798162

Skudlarski, P., Jagannathan, K., Anderson, K., Stevens, M. C., Calhoun, V. D., Skudlarska, B. A., & Pearlson, G. (2010). Brain Connectivity Is Not Only Lower but Different in Schizophrenia: A Combined Anatomical and Functional Approach. *Biological Psychiatry*, *68*(1), 61–69. https://doi.org/10.1016/j.biopsych.2010.03.035

Sohal, V. S., Zhang, F., Yizhar, O., & Deisseroth, K. (2009). Parvalbumin neurons and gamma rhythms enhance cortical circuit performance. *Nature*, *459*(7247), 698–702. https://doi.org/10.1038/nature07991

Solomons, C. D., & Shanmugasundaram, V. (2019). A review of transcranial electrical stimulation methods in stroke rehabilitation. *Neurology India*, *67*(2), 417. https://doi.org/10.4103/0028-3886.258057

Sommer, C. J. (2017). Ischemic stroke: Experimental models and reality. *Acta Neuropathologica*, *133*(2), 245–261. https://doi.org/10.1007/s00401-017-1667-0

Song, W., Kerr, C. C., Lytton, W. W., & Francis, J. T. (2013). Cortical Plasticity Induced by Spike-Triggered Microstimulation in Primate Somatosensory Cortex. *PLOS ONE*, *8*(3), e57453. https://doi.org/10.1371/journal.pone.0057453

Stagg, C. J., Wylezinska, M., Matthews, P. M., Johansen-Berg, H., Jezzard, P., Rothwell, J. C., & Bestmann, S. (2009). Neurochemical Effects of Theta Burst Stimulation as Assessed by

Magnetic Resonance Spectroscopy. *Journal of Neurophysiology*, *101*(6), 2872–2877. https://doi.org/10.1152/jn.91060.2008

Stanis, N., Khateeb, K., Zhou, J., Wang, R. K., & Yazdan-Shahmorad, A. (2023). Protocol to study ischemic stroke by photothrombotic lesioning in the cortex of non-human primates. *STAR Protocols*, *4*(3), 102496. https://doi.org/10.1016/j.xpro.2023.102496

Stark, E., Eichler, R., Roux, L., Fujisawa, S., Rotstein, H. G., & Buzsáki, G. (2013). Inhibition-Induced Theta Resonance in Cortical Circuits. *Neuron*, *80*(5), 1263–1276. https://doi.org/10.1016/j.neuron.2013.09.033

Stinear, C. M., Lang, C. E., Zeiler, S., & Byblow, W. D. (2020). Advances and challenges in stroke rehabilitation. *The Lancet Neurology*, *19*(4), 348–360. https://doi.org/10.1016/S1474-4422(19)30415-6

Tajiri, N., Dailey, T., Metcalf, C., Mosley, Y. I., Lau, T., Staples, M., van Loveren, H., Kim, S. U., Yamashima, T., Yasuhara, T., Date, I., Kaneko, Y., & Borlongan, C. V. (2013). In vivo animal stroke models: A rationale for rodent and non-human primate models. *Translational Stroke Research*, *4*(3), 308–321. https://doi.org/10.1007/s12975-012-0241-2

Tehovnik, E. J., Tolias, A. S., Sultan, F., Slocum, W. M., & Logothetis, N. K. (2006). Direct and Indirect Activation of Cortical Neurons by Electrical Microstimulation. *Journal of Neurophysiology*, *96*(2), 512–521. https://doi.org/10.1152/jn.00126.2006

Tehse, J., & Taghibiglou, C. (2019). The overlooked aspect of excitotoxicity: Glutamate-independent excitotoxicity in traumatic brain injuries. *European Journal of Neuroscience*, *49*(9), 1157–1170. https://doi.org/10.1111/ejn.14307

Thiebaut de Schotten, M., Tomaiuolo, F., Aiello, M., Merola, S., Silvetti, M., Lecce, F., Bartolomeo, P., & Doricchi, F. (2014). Damage to White Matter Pathways in Subacute and Chronic Spatial Neglect: A Group Study and 2 Single-Case Studies with Complete Virtual "In Vivo" Tractography Dissection. *Cerebral Cortex*, *24*(3), 691–706. https://doi.org/10.1093/cercor/bhs351

Thielscher, A., & Kammer, T. (2004). Electric field properties of two commercial figure-8 coils in TMS: Calculation of focality and efficiency. *Clinical Neurophysiology*, *115*(7), 1697–1708. https://doi.org/10.1016/j.clinph.2004.02.019

Tsao, C. W., Aday, A. W., Almarzooq, Z. I., Alonso, A., Beaton, A. Z., Bittencourt, M. S., Boehme, A. K., Buxton, A. E., Carson, A. P., Commodore-Mensah, Y., Elkind, M. S. V., Evenson, K. R., Eze-Nliam, C., Ferguson, J. F., Generoso, G., Ho, J. E., Kalani, R., Khan, S. S., Kissela, B. M., … null, null. (2022). Heart Disease and Stroke Statistics—2022 Update: A Report From the American Heart Association. *Circulation*, *145*(8), e153–e639. https://doi.org/10.1161/CIR.0000000000001052

Uemura, Y., Kowall, N. W., & Moskowitz, M. A. (1991). Focal ischemia in rats causes time-dependent expression of c-fos protein immunoreactivity in widespread regions of ipsilateral cortex. *Brain Research*, *552*(1), 99–105. https://doi.org/10.1016/0006-8993(91)90665-I

Venkataraman, A., Whitford, T. J., Westin, C.-F., Golland, P., & Kubicki, M. (2012). Whole brain resting state functional connectivity abnormalities in schizophrenia. *Schizophrenia Research*, *139*(1), 7–12. https://doi.org/10.1016/j.schres.2012.04.021

Villamar, M. F., Santos Portilla, A., Fregni, F., & Zafonte, R. (2012). Noninvasive Brain Stimulation to Modulate Neuroplasticity in Traumatic Brain Injury. *Neuromodulation: Technology at the Neural Interface*, *15*(4), 326–338. https://doi.org/10.1111/j.1525-1403.2012.00474.x

Vink, J. J. T., van Lieshout, E. C. C., Otte, W. M., van Eijk, R. P. A., Kouwenhoven, M., Neggers, S. F. W., van der Worp, H. B., Visser-Meily, J. M. A., & Dijkhuizen, R. M. (2023). Continuous Theta-Burst Stimulation of the Contralesional Primary Motor Cortex for Promotion of Upper Limb Recovery After Stroke: A Randomized Controlled Trial. *Stroke*, *54*(8), 1962–1971. https://doi.org/10.1161/STROKEAHA.123.042924

Viswanathan, A., & Freeman, R. D. (2007). Neurometabolic coupling in cerebral cortex reflects synaptic more than spiking activity. *Nature Neuroscience*, *10*(10), 1308–1312. https://doi.org/10.1038/nn1977

von Bornstädt, D., Houben, T., Seidel, J. L., Zheng, Y., Dilekoz, E., Qin, T., Sandow, N., Kura, S., Eikermann-Haerter, K., Endres, M., Boas, D. A., Moskowitz, M. A., Lo, E. H., Dreier, J. P., Woitzik, J., Sakadžić, S., & Ayata, C. (2015). Supply-Demand Mismatch Transients in Susceptible Peri-infarct Hot Zones Explain the Origins of Spreading Injury Depolarizations. *Neuron*, *85*(5), 1117–1131. https://doi.org/10.1016/j.neuron.2015.02.007

Vöröslakos, M., Takeuchi, Y., Brinyiczki, K., Zombori, T., Oliva, A., Fernández-Ruiz, A., Kozák, G., Kincses, Z. T., Iványi, B., Buzsáki, G., & Berényi, A. (2018). Direct effects of transcranial electric stimulation on brain circuits in rats and humans. *Nature Communications*, *9*(1), 483. https://doi.org/10.1038/s41467-018-02928-3

Vos, T., Lim, S. S., Abbafati, C., Abbas, K. M., Abbasi, M., Abbasifard, M., Abbasi-Kangevari, M., Abbastabar, H., Abd-Allah, F., Abdelalim, A., Abdollahi, M., Abdollahpour, I., Abolhassani, H., Aboyans, V., Abrams, E. M., Abreu, L. G., Abrigo, M. R. M., Abu-Raddad, L. J., Abushouk, A. I., … Murray, C. J. L. (2020). Global burden of 369 diseases and injuries in 204 countries and territories, 1990–2019: A systematic analysis for the Global Burden of Disease Study 2019. *The Lancet*, *396*(10258), 1204–1222. https://doi.org/10.1016/S0140-6736(20)30925-9

Wagner, T. A., Zahn, M., Grodzinsky, A. J., & Pascual-Leone, A. (2004). Three-dimensional head model Simulation of transcranial magnetic stimulation. *IEEE Transactions on Biomedical Engineering*, *51*(9), 1586–1598. IEEE Transactions on Biomedical Engineering. https://doi.org/10.1109/TBME.2004.827925

Wang, F., Xie, X., Xing, X., & Sun, X. (2022). Excitatory Synaptic Transmission in Ischemic Stroke: A New Outlet for Classical Neuroprotective Strategies. *International Journal of Molecular Sciences*, *23*(16), Article 16. https://doi.org/10.3390/ijms23169381

Wang, L.-C., Wei, W.-Y., Ho, P.-C., Wu, P.-Y., Chu, Y.-P., & Tsai, K.-J. (2021). Somatosensory Cortical Electrical Stimulation After Reperfusion Attenuates Ischemia/Reperfusion Injury of Rat Brain. *Frontiers in Aging Neuroscience*, *13*. https://doi.org/10.3389/fnagi.2021.741168

Wessels, T., Wessels, C., Ellsiepen, A., Reuter, I., Trittmacher, S., Stolz, E., & Jauss, M. (2006). Contribution of Diffusion-Weighted Imaging in Determination of Stroke Etiology. *American Journal of Neuroradiology*, *27*(1), 35–39.

Westlake, K. P., & Nagarajan, S. S. (2011). Functional Connectivity in Relation to Motor Performance and Recovery After Stroke. *Frontiers in Systems Neuroscience*, *5*. https://doi.org/10.3389/fnsys.2011.00008

Whitfield-Gabrieli, S., Thermenos, H. W., Milanovic, S., Tsuang, M. T., Faraone, S. V., McCarley, R. W., Shenton, M. E., Green, A. I., Nieto-Castanon, A., LaViolette, P., Wojcik, J., Gabrieli, J. D. E., & Seidman, L. J. (2009). Hyperactivity and hyperconnectivity of the default network in schizophrenia and in first-degree relatives of persons with schizophrenia. *Proceedings of the National Academy of Sciences*, *106*(4), 1279–1284. https://doi.org/10.1073/pnas.0809141106

Widge, A. S. (2024). Closing the loop in psychiatric deep brain stimulation: Physiology, psychometrics, and plasticity. *Neuropsychopharmacology*, *49*(1), 138–149. https://doi.org/10.1038/s41386-023-01643-y

Widge, A. S., & Miller, E. K. (2019). Targeting Cognition and Networks Through Neural Oscillations: Next-Generation Clinical Brain Stimulation. *JAMA Psychiatry*, *76*(7), 671–672. https://doi.org/10.1001/jamapsychiatry.2019.0740

Wiegert, J. S., Mahn, M., Prigge, M., Printz, Y., & Yizhar, O. (2017). Silencing Neurons: Tools, Applications, and Experimental Constraints. *Neuron*, *95*(3), 504–529. https://doi.org/10.1016/j.neuron.2017.06.050

Woitzik, J., Hecht, N., Pinczolits, A., Sandow, N., Major, S., Winkler, M. K. L., Weber-Carstens, S., Dohmen, C., Graf, R., Strong, A. J., Dreier, J. P., Vajkoczy, P., & Group, F. the C. study. (2013). Propagation of cortical spreading depolarization in the human cortex after malignant stroke. *Neurology*, *80*(12), 1095–1102. https://doi.org/10.1212/WNL.0b013e3182886932

Yazdan-Shahmorad, A., Diaz-Botia, C., Hanson, T. L., Kharazia, V., Ledochowitsch, P., Maharbiz, M. M., & Sabes, P. N. (2016). A Large-Scale Interface for Optogenetic Stimulation and Recording in Nonhuman Primates. *Neuron*, *89*(5), 927–939. https://doi.org/10.1016/j.neuron.2016.01.013

Yazdan-Shahmorad, A., Kipke, D. R., & Lehmkuhle, M. J. (2011). Polarity of cortical electrical stimulation differentially affects neuronal activity of deep and superficial layers of rat motor cortex. *Brain Stimulation*, *4*(4), 228–241. https://doi.org/10.1016/j.brs.2010.11.004

Yazdan-Shahmorad, A., Kipke, D. R., & Lehmkuhle, M. J. (2013). High gamma power in ECoG reflects cortical electrical stimulation effects on unit activity in layers V/VI. *Journal of Neural Engineering*, *10*(6), 066002. https://doi.org/10.1088/1741-2560/10/6/066002

Yazdan-Shahmorad, A., Lehmkuhle, M. J., Gage, G. J., Marzullo, T. C., Parikh, H., Miriani, R. M., & Kipke, D. R. (2011). Estimation of electrode location in a rat motor cortex by laminar analysis of electrophysiology and intracortical electrical stimulation. *Journal of Neural Engineering*, *8*(4), 046018. https://doi.org/10.1088/1741-2560/8/4/046018

Yazdan-Shahmorad, A., Silversmith, D. B., Kharazia, V., & Sabes, P. N. (2018). Targeted cortical reorganization using optogenetics in non-human primates. *eLife*, *7*. https://doi.org/10.7554/eLife.31034

Yazdan-Shahmorad, A., Tian, N., Kharazia, V., Samaranch, L., Kells, A., Bringas, J., He, J., Bankiewicz, K., & Sabes, P. N. (2018). Widespread optogenetic expression in macaque cortex obtained with MR-guided, convection enhanced delivery (CED) of AAV vector to the thalamus. *Journal of Neuroscience Methods*, *293*, 347–358. https://doi.org/10.1016/j.jneumeth.2017.10.009

Yenari, M. A., Kauppinen, T. M., & Swanson, R. A. (2010). Microglial Activation in Stroke: Therapeutic Targets. *Neurotherapeutics*, *7*(4), 378–391. https://doi.org/10.1016/j.nurt.2010.07.005

Zanos, S., Rembado, I., Chen, D., & Fetz, E. E. (2018). Phase-Locked Stimulation during Cortical Beta Oscillations Produces Bidirectional Synaptic Plasticity in Awake Monkeys. *Current Biology*, *28*(16), 2515-2526.e4. https://doi.org/10.1016/j.cub.2018.07.009

Zhou, J., Khateeb, K., Gala, A., Rahimi, M., Griggs, D. J., Ip, Z., & Yazdan-Shahmorad, A. (2022). Neuroprotective effects of electrical stimulation following ischemic stroke in non-human primates. *2022 44th Annual International Conference of the IEEE Engineering in Medicine & Biology Society (EMBC)*, 3085–3088. https://ieeexplore.ieee.org/abstract/document/9871335/

Zrenner, C., Desideri, D., Belardinelli, P., & Ziemann, U. (2018). Real-time EEG-defined excitability states determine efficacy of TMS-induced plasticity in human motor cortex. *Brain Stimulation*, *11*(2), 374–389. https://doi.org/10.1016/j.brs.2017.11.016